PROCESSING AND CHARACTERIZATION OF CARBON BLACK-FILLED ELECTRICALLY CONDUCTIVE NYLON-12 NANOCOMPOSITES PRODUCED BY SELECTIVE LASER SINTERING

A Dissertation
Presented to
The Academic Faculty

by

Siddharth Ram Athreya

In Partial Fulfillment
of the Requirements for the Degree
Doctor of Philosohy in the
George W. Woodruff School of Mechanical Engineering

Georgia Institute of Technology
May 2010

PROCESSING AND CHARACTERIZATION OF CARBON BLACK-FILLED ELECTRICALLY CONDUCTIVE NYLON-12 NANOCOMPOSITES PRODUCED BY SELECTIVE LASER SINTERING

Approved by:

Dr. Suman Das, Co-chair
School of Mechanical Engineering
Georgia Institute of Technology

Dr. Kyriaki Kalaitzidou, Co-chair
School of Mechanical Engineering
Georgia Institute of Technology

Dr. David Rosen
School of Mechanical Engineering
Georgia Institute of Technology

Dr. Satish Kumar
School of Polymer, Textile and Fiber Engineering
Georgia Institute of Technology

Dr. Gleb Yushin
School of Materials Science and Engineering
Georgia Institute of Technology

Date Approved: February 17, 2010

To my parents

ACKNOWLEDGEMENTS

Today, as I complete my dissertation and look back at the last four and a half years of my life as a graduate student, I am overwhelmed by a feeling of accomplishment. However, I have to acknowledge that I would not be in this position today had I not received help and guidance from several people.

First, I would like to thank my advisor Dr. Suman Das for his guidance and confidence in my abilities. His deep knowledge of and insights on the latest research topics have been a source of inspiration for me during my graduate studies. My co-advisor, Dr. Kyriaki Kalaitzidou's expertise in polymer science has also been invaluable. Her cheerful nature and willingness to help have always amazed me. I thank both of them for instilling a scientific temper in me.

My PhD reading committee members: Dr. David Rosen, Dr. Satish Kumar, and Dr. Gleb Yushin provided me with insightful comments during my PhD Proposal presentation. I thank the Materials Property Research Lab at Georgia tech, Dr. Jonathan Colton, Dr. Haskell Beckham, Dr. Mohan Srinivasarao, and Dr. Donggang Yao for giving me access to the equipment in their labs.

I would like to thank all my colleagues in the Direct Digital Manufacturing Lab. I have cherished the friendship of Sudipta, Bhai, Shanti, Ugur, Akshay, and Akshi. I am also grateful to Sarang, Xuxia, and Ryan for tolerating my frequent requests for using their characterization equipment.

Finally, I would like to express my sincere gratitude and thanks to my parents, without whose hard work, sacrifices and planning I would not be in this position today. I thank both my sisters for their love and affection. To them, I dedicate this thesis.

TABLE OF CONTENTS

LIST OF TABLES

Page

LIST OF FIGURES

Page

SUMMARY

Electrically conductive polymer composites are suitable for use in the manufacture of antistatic products and components for electronic interconnects, fuel cells and electromagnetic shielding. The most widely used processing techniques for producing electrically conductive polymer composites place an inherent constraint on the geometry and architecture of the part that can be fabricated. Hence, this thesis investigates selective laser sintering (SLS), a rapid prototyping technique, to fabricate and characterize electrically conductive nanocomposites of Nylon-12 filled with 4% by weight of carbon black. The objective of the dissertation was to study the effects of the SLS process on the microstructure and properties of the nanocomposite. The effect of laser power and the scan speed on the flexural modulus and part density of the nanocomposite was studied. The set of parameters that yielded the maximum flexural modulus and part density were used to fabricate specimens to study the tensile, impact, rheological and viscoelastic properties. The electrical conductivity of the nanocomposite was also investigated. The thermo-mechanical properties and electrical conductivity of the nanocomposites produced by SLS were compared with those produced by extrusion-injection molding.

The structure and morphology of the SLS-processed and extrusion-injection molded nanocomposites were characterized using gas pycnometry, gel permeation chromatography, differential scanning calorimetry, electron microscopy, polarized light microscopy and x-ray diffraction. Physical models were developed to explain the effects of the processing technique on the structure and properties of the nanocomposites.

Finally, a one-dimensional heat transfer model of the SLS process that accounted for sintering-induced densification and thermal degradation of the polymer was implemented in order to study the variation in part density with respect to the energy density of the laser beam.

This dissertation demonstrated that SLS can be successfully used to fabricate electrically conductive polymer nanocomposites with a relatively low percolation threshold. This capability combined with the ability of SLS to fabricate complicated three-dimensional objects without part-specific tooling could open up several new opportunities.

CHAPTER 1 INTRODUCTION

Polymer nanocomposite technology is a developing field in which nanoscale fillers are blended with a polymer to produce materials with novel characteristics. A wide range of polymers including thermoplastics, thermosets and elastomers have been used to produce nanocomposites. The most commonly used fillers are nanoclays, nanosilicas, nanoceramics and carbon based nanoparticles. The properties imparted by the nanoparticles to the polymer can be remarkable. Polymer nanocomposites have the potential to create a whole new generation of products with significantly improved performance characteristics. They represent a class of materials that is a radical alternative to conventional polymer composites. These novel materials have generated great interest due to significantly enhanced physical, mechanical, electrical, thermal, and barrier properties at low filler contents [1-3].

The objective of this doctoral dissertation is to process an electrically conductive polymer nanocomposite by selective laser sintering (SLS), a solid freeform fabrication (SFF) or a layered manufacturing (LM) technique. This dissertation focuses on characterizing the structure and morphology of the nanocomposite in order to relate its properties with the SLS process. This chapter focuses on providing an introduction and description of previous research pertaining to electrically conductive polymer composites and selective laser sintering. Section 1.4 provides the motivation and a statement of research. Section 1.5 provides an outline for this dissertation.

1.1 Electrically Conductive Polymer Composites

Progress in the science of polymeric materials has witnessed a dramatic development and search for polymers and polymer-based composite materials that have properties similar to metals, ceramics and glass. Among the many useful properties, electrical conductivity of polymer-based composites is one of the most important. It has been observed that addition of carbon-based fillers such as graphite, carbon black, carbon nanotubes, and carbon fibers to insulating polymers results in a drop in resistivity of the composite [4]. A sharp drop in resistivity is observed at a critical concentration of the filler. This concentration is called the percolation threshold. Many conductive polymer composites exhibit percolation behavior [5, 6]. The percolation behavior of electrically conductive polymer composites (ECPC) has been exploited to fabricate components for a wide range of applications. ECPCs find use in the fabrication of devices for electromagnetic radiation shielding, electrostatic discharge, medical equipment, cables, transducers and gas sensors [7]. A major advantage of this class of materials is the ability to vary the conductivity by adjusting the concentration of the conductive filler in the polymer-filler mixture. Moreover, unlike metal fillers, carbon-based fillers do not have a tendency to oxidize and form an insulating layer on the surface [8]. Another benefit is that they are lighter than metals.

Some of the commonly used processing techniques of ECPCs such as melt mixing have the following disadvantages. Firstly, melt mixing involves the heating of the polymer-filler mixture above the softening temperature of the polymer and employing a shearing action to adequately blend the filler parts. It has been observed that the shearing action results in the dispersion and breaking down of the agglomerates of conductive

fillers such as carbon black. However, excessive shear forces can lead to an increase in the percolation threshold [9]. Agari et al [10] studied the effects of different mixing conditions on the electrical conductivity of polyethylene-filled graphite particles. It was reported that parts made by melt mixing had the highest percolation thresholds. This was attributed to the fact that the shearing forces resulted in filler particles with the lowest aspect ratios. Hence, parts made by melt mixing required the highest filler concentrations for the formation of a conductive network. Secondly, ECPCs that require high concentrations of the conductive filler are difficult to process by melt mixing due to a sharp increase in melt viscosity [4]. Thirdly, high shearing forces in melt mixing cause the conductive filler particles to migrate from regions of high shear stress to regions of low shear stress during the mixing and molding process [11]. This results in uneven distributions of the filler particle in the final component which might result in non-uniform properties. This is highly undesirable since it is not within the control of the designer. Lastly, the fabrication of functionally graded parts is not possible.

Selective laser sintering (SLS) has the potential to address some, if not all these issues. The following section gives a brief introduction to operating principles of this manufacturing technique.

1.2 Selective Laser Sintering

Selective laser sintering is a type of solid freeform fabrication (SFF) or layered manufacturing (LM) technique. SFF [12] is a completely automated process that can fabricate 3-dimensional (3D) parts without the need for part specific tools or fixtures. In most SFF processes, a 3D CAD model of the part is sliced by the computer and

systematically recreated layer upon layer to form the 3D part. A schematic diagram of the SLS process is shown in Figure 1.1.

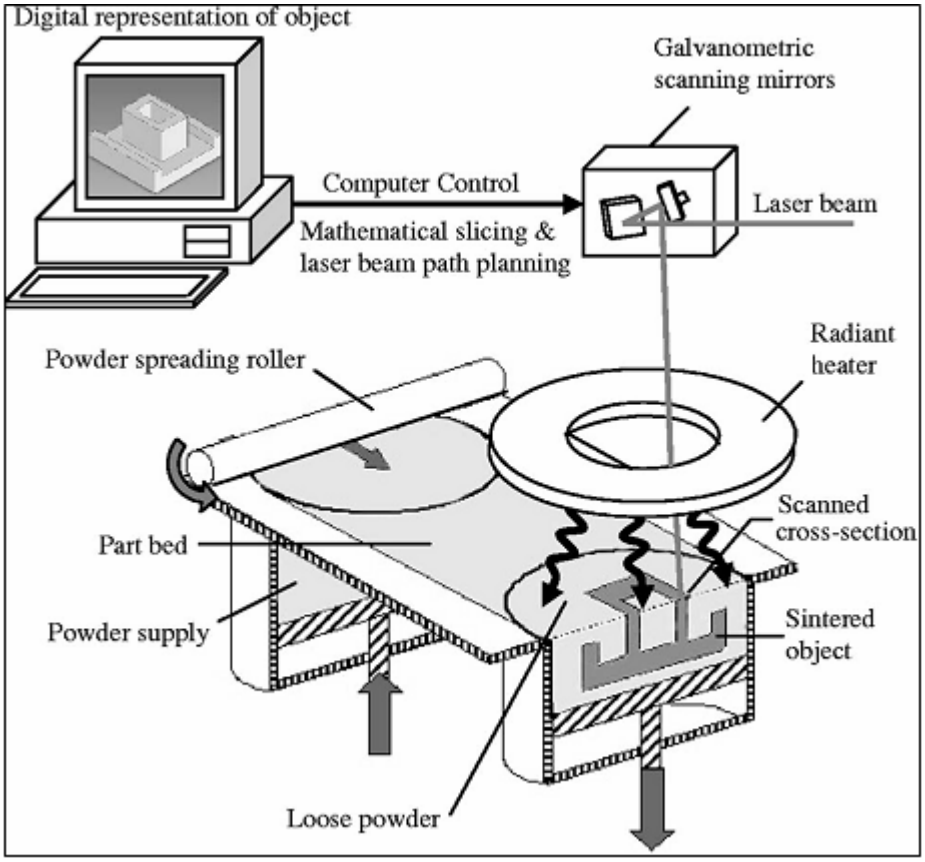

Figure 1.1 Schematic diagram of the Selective Laser Sintering Process.

SLS was invented by Dr. Carl Robert Deckard [13] in 1988. The SLS process like other LM processes starts with a CAD model of the part to be built. The CAD file is subsequently sliced at discrete intervals (approximately 100 – 200 μm) and the resulting cross-sections are stored sequentially in a "build file". Scanning algorithms are used to plan the path of the laser for each cross-section which is scanned onto a preheated bed of powder. Exposure to the scanning laser elevates the temperature of the powder to the

point of melting, resulting in the sintering of the particles. After scanning an entire cross-section onto the powder surface, the power bed is lowered by a distance equal to the slice layer thickness used in the build process and a fresh layer of powder is deposited by a roller mechanism. The next cross-section is then laser-sintered deep enough to fuse it to the underlying layer and in this way, by sintering layer upon layer, the entire part is fabricated.

Some of the important advantages of SLS are as follows:

1. Ability to manufacture complex 3D parts without any tools or fixtures
2. A wide range of materials can be processed. Polymers, metals, ceramics and composites have been successfully fabricated by SLS [14].
3. Ability to fabricate 1-dimensional (1D) functionally graded parts [15, 16].
4. SLS does not require CAD software developed support structures and hence does not require time for support structure removal.
5. SLS, unlike melt mixing methods, does not use a shearing action to blend the polymer when it is in a melt or near-melt state. With reference to the melt-mixing related processing issues that were raised in section 1.1, SLS is comparatively benign in the sense that it does not break down the conductive filler particles or cause migration of the filler particles leading to uneven distributions.

SLS was initially used for fabricating prototypes to aid visualization [12, 14] . However, over the last few years, significant effort has been focused on using SLS for making tissue engineering scaffolds [17-19] and drug delivery devices [20]. More recently, SLS has been used in rapid tooling [21] applications and to fabricate fuel cell [22] components and flexible electronics [23-25].

The primary objective of this project is to process and characterize an electrically conductive polymer nanocomposite by SLS. The material system under investigation in this work is Nylon 12 – carbon black (4 % by weight). Since the macroscopic properties of polymer nanocomposites are greatly dependent on the processing technique, the emphasis of this dissertation is to study the SLS processing-material structure-property relationships.

1.3 Literature Survey

The current scientific literature on areas central to this doctoral dissertation deals with various aspects and is rather expansive. The following sub-sections intend to give a literature review of the following key areas: processing of electrically conductive polymer composites and research in selective laser sintering.

1.3.1 Synthesis of Electrically-Conductive Nanocomposites

Factors affecting the percolation threshold and the electrical resistivity of electrically conductive polymer composites have been the focus of many studies. The most important factors are the processing technique, processing parameters, properties of the polymer matrix and the type of conductive filler [4, 8]. This section gives a literature survey of the three most commonly used processing techniques for the synthesis of ECPCs, namely,

(a) Melt mixing, (b) *In-situ* polymerization, and (c) Solution processing

It is important to note that there are two classes of ECPCs, as follows:

(a) Composites with an intrinsically conductive polymer

(b) Composites with a conductive filler and an insulating polymer matrix.

This section deals with ECPCs composed of a conductive nano-scale filler and an insulating polymer matrix. Special emphasis is given to carbon black-based ECPCs.

1.3.1.1 Melt Mixing

Melt mixing has been widely used for the preparation of carbon black-based ECPCs. This method involves mixing the nano-scale particles with the polymer and simultaneously heating this mixture above the softening point of the polymer. A mixing process that induces shear forces, also known as compounding is used to disperse the filler in the polymer melt. Commonly used types of compounding equipment are internal mixers, two roll mills, extruders and chaotic mixers. The choice of the compounding equipment [26], processing technique [27-29], process parameters during compounding, such as mixing time [9, 30] and temperature [31], type and structure of the carbon black [30], and morphology of the polymer [30] have a profound effect on the percolation threshold and electrical resistivity of the composite.

Bigg [30] investigated the effect of carbon black structure, morphology of the polymer, and mixing time on the electrical conductivity of carbon black-based ECPCs. Three types of carbon black, with varying structure and three polymers with varying degrees of crystallinity were considered. An electrically heated two roll mill was used to compound each of the blends for varying lengths of time. The blends were finally compression molded into sheets. The results showed that carbon black with high porosity yielded composites with lower resistivity than composites prepared using highly structured carbon black for identical concentrations. Furthermore, the resistivity of composites filled with high porosity carbon black is less sensitive to mixing time than composites filled with high structure carbon blacks. The results also indicated that

polymers with higher degree of phase separation had higher abilities to form segregated networks of the conductive filler. Polypropylene, the only semicrystalline polymer investigated in the study had the lowest resistivity among the three polymers whereas polycarbonate, a single phase amorphous polymer had the highest resistivity. This observation was explained by the premise that the carbon black was segregated to the amorphous region of the polymer, thereby increasing its effective concentration. However, this premise was not microscopically verified. Similar results were obtained by Cembrola [9] who studied the effects of mixing time and type of carbon black on the resistivity of carbon black – rubber composites. Beyond a certain optimal mixing time, the resistivity increased as the agglomerates got broken down, hindering the formation of a conductive network.

Bayer et al [27-29] studied the electrical properties of a carbon black – polyethylene (PE) composite processed using a mold that induced an elongational flow component during injection molding. They reported that the elongational flow component oriented the carbon black particles in axial channels. The resulting anisotropic distribution of carbon black resulted in a lower percolation threshold than samples made by compression molding as well as resitivities that were lower by two to three orders of magnitude than the latter.

Jana et al [26] investigated the effect of the compounding method on the percolation behavior of vapor grown carbon nanofiber-poly(methyl-methacrylate) composites. The electrical properties of samples prepared by a chaotic mixer were compared with those prepared by an internal mixer. The percolation threshold of composites prepared by chaotic mixing was 2 wt. % whereas it was 6 wt. % for

composites prepared by internal mixing. This was attributed to the fact that the nanofibers were aligned in the direction of flow in the composites prepared by chaotic mixing whereas the alignment was random in the composites prepared by internal mixing. It was also observed that the average fiber length was higher in the case of the composites manufactured by the internal mixer This was a result of the comparatively higher shearing forces in the internal mixer for the same mixing conditions. The greater fiber lengths as well as the presence of aligned fibers resulted in a lower percolation threshold of the chaotic mixer composites.

In recent years, there have been attempts to fabricate immiscible polymer blend-based ECPCs by injection molding [11, 32-34] and extrusion [35]. Foulger [33] studied the percolation behavior of a poly(ethylene-co-vinyl acetate) (EVA) and high density polyethylene (HDPE) blend – carbon black composite. The percolation threshold of the blend was lower than that of the individually filled polymers. The reduction in resistivity was explained by the fact that carbon black selectively locates either in one of the polymer phases or at their interface and thereby increases its effective concentration. Similar results were reported by Yui et al [11] who studied the percolation behavior of a blend of polypropylene and HDPE. The low percolation threshold was explained by the preferential location of the carbon black particles in the HDPE phase. This was experimentally verified by electron microscopy. Li et al [35] modified the post-percolation regime of a PE and poly(ethylene terephthalate) (PET) blend – carbon black composite by the addition of insulating nanoparticles (calcium carbonate nanoparticles). The nanoparticles and the carbon black were shown to preferentially locate themselves in the PET phase. An increase in resistivity was recorded for increasing concentrations of

the nanoparticles. This suggested that the nanoparticles were being pushed outwards towards the interface of the two polymers. This phenomenon was used to broaden the post-percolation regime by controlling the concentration of the nanoparticles and thereby increasing the reproducibility of the material properties. Table 1.1 lists several values of percolation threshold of carbon black filled ECPCs that have been reported in the literature. Among the melt mixing techniques, the lowest percolation threshold was achieved using compression molding

Table 1.1 Percolation thresholds for carbon black filled electrically conductive polymer composites

Polymer	Percolation threshold	Processing technique	Comments	Reference
Poly (2-ethylhexyl methacrylate)	6 wt. %	*In-situ* polymerization		[36]
Polystyrene	3 vol. %	*In-situ* polymerization		[37]
Polyurethane	4.6 vol. %	Solution processing	Electrospun into fiber webs	[5]
Polycaprolactone	7 wt. %	Solution processing	Electrospun into fibers	[6]
Epoxy resin	0.06 vol. %	Solution processing	Achieved low percolation thresholds by controlling ionic conc.	[38]
Nylon 6	1 wt. %	*In-situ* polymerization (ISP) and melt mixing.	Masterbatch made by ISP and diluted by melt mixing	[39]
Nylon 6	6 wt. %	Melt mixing		[39]
Nylon 6	9 wt. &	Compression molding		[40]
Nylon 6	25 wt. %	Melt mixing		[41]
Polyethylene	0.25–0.65 vol. %	Compression molding	3 types of CB studied	[42]

1.3.1.2 In-Situ Polymerization

In-situ polymerization involves the dispersion of the filler particles in a monomer followed by a polymerization reaction. Depending on the required molecular weight and molecular weight distribution of the polymer, radical, anionic, chain transfer and ring opening polymerizations may be used [43]. It is a very versatile technique since almost any polymer can be processed by this technique but is particularly useful for processing thermally unstable and insoluble polymers [43]. Regarding the processing of electrically conductive nanocomposites by *in-situ* polymerization, most of the work has been focused on carbon nanotube-based composites [2, 44-47]. *In-situ* polymerization has also been used to prepare carbon black-based ECPCs [36, 37, 48]. Li et at [37] prepared amorphous polystyrene (PS)–carbon black composites by *in-situ* polymerization. A percolation threshold of 3.3 vol. % was achieved. This was attributed to the fact that, prior to polymerization, the monomers could penetrate into the carbon black agglomerates and aid the formation of a conductive network.

1.3.1.3 Solution Processing

Solution processing techniques have been widely used for the preparation of carbon black [38, 49-52] and carbon nanotube-based [3, 53-55] electrically conducting polymer composites. Solution processing techniques, in general, have three steps: dispersing the nano-scale filler in a solvent, mixing this suspension with the polymer in an appropriate solvent and drying the composite solution. An alternative method that is widely used is the mixing of the nano-scale filler suspension in a resin which is cured by the addition of a hardener [3].

Schueler et al [38] studied the electrical percolation behavior by applying the science of colloids to polymer composites. Carbon black, an epoxy resin and an amine hardener were used to prepare an ECPC. The authors believed that percolation behavior of carbon black filled epoxy composites should not be explained with a geometric or statistical model [56] but from the viewpoint of colloid science where attractive and repulsive forces between the carbon black particles affect the development of agglomerates. Two methods were used to synthesize the composites. One of the methods used an electrolyte to reduce the Coulombic barrier between the carbon black particles. A percolation threshold of 0.06 vol. % was achieved through this processing route. It was shown that the dispersion of carbon black is electrostatically stabilized and an increase in ionic concentration achieved by the addition of an electrolyte lowers the percolation threshold. Particle agglomeration can also be induced by the use of electric fields. Prasse et al [50] and Schwarz et al [52] applied DC and AC electric fields respectively during the curing of the resin. The final resistivity of the composite for a given carbon black content could be controlled by varying the duration and strength of the electric field as well as the curing temperature.

The effect of viscosity of the epoxy solution on network formation of conductive nano-scale fillers was studied by Choi et al [57]. Vapor grown carbon nanofibers-based composites were prepared using a low and high viscosity epoxy solutions. The composite prepared with the low viscosity resin had a lower resistivity than the composite made by the high viscosity resin. The authors reported that lower viscosities resulted in a better dispersion of the nanofibers and aided the formation of a conductive network

A solution mixing/solvent removal technique has been employed for synthesizing ECPCs [58]. The drying procedure determines the final state of the composite. The composite could be in a pasty form [58], thin film [59] produced by spin casting, or in the form of a fiber produced by electrospinning. Electrospinning is a technique that processes a polymer solution or a melt into fibers with diameters ranging from a few nanometers to a few microns. Additives such as carbon black [5, 6, 60, 61], carbon nanotubes [62, 63] and carbon nanofibers [64] have been added to the solution/melt to tailor the mechanical and electrical properties of the fibers.

Chuangchote et al [60] investigated the mechanical, electrical and rheological properties of poly (vinyl alcohol)–carbon black nanofiber mats produced by electrospinning. The morphology and average diameter of the composite fibers were compared to those of the pure polymer. The authors reported that the Young's modulus of the fiber mats increased with increasing carbon black content. A loading of 10 wt. % of carbon black resulted in the doubling of the Young's modulus over that of fibers made from pure polymer. However, a significant drop in elongation at break was reported. Hwang et al [5] studied the electrical, mechanical and thermal properties of polyurethane-carbon black nanofibers synthesized by electrospinning. A percolation threshold of 4.6 vol. % was reported.

Tiwari et al [6] synthesized polycaprolactone-carbon black nanocomposite fibers by electrospinning. The authors investigated the possibility of using these fibers as noncyclic strain sensors. The effect of carbon black loading on the electrical conductivity of the fibers was experimentally studied. A percolation threshold of 7 wt. % was reported. Experiments demonstrated that at high strains, the fibers became

nonconductive. The stretching process disrupted the network of carbon black particles and resulted in an increase in resistivity. The authors proposed a two-dimensional model to describe the variation of electrical resistance with strain. A reasonable agreement between the model and the experimental results was reported.

1.3.2 Selective Laser Sintering

Polymer powders were the first materials to be used in SLS. The most commonly used polymers have been polyamide, polycarbonate and polystyrene. Many studies [65-68] have focused on optimizing the process parameters as well as studying the effects of SLS process parameters on the mechanical properties of components made from a pure polymer. The electrical properties such as the dielectric constant and dissipation factor of polymeric materials processed by SLS have been the focus of very few studies [69]. Caulfield et al [68] studied the effects of increasing energy density of the laser on the density and mechanical properties of polyamide components. The Young's modulus, tensile strength and elongation at break increased with increasing energy densities but began to decrease after a critical value. This was explained by the fact that increasing energy densities resulted in greater powder consolidation and stronger inter-layer bonding which resulted in stronger parts. However, energy densities greater than a critical value damaged the polymer and thereby decreased the mechanical properties.

The SLS processing of immiscible polymer blends of Nylon-12 (PA12)/high density polyethylene (HDPE) and Nylon-6 (PA6)/Nylon-12 has been investigated [70, 71]. The effects of the composition of the mixture and the processing conditions on the properties of the specimens were investigated. In the case of the PA12/HDPE system, the low chemical affinity between the two polymers resulted in a heterogeneous

microstructure. The microstructure contained either co-continuous or dispersed domains depending on the quantity of HDPE. A similar microstructure was detected in the case of the PA6/PA12 blend. The melt flow index and the rheological behavior of the individual polymers were found to have a significant effect on the porosities and microstructures of the specimens.

SLS has been used to fabricate tissue engineering scaffolds and drug delivery devices [17-20, 72, 73]. SLS is particularly useful for this application since it has capability of fabricating extremely complex 3D parts which may have an inner porous network without any part specific tooling. Williams et al [17] fabricated tissue engineering scaffolds using polycaprolactone (PCL) by SLS. The authors successfully fabricated scaffolds which had an external shape derived from CT/MRI data and an internal porous structure into which bone regenerating protein could be seeded. They reported that the part dimensions varied by around 3-8% from the designed dimensions. Popov et al [19] fabricated tissue engineering scaffolds by mixing a small quantity of biocompatible carbon black with a biodegradable polymer. *In Vitro* tests of the scaffolds showed a high level of biocompatibility. Leong et al [20] fabricated and characterized a drug delivery device made of PCL by SLS. Methylene blue was chosen to be the drug. Experimental results indicated that the drug was evenly distributed in the fabricated device and was not affected by the sintering.

The addition of fillers into the polymer has often resulted in improved structural and functional properties of the component. Hence, processing of polymer composites by SLS and the preparation of polymer composite powders for SLS applications has increasingly become the focus of many studies [15, 16, 74-81]. Creasy et al [74]

investigated the densities and sintering characteristics of Nylon-6/clay nanocomposite powders. Commercially available pellets of neat Nylon-6 and Nylon-6/clay nanocomposites were cryogenically milled to produce powders suitable for use in the SLS process. Cryogenic milling produced powders with an irregular size, shape and a wide particle size distribution. The authors reported a lower sintering rate and a lower density for the sintered nanocomposite in comparison with the neat polymer. Higher temperature set-points were recommended for the nanocomposite powders during the SLS process. Mazzoli et al [78] prepared an aluminum-polyamide composite by SLS. The authors reported that the resulting parts had a good surface finish, high dimensional accuracy and high stiffness. Zheng et al [79] fabricated nano-Al_2O_3 polystyrene composites by SLS. The nanoparticles were coated with PS by emulsion polymerization. The authors reported an increase in tensile strength of up to 300 % and an increase in impact strength of up to 50 %. Chunze et al [80] prepared a Nylon-12/nanosilica composite powder by a dissolution-precipitation method. The nanoparticles were treated with a silane coupling agent prior to being dispersed in a Nylon-12/alcohol solution. The nanosilica was reported to have a heterogeneous nucleation effect on Nylon-12 and was found to be uniformly dispersed in the polymer matrix. The tensile properties and the impact strength of the SLS-processed nanocomposite were higher than that of the neat polymer. Chung et al [15] investigated the mechanical properties of a Nylon-11/silica nanocomposite manufactured by SLS. A composite powder prepared by a rotary tumbling method of the neat polymer powder and the nanosilica powder was used in the SLS process. The authors reported a non-linear variation in the mechanical properties as a function of the filler content. Moreover, the layer-by-layer manufacturing approach of

SLS was exploited by the authors to fabricate one-dimensional functionally graded components made from blends of Nylon 11 – glass beads as well as blends of Nylon-11/nanosilica powder [15, 16].

Metal and ceramic components have been fabricated using both direct SLS and indirect SLS. In indirect SLS, polymer-coated metal/ceramic powders are used in the SLS process. During the sintering process, the polymer melts and acts as a binder for the metal/ceramic particles to yield a green part. The polymeric binder is thermally decomposed to yield a brown part that is subsequently infiltrated with a molten metal. Liu et al [82] fabricated metal green parts by indirect SLS of iron-epoxy resin powder. They successfully subjected the green parts to decomposition, secondary sintering and infiltration by liquid bronze. Kruth et al [21] reviewed the SLS of metals and cermets. Evans et al [83] reviewed the fabrication of fully functional SiC by indirect SLS.

In recent years, SLS has been used for novel applications in the areas of microfabrication, microelectronics and electrically conductive polymer composites that are used in fuel cells. Ko et al [23-25] demonstrated the fabrication of organic field effect transistors with submicron resolution by SLS of inkjet printed metal nanoparticles. This is particularly useful for fabricating large area printed electronics at a low cost and high resolution. Clare et al [84] fabricated piezoelectric materials on silicon substrates by the SLS of Barium Titanate-polymer composite films. Chen et al [22] fabricated and tested a fuel cell collector by SLS of a graphite-phenolic polymer blend. The polymer was thermally decomposed and the resulting brown part was successfully infiltrated with a conducting epoxy resin. Computer simulations of the fuel cell performance were used to generate new designs of non-planar plates that maximized the surface area to volume

ratio as well as improved the packaging capability of individual plates into various products.

1.4 Motivation and Statement of Research

The study of ECPCs has mainly focused on evaluating the effects of the processing technique and the properties of the polymer and the conductive filler on the mechanical and electrical properties of the composite. A majority of the work has used melt mixing techniques to synthesize the ECPCs. However, melt mixing methods have several disadvantages as discussed earlier. Moreover, there is an inherent constraint on the geometry and architecture of the part that can be fabricated. Hence, the motivation of this dissertation is to investigate the processing of an ECPC using SLS. The ultimate goal of this research is to investigate the fundamental scientific and engineering aspects of processing electrically conductive polymer nanocomposites by selective laser sintering and establish the future capability of designing and fabricating functionally graded three-dimensional parts in such nanocomposite formulations. In this context, the three main research objectives of this study are to:

1. Investigate the processing of a polyamide 12-carbon black ECPC by SLS and to optimize the process parameters in order to maximize the flexural modulus and to subsequently evaluate and compare the mechanical properties, electrical properties and viscoelastic properties of the SLS produced parts with those made by a conventional process such as injection molding.
2. Develop physical models to explain the variation in the mechanical and electrical properties by studying the process-structure-property relationships.

3. Develop a coupled heat transfer and sintering model to estimate optimal SLS process parameters by studying the effect of carbon black on the thermal degradation of the polymer in the SLS process.

1.5 Dissertation Organization

Chapter 2 focuses on the use of SLS to manufacture polymer nanocomposites by incorporating carbon black into Nylon-12. A brief background of the characteristics of polymer powders that can be processed by SLS is provided. The method used to prepare the material for SLS processing is described. The SLS process parameters are optimized in order to maximize the flexural modulus of the resulting parts. The variation of the flexural modulus and porosity of the parts with respect to the process parameters and the characterization of the structure and morphology of the neat polymer and polymer nanocomposite are also reported.

Chapter 3 reports on the properties and characterization of the SLS-processed neat Nylon-12 and Nylon-12/carbon black nanocomposites. The optimized process parameters obtained in chapter 2 are used to fabricate specimens for evaluating the thermo-mechanical properties and the electrical conductivity. The thermo-mechanical properties and the electrical conductivity of the nanocomposites prepared by SLS are compared with those prepared by extrusion-injection molding. The characterization of the morphology and microstructure of the nanocomposites prepared by SLS and extrusion-injection molding is described. Finally, the relationship between the process, microstructure and properties is elucidated.

Chapter 4 describes a one-dimensional thermal model used for studying the variation in part density of SLS-processed neat Nylon-12 and Nylon-12/carbon black

nanocomposites with respect to the energy density of the laser beam. The effects of sintering induced densification and thermal degradation of the polymer are taken into consideration. The results of the model are compared with experimental results.

Chapter 5 revisits the research objectives of this doctoral dissertation and summarizes the key contributions of this work. The limitations of this work and avenues for future work are discussed.

CHAPTER 2 PROCESSING OF A CARBON BLACK-FILLED NYLON-12 NANOCOMPOSITE BY SELECTIVE LASER SINTERING

Selective laser sintering is a type of solid freeform fabrication technique that requires the feedstock material to be in a powder form. The controlled application of thermal energy results in the coalescence of the powder. SLS has been used to manufacture near-fully dense parts from powders that have porosities in the range of 50% - 60%. The porosity in SLS processed parts is strongly dependent on the process parameters such as the laser power, the laser scan speed, the laser scan spacing and various powder temperature set-points. SLS can be used to manufacture near-fully dense parts by varying the process parameters such that a fine balance between the two conflicting phenomena of sintering induced densification of the powder and thermally induced de-polymerization is achieved. Since porosity is known to have a deleterious effect on the modulus and strength of polymeric parts, the objective of maximizing the elastic modulus of SLS-processed polymer nanocomposites is closely related with the task of minimizing the porosity.

This chapter focuses on employing SLS to manufacture polymer nanocomposites by incorporating carbon black, an electrically conductive nano-material, into Nylon-12. A brief background of the characteristics of polymer powders that can be processed by SLS is provided. The SLS process parameters are optimized in order to maximize the flexural modulus of the resulting parts. The variation of the flexural modulus and porosity of the parts with respect to the process parameters and the characterization of the structure and morphology of the neat polymer and polymer nanocomposite are also reported.

2.1 Materials-Preparation and Processing

The SLS process has been used to process amorphous and semi-crystalline thermoplastic polymer powders. The nature of the SLS process places restrictions on the properties of the powder. The following sub-section provides a brief summary of the important factors that affect the processing of a polymeric powder by SLS.

2.1.1 Polymer powder properties

The SLS processing of a polymer involves low shear rates or near-zero shear rates. The main driving force behind particle densification is a reduction in surface energy. The SLS process is analogous to the conventional sintering process. Frenkel et al [85] developed one of the earliest models to describe the early stages of viscous sintering. Frenkel's model describes the growth of the inter-particle neck radius with respect to time as follows:

$$\left(\frac{x}{a}\right)^2 = \frac{3}{2\pi}\frac{\sigma}{a\eta}t \tag{2.1}$$

where x is the radius of the inter-particle neck, a is the particle radius, σ is the surface tension, η is the viscosity and t denotes time. A schematic of the model is shown below in Figure 2.1. In Frenkel's model, the relevant thermo-physical properties are the surface tension, viscosity and particle size. The model predicts an increased sintering rate for powders with higher surface tension and lower viscosity and particle size. A similar dependence on material properties (σ, η and, a) can be found in Pokluda's model that describes complete particle coalescence [86].

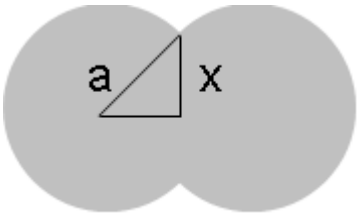

Figure 2.1 Schematic of neck formation during sintering of two particles.

The temperature dependence of viscosity is a significant factor in the SLS process and is dependent on whether the polymer is amorphous or semi-crystalline. Amorphous polymers experience only a gradual softening above the glass transition temperature rather than a sharp drop in the viscosity above the melting temperature like in the case of semi-crystalline polymers. This sharp drop in viscosity for semi-crystalline polymers can result in very low melt viscosities and can aid in near-complete coalescence of the powder. In contrast, the SLS processing of amorphous polymers usually results in porous parts.

The viscosity of polymers at low shear rates is known to be a strong function of their molecular weight [87]**.** The viscosity is known to be related to the molecular weight as follows:

$$\eta = k'\left(M_w\right)^{3.4} \tag{2.2}$$

The strong dependence on molecular weight indicates that for SLS applications, a low molecular weight is preferable. A low molecular weight polymer will have a low melt viscosity and thereby have superior sintering characteristics.

A further consideration relevant to the SLS process is the shape and size of the polymer particles. Since the layer thickness in SLS usually lies between 100 μm and 200 μm, powders no larger than 100 μm along with a narrow particle size distribution are

usually preferred. Moreover, powders with a regular near-spherical geometry are preferred due to surface finish considerations.

From the above discussion, it can be inferred that the thermo-physical properties of the polymer powder are very important for the SLS process. An appropriate choice of a polymer with high surface energy, low melt viscosity and small particle size is critical for fabricating near-fully dense parts.

2.1.2 Materials selection

In this study, Nylon-12 powder (Figure 2.2) with the trade name VESTOSINT® X 1553 white (Evonik Industries, Essen, Germany) was chosen since it is one of the few commercially available materials that possesses the requisite thermo-physical properties required for SLS-processing, as outlined in the previous section. It is a white, odorless, semicrystalline thermoplastic polymer (average particle diameter between 50 μm and 100 μm) having a low molecular weight and a melting temperature in the range of 176-184^{o}C [88]. The reinforcement employed in the study is nano-sized carbon black (KETJENBLACK EC-600 JD, Akzo Nobel Polymer Chemicals LLC). This highly structured carbon black has high electrical conductivity (in the range of 10 – 100 S/cm), high degree of porosity and surface area of 1250 m^2/g [89].

Carbon black is mainly composed of primary particles of carbon clustered together in *aciniform* morphology. The term *aciniform* refers to a “clustered like grapes” structure in which the primary particles are fused to each other via a chemical bond to form clusters of branched, irregular shapes. This *aciniform* structure is usually referred to as an aggregate in carbon black related literature. The aggregates of carbon black have a tendency to form loosely held agglomerates held together by weak Van der Waals and

electrostatic forces [90]. Carbon black in its nascent form is a fluffy powder primarily comprised of these loosely held agglomerates and is thereby difficult to handle and transport. Manufacturers usually resolve this issue by “pelletizing” the carbon black into beads of approximately 3-5 mm in diameter. The Ketjenblack is a high structure carbon black commercially available as pellets. A high structure carbon black has a less closed packing of primary particles and is generally easier to disperse than a comparable low structure carbon black. Prior to the blending of the carbon black and Nylon-12 for use in the SLS process, the commercially procured Ketjenblack pellets had to be broken down into either aggregates or much smaller agglomerates. The procedure that was adopted in this study is outlined below.

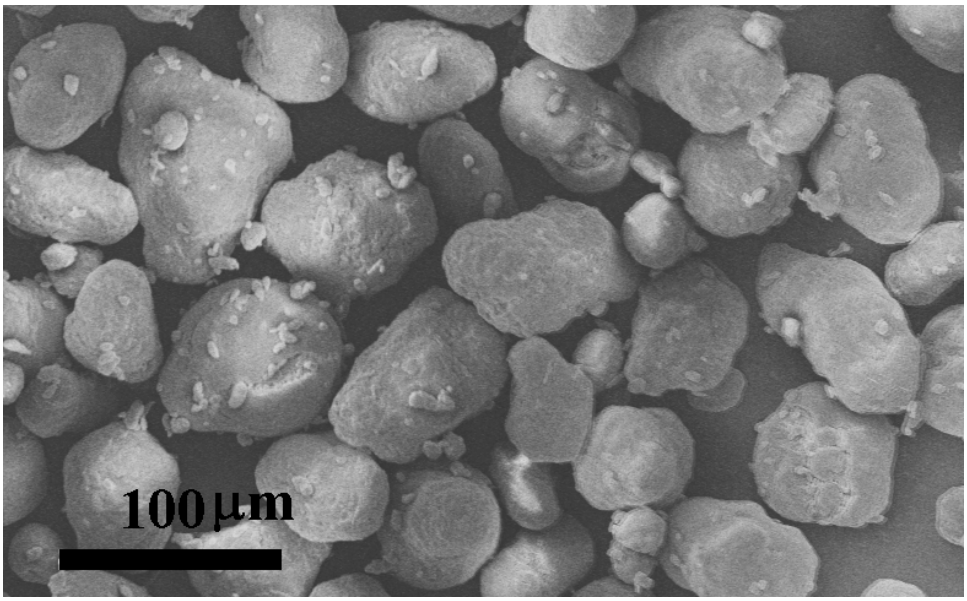

Figure 2.2 SEM image of VESTOSINT Nylon-12 powder

High wear-resistant zirconia grinding media (Glenmills Inc., Clifton, New Jersey, USA) having a diameter of 5 mm was used to ball-mill the carbon black pellets in a rotary tumbler (784 AVM, U.S. Stoneware, Ohio, USA) for 24 hours. The ball-milled

carbon black was sieved using a US standard 140 mesh sieve with 106 µm opening. A dilute suspension of the sieved, ball-milled carbon black in isopropyl alcohol was used for preparing samples for TEM imaging and is shown in Figure 2.3a. A SEM image of the sieved, ball-milled carbon black in a dry state is seen in Figure 2.3b**.**

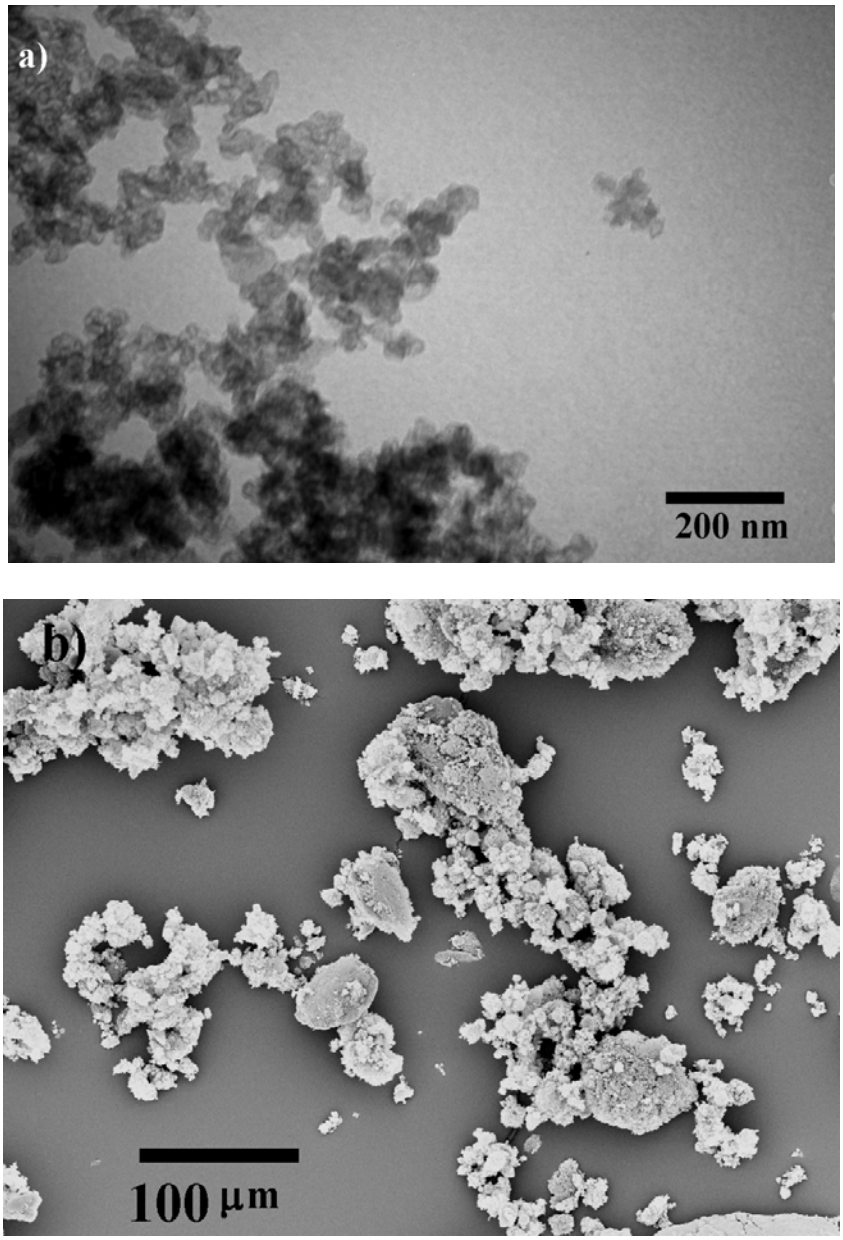

Figure 2.3 a) TEM image of primary particles and aggregates of carbon black and, b) SEM image of sieved, ball-milled carbon black in a dry, powdery state.

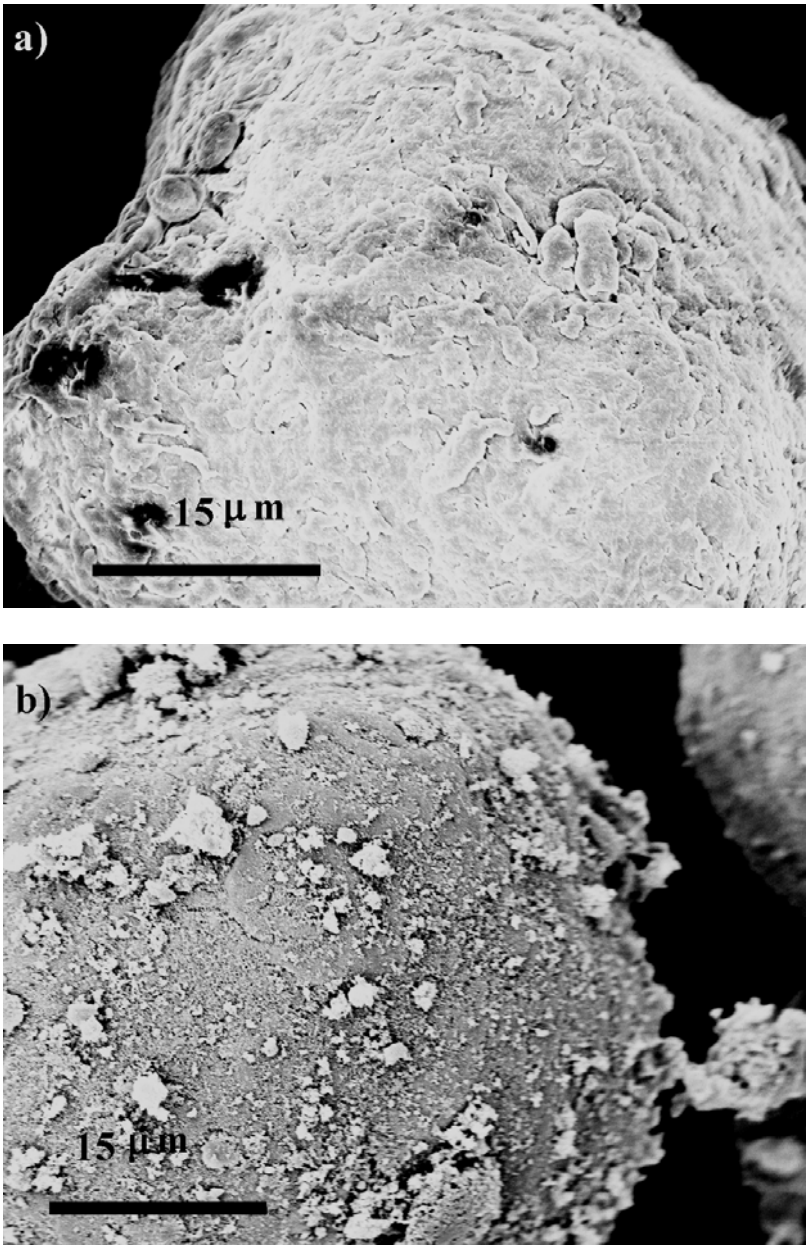

Figure 2.4 SEM images of a) Nylon-12 particle, and b) Carbon black coated Nylon-12 particle.

The sieved carbon black was then blended with the pure Nylon-12 powder in a rotary tumbler for 24 hours. In prior work by Kalaitzidou et al [91], a loading of 4 wt% of carbon black was shown to be sufficient to induce electrical conductivity in polymer composites, and was thus chosen as the nano-filler loading for this study. Carbon black was chosen due to its potential for nanoscale mechanical reinforcement and due to the

low aspect ratio and the size (1-10 μm as seen in Figure 2.4b) of its agglomerates, which makes it suitable for processing by SLS. A high magnification scanning electron microscope image of a Nylon-12 particle and a carbon black-coated Nylon-12 composite particle are shown in Figure 2.4a and Figure 2.4b, respectively. The pure Nylon-12 powder and the carbon black-coated Nylon-12 powder were processed in a Sinterstation® 2000 (3D Systems Inc., Rock Hill, South Carolina, USA) SLS machine. Henceforth in this chapter, the SLS processed pure Nylon-12 and the Nylon-12 carbon black composite will be referred to as the PA SLS and PA-4CB SLS systems respectively.

2.2 SLS Process Parameter Optimization

The supplied energy input and the part build orientation within the build platform influence the mechanical properties of parts fabricated using SLS. The energy input also known as the energy density is a function of the laser power, the laser scan speed, the laser scan spacing and is defined as follows:

$$\text{Energy density} = \frac{P}{S \cdot H} \tag{2.3}$$

where P is the laser power, S is the laser scan speed and H is the laser scan spacing. The other important parameters that affect the quality and microstructure of a part manufactured through SLS are the part-side temperature set-point (which defines the surface temperature of the powder bed scanned by the laser beam), the powder feed temperature set-point (which defines the surface temperature of the powder in the supply bins), the powder layer thickness and the roller speed.

For parts with a simple geometry, the part build orientation may be defined as the orientation of the long axis of the part with respect to the direction of movement of the roller. Parts fabricated using the same process parameters but having a different build orientation have been shown to have different mechanical properties [92]. In order to maintain consistency, in this study, all parts were oriented parallel to the direction of the movement of the roller.

In this dissertation, only the laser power and the laser scan speed were varied at discrete intervals. The laser scan spacing was set at 152.4 μm (6 mils) since this value corresponds to a beam overlap factor (beam diameter divided by the scan spacing) of around 3 and has been used in earlier studies to process polymer composites at low loading levels [15, 16] .

SLS is a manufacturing process that involves fusing layers of powders using a laser beam. The thermal conditions such as temperature set-points and temperature gradients have a significant effect on the final properties of parts fabricated via SLS. The processing of a neat polymer by SLS constitutes homologous wetting and involves the spreading of a thin layer of polymer melt over a previously formed layer of the same material. The thin layer of polymer melt spreads over the previously formed layer until the solidification process is complete. The angle of contact that the newly formed layer forms over the previously formed substrate has been shown to be directly proportional to the square root of the Stefan number [93]. In the context of SLS, it is beneficial to have as low an angle of contact as possible. Since the Stefan number is directly proportional to the temperature difference of the two phases, maintaining a substrate temperature (part-side temperature set point) as close to the melting temperature as possible would ensure a

low angle of contact would be achieved. Maintaining a high temperature set-point also minimizes the rate of solidification of the newly formed layer of polymer melt. A slow cooling rate allows the polymer to flow for a greater duration of time and thereby more effectively reduce any residual stresses that might develop during the sintering process. A high temperature set-point minimizes the thermal gradients around the sintered region and reduces the out-of-plane curling and distortion. However, an excessively high temperature set-point results in significant caking of unused powder at the end of the SLS process.

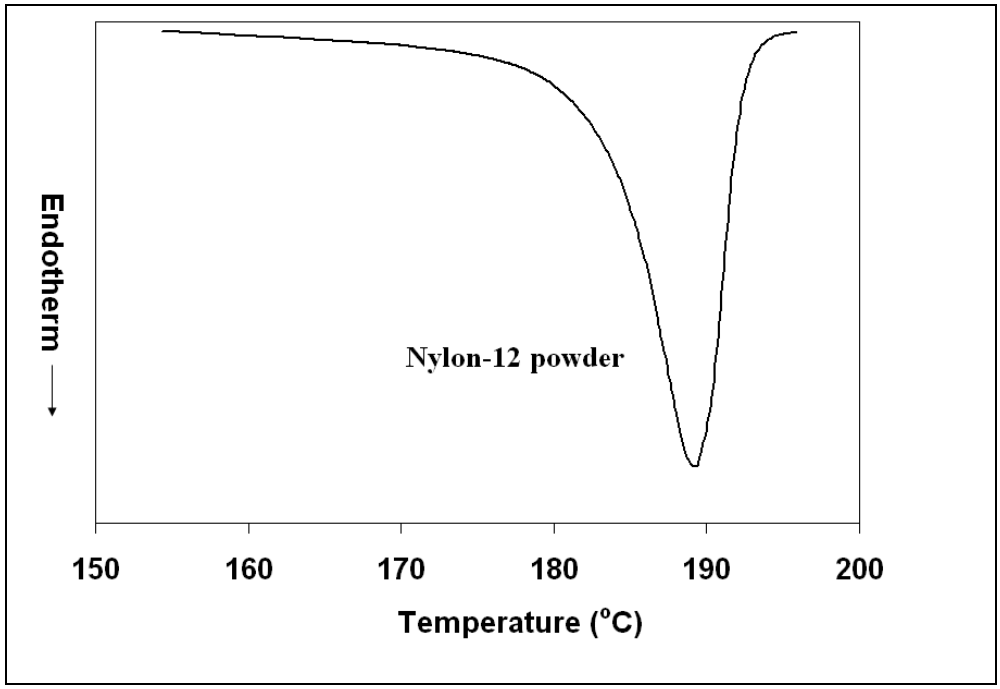

Figure 2.5 Melting endotherm of the Nylon-12 powder used in this study.

Prior to determining the part-side temperature set-point in SLS, the melting characteristics of the polymer powder have to be ascertained. The melting behavior of the Nylon-12 powder used in this study is shown in Figure 2.5. The melting endotherm

experiences a change in slope at approximately 172^{o}C. A part side temperature set-point greater than 172^{o}C resulted in significant caking of the unused powder. Hence, in this study, a part side temperature set-point of 172^{o}C was chosen for processing neat Nylon-12 powder. In the case of the Nylon-12 carbon black nanocomposite, visual inspection suggested minimal caking of powder until a set-point of 174^{o}C. This can probably be explained by the fact that the addition of fillers to a polymer results in lowering the rate of sintering.

Similar to the part-side temperature set-point, if the powder feed temperature set-point was too high, the roller was not able to deliver the powder across the entire build area. Lowering the temperature set-points below a critical value resulted in curling of the sintered region. It is important to note that the temperature setpoints were not experimentally calibrated in this study. The Nylon-carbon black composite powder was much darker than the neat Nylon powder and is likely to have had a different emissivity which in turn would have affected the pyrometer reading in the Sinterstation® 2000 machine. Hence, the temperature setpoints are only meant to serve the purpose of an input parameter. Powder layer thickness was chosen to be 101.6 μm (4 mils) since the average size of the polymer particles is less than 100 μm. The roller speed was set at 0.0762 m/s (3 in/s), the lowest allowable value on the Sinterstation® 2000 machine, to ensure that the powder was uniformly spread across the entire build area.

Table 2.1 Summary of process parameters investigated for processing Nylon-12 (PA SLS) and Nylon-12 –carbon black (PA-4CB SLS) composite powders

Process parameter	PA SLS	PA-4CB SLS
Laser power	3W-7W (intervals of 1W)	3W-7W (intervals of 1W)
Laser scan speed	0.762 m/s – 1.524 m/s (intervals of 0.254 m/s)	0.762 m/s – 1.524 m/s (intervals of 0.254 m/s)
Laser scan spacing	152.4 μm	152.4 μm
Part-side temperature set-point	172^{o}C	174^{o}C
Powder feed temperature set-point	80^{o}C	80^{o}C
Roller speed	0.0762 m/s (3 in/s)	0.0762 m/s (3 in/s)
Powder layer thickness	101.6 μm	101.6μm

The range of parameters investigated for the polymer powder and the composite powder are summarized in Table 2.1. The laser power was varied from 3W to 7W (in intervals of 1W) and the laser scan speed was varied between 0.762 m/s and 1.542 m/s (30 in/s to 60 in/s) in intervals of 0.254 m/s (10 in/s). The aim of undergoing this exercise was to explore a wide range of laser powers and scan speeds and to identify the combinations that yielded the highest flexural modulus. Specimens made with combinations of laser powers and scan speeds as mentioned above were fabricated and subjected to flexural testing. The combinations that yielded specimens with the highest flexural modulus were used as a starting point for subsequent refinement of the parameters. It should be noted that the values of laser power listed above are machine setpoints. The actual laser power

available within the machine differs from the setpoints A Molectron laser power meter (Coherent, Santa Clara, California, USA) was used to calibrate the laser setpoints. A map of setpoints to the actual measured power is shown in Table 2.2.

Table 2.2 Mapping of laser power setpoint to measured laser power

Laser power setpoint (W)	Measured laser power (W)
3	3.08
4	3.80
5	4.30
6	4.85
7	5.40

2.3 Characterization Techniques

The flexural properties of the composites were characterized using a UTS testing machine as per ASTM D790 (three point bend test) at a test speed of 0.05 in/min. Fracture surfaces of the neat polymer and the composite obtained by Izod impact testing were used to study the morphology with a Zeiss Ultra 60 (Carl Zeiss, Oberkochen, Germany) scanning electron microscope (SEM) at an accelerating voltage of 5 kV- 20 kV. The crystallinity characteristics of the neat polymer and composite were assessed through the X-ray diffraction patterns obtained using a X'Pert Pro Alpha 1 diffractometer (PANalytical, Almelo, Netherlands) in the Bragg-Brentano geometry using a monochromatic, filtered Cu Kα1 radiation. X-ray photoelectron spectroscopy was performed using a SSX-100 system (Surface Science Laboratories, Mountain View, CA) with a spot size of 400 μm. A Seiko 220 differential scanning calorimeter (Seiko

Instruments, Chiba, Japan) was used to measure the melting temperature and the heat of fusion. Samples weighing 5-10 mg were heated at 5^{o}C/min to obtain the melting curves.

The porosity of the composites made by SLS was determined using a method developed previously and reported elsewhere [66]. Each of the flexure test coupons was cleaved parallel to the build direction using a single-edged razor blade. A black colored wax was applied on the surface of the cleaved Nylon-12 parts. The wax remained in the void spaces when the excess was wiped off providing an increased contrast when viewed under an optical microscope. In the case of the cleaved PA-4CB SLS parts, the pores were clearly distinguishable under an optical microscope and hence there was no need to treat the cleaved surface. Fifty photomicrographs were taken across the thickness of each test specimen using a Leica optical microscope and analyzed using ImageJ [94] image analysis software. A thresholding operation was performed on each image prior to calculation of the area fraction of the pores using the "analyze particles" function in ImageJ. It is important to note that this sample preparation technique may induce artifacts on the sample and cannot account for porosity arising due to agglomeration of nanoparticles. Hence, it can be used to obtain only a rough estimate of the porosity of polymer nanocomposites.

2.4 Results and Discussion

2.4.1 Dependence of Flexural Modulus on Energy Density

The flexural modulus of composites made by the combinations of laser powers and scan speeds listed in Table 2.1 is shown in Figure 2.6. In the case of the PA SLS system, a maximum flexural modulus of approximately 1750 MPa was achieved

using a laser power of 3.08W and scan speed of 0.762 m/s. In the case of the PA-4CB SLS system, a maximum flexural modulus of only 1450 MPa was achieved using the combinations of laser power and scan speed as follows: (3.8W, 0.762 m/s), (4.85W, 1.016 m/s), (5.4W, 0.762 m/s) and (5.4W, 1.016 m/s). Most of the other combinations of laser power and scan speed yielded a flexural modulus lower than 1450 MPa. The combination of (3.8W, 0.762 m/s) was chosen as the "optimum" parameter set as opposed to the other combinations mentioned above because higher laser powers resulted in significant secondary sintering and poor dimensional accuracy of the parts.

Similar results have been obtained for low loading of nanosilica powder in nylon 11/nanosilica nanocomposites prepared by SLS [15]. The modulus of nanocomposites is not a simple function of the volume fraction of the filler as is the case in conventional micro-composites. Rather, it also depends on the degree of crystallinity, the spherulite size, the lamella thickness, the crystalline long range order, the properties of the filler, and the state of dispersion and distribution of the filler in the composite [95]. The melting endotherms of the PA SLS and PA-4CB SLS systems as obtained through DSC are shown in Figure 2.7. Both systems have two melting peaks at approximately 181^{o}C and 189^{o}C. The peak at 189^{o}C corresponds to the melting peak of the powder (189.4^{o}C). This indicates that a certain portion of the original powder particles does not melt during SLS processing and is retained in its original form in the final part. Similar results have been reported in earlier studies [96].

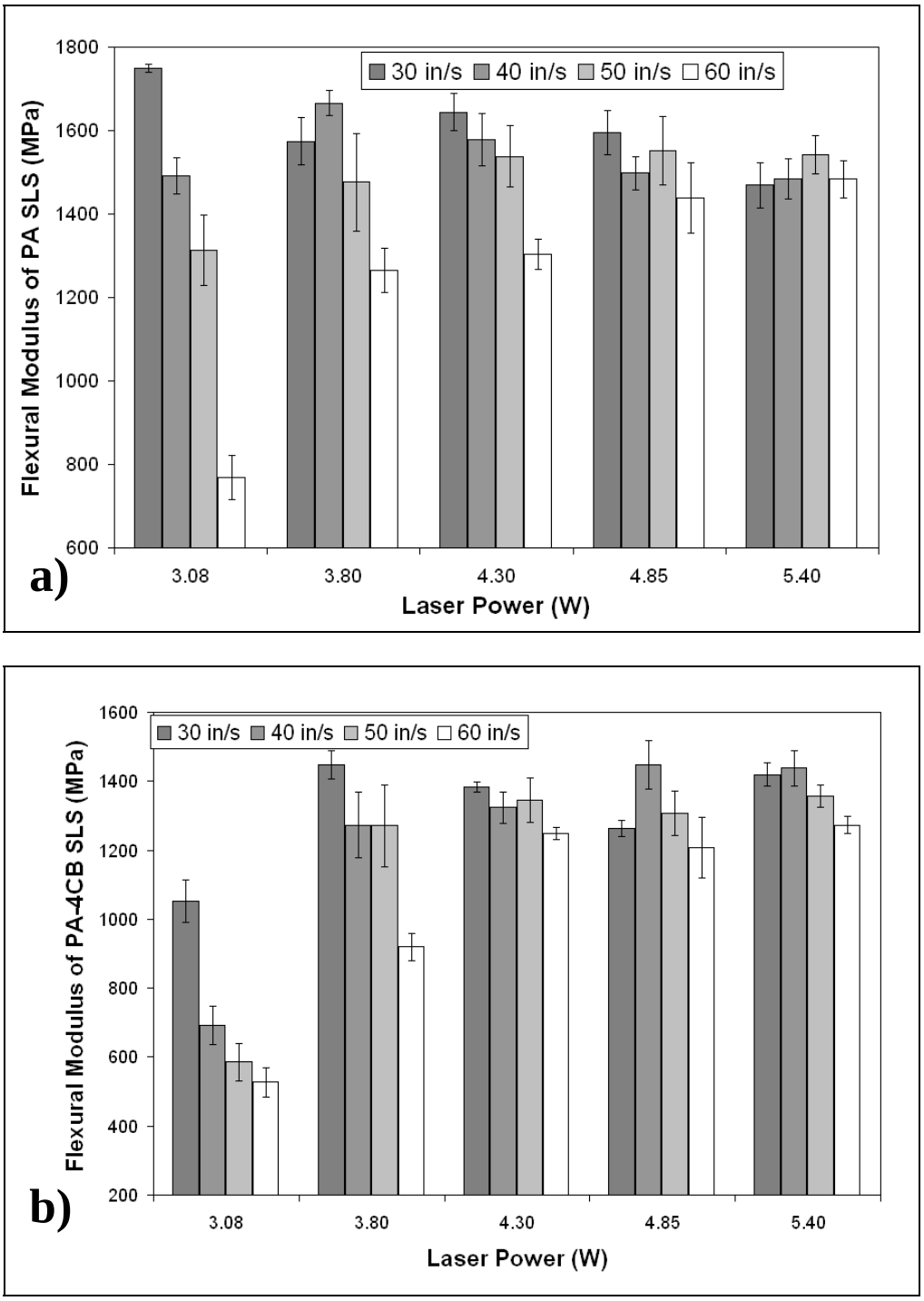

Figure 2.6 Variation of flexural modulus with respect to measured laser power and scan speed for a) PA SLS, and b) PA-4CB SLS.

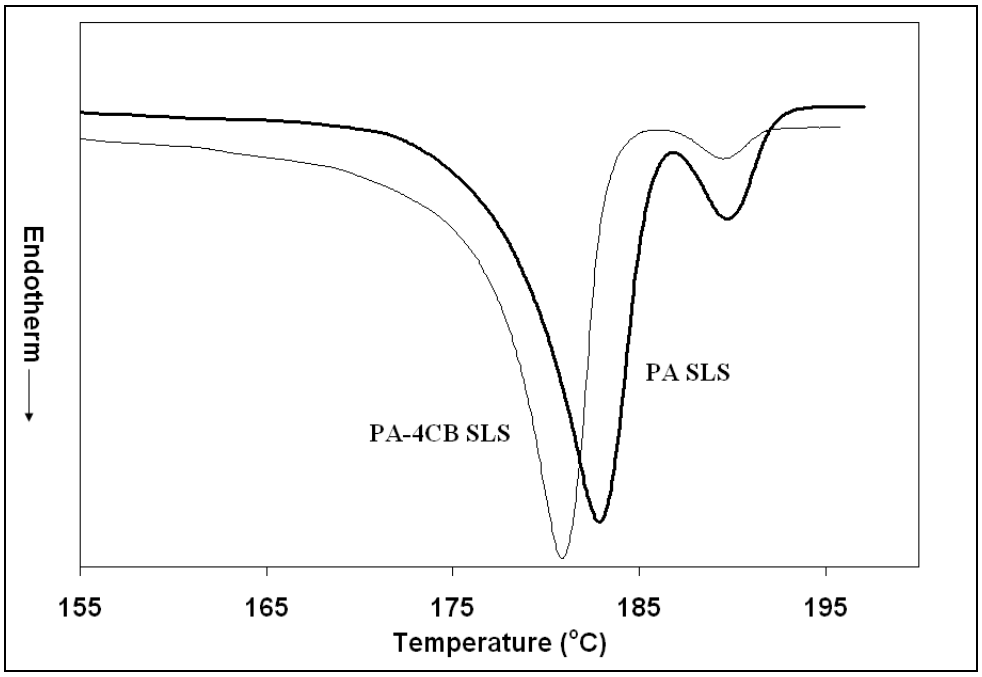

Figure 2.7 Melting endotherms of PA SLS and PA-4CB SLS systems obtained by DSC.

Polarized optical microscopy images of Nylon-12 processed by SLS indicated the presence of unmelted particle cores [97]. The presence of incompletely melted particles can also be inferred from the XRD patterns as shown in Figure 2.8. The presence of a small "bulge" towards the right side of the peaks corresponds to the crystallites that remain unmelted and are retained in the final part. The "bulge" is more prominent in the case of the XRD peak of PA SLS. This observation is also reflected as a larger melting peak for PA SLS at around 189^{o}C as compared to that of PA-4CB SLS (Figure 2.7). The melting endotherms and XRD patterns also indicate that there is no significant difference in the degree of crystallinity (calculated from the area under the DSC melting endotherm) or the crystalline lamellae thickness (calculated from the full width at half maximum from the XRD patterns).

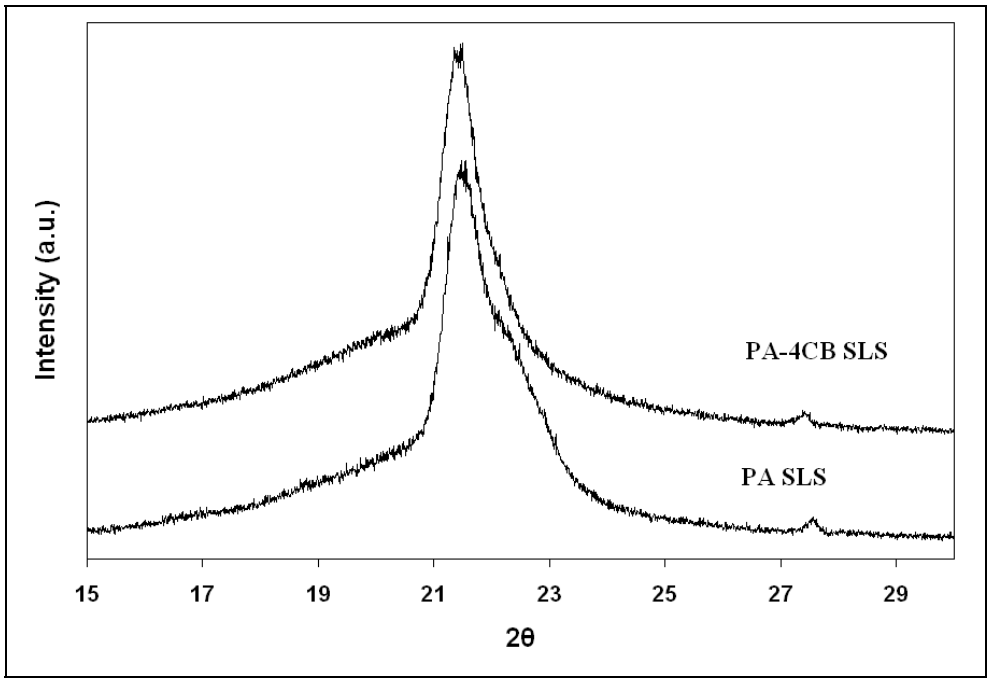

Figure 2.8 XRD patterns of PA SLS and PA-4CB SLS systems.

A possible explanation for the reduction in flexural modulus could lie in the state of dispersion of the carbon black in the composite. SEM images of the fracture surfaces of the PA SLS and PA-4CB SLS systems (processed using the optimal parameter sets) are shown in Figure 2.9a and Figure 2.9b respectively. A highly segregated structure in the PA-4CB SLS system is evident in Figure 2.9b. The bright areas in Figure 2.9b correspond to carbon black-rich regions in the PA-4CB SLS system. It is similar to the microstructures found in sintered [98] and compression molded [99] polymer-carbon black composites. A highly segregated structure has lesser area of contact between the polymer and the reinforcing agent as compared to a structure with uniformly dispersed carbon black. A more comprehensive analysis of the reasons behind the reduction in flexural modulus is presented in chapter 3.

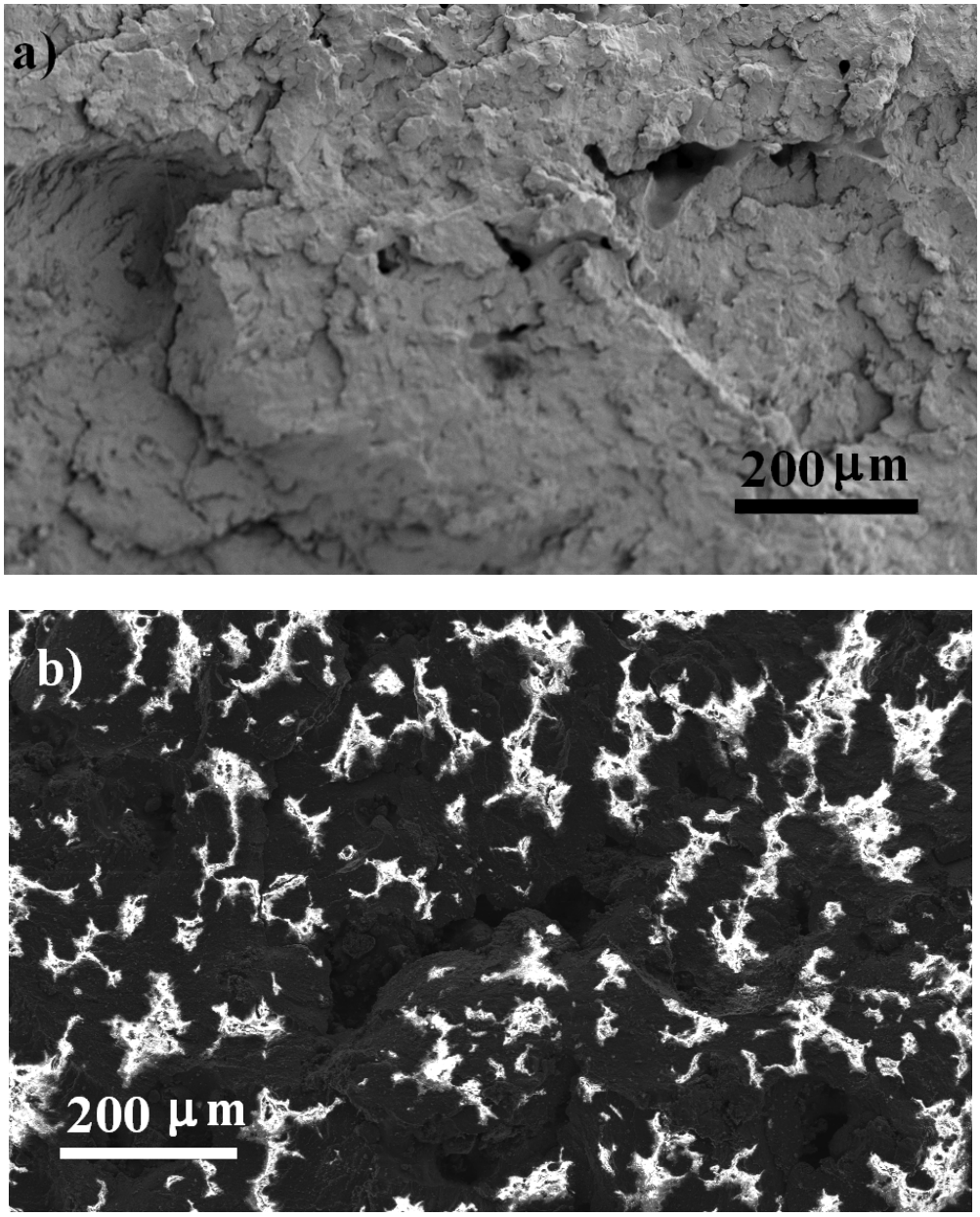

Figure 2.9 SEM images of fracture surfaces of a) PA SLS, and b) PA-4CB SLS.

2.4.2 Dependence of Porosity on Energy Density

The porous nature of parts produced by SLS has been shown to affect their mechanical properties [12]. Porosity in parts produced by SLS can occur due to at least two reasons. First, the application of thermal and laser energy leads to particle coalescence in the

scanned areas of the powder bed. Inadequate energy levels and time scales leads to incomplete particle densification and can be inferred from SEM images of fracture surfaces of impact tested specimens as seen in Figure 2.10. Second, excessive laser energy levels can result in extremely high temperatures which can lead to polymer pyrolysis, which manifests itself in the form of porosity. The addition of carbon black to the polymer can further aggravate this phenomenon due to strong absorption of CO_2 laser radiation and consequent localized heating [100].

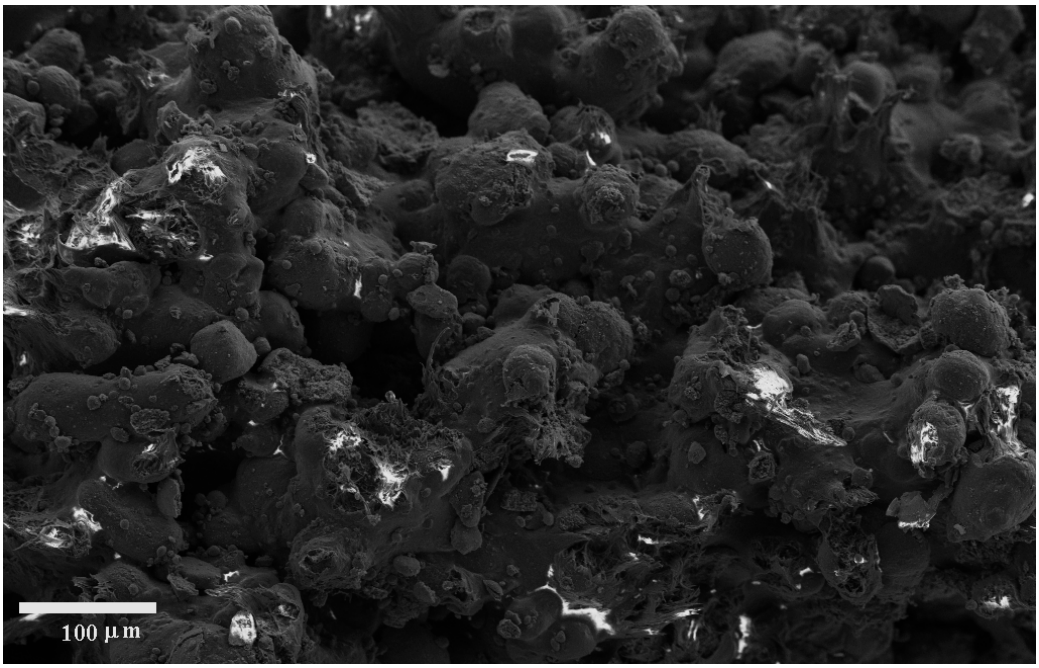

Figure 2.10 SEM image of the fracture surface of impact tested PA-4CB SLS specimen processed using a laser power of 3.08W and a laser scan speed of 1.524 m/s. Inadequate energy levels resulted in incomplete densification of the polymer inferred from the presence of polymer particles on the fracture surface and reduced levels of carbon black-rich regions.

The phenomena of laser-induced densification and laser induced degradation of the polymer occur concurrently. However, the relative significance of each phenomenon varies with energy density. Figure 2.11 illustrates the typical variation of porosity with

respect to energy density of neat polymeric parts processed by SLS. Increasing energy density initially results in greater polymer densification and consequently lower porosity. However, beyond a certain critical energy density, thermal degradation of the polymer begins to play a dominating role and is reflected in higher porosities.

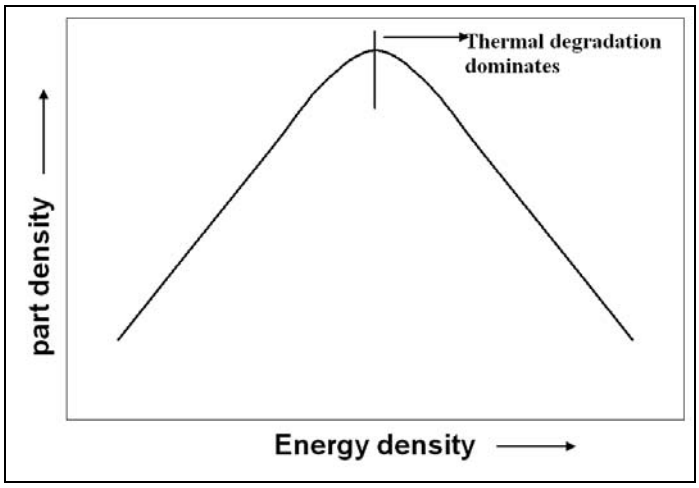

Figure 2.11 Typical variation of part density with energy density for neat polymers processed by SLS.

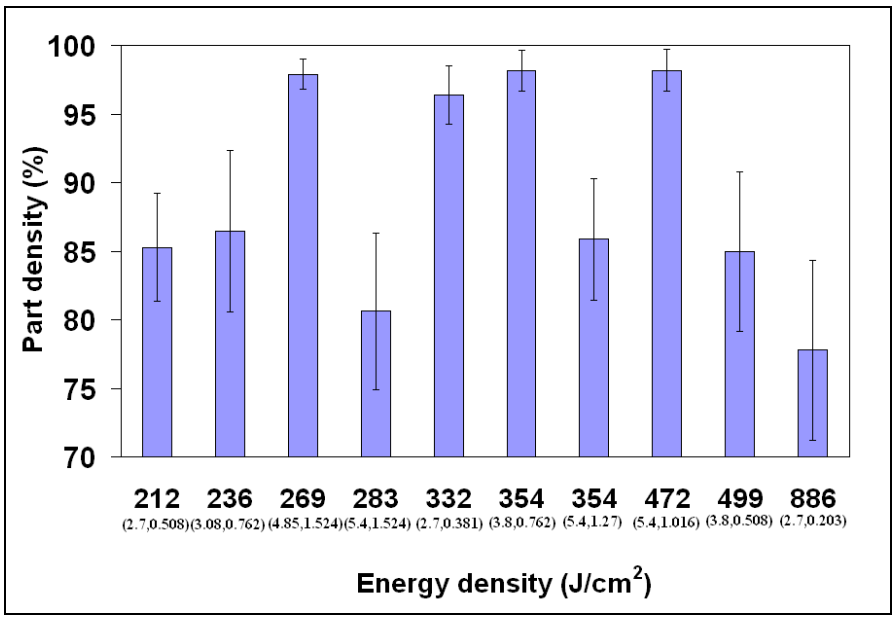

Figure 2.12Variation of part density of PA-4CB SLS system with respect to energy density. The label (within brackets) for each bar on the x-axis denotes measured laser power in watts, laser scan speed in m/sec.

Since one of the aims of this study is to identify the SLS process parameters that produce parts with the maximum flexural modulus, it is important to produce parts that are fully dense or as close to fully dense as possible. The porosity of PA-4CB SLS parts fabricated using some of the process parameters mentioned in Table 2.1 was investigated by the procedure described in section 2.3 and is summarized in Figure 2.12.In contrast with neat polymers, the part density of the PA-4CB SLS system does not entirely depend on the energy density. Parts fabricated using the same energy density but with higher laser powers (and consequently higher laser scan speeds) have significantly lower part density. This could be probably due to a stronger dependence of carbon black-induced localized heating on the laser power than on the energy density. This phenomenon is studied in more detail in chapter 4. In the case of the PA SLS system, parts made only by the optimal parameter set were analyzed from a porosity standpoint. The optimal parameter set for the PA SLS system (3.08W, 0.762 m/sec) and the PA-4CB SLS system (3.8W, 0.762 m/sec) produced parts with an average porosity of 3% (97% dense) and 4% (96% dense), respectively. The addition of fillers to polymers has experimentally been shown to reduce the sintering rate [101]. This explains the fact the energy density corresponding to the optimal parameter set for the PA-4CB SLS system is higher than that of the PA SLS system as more energy is required to achieve the same degree of densification. Representative optical micrographs that were used for porosity calculations are shown in Figure 2.13.

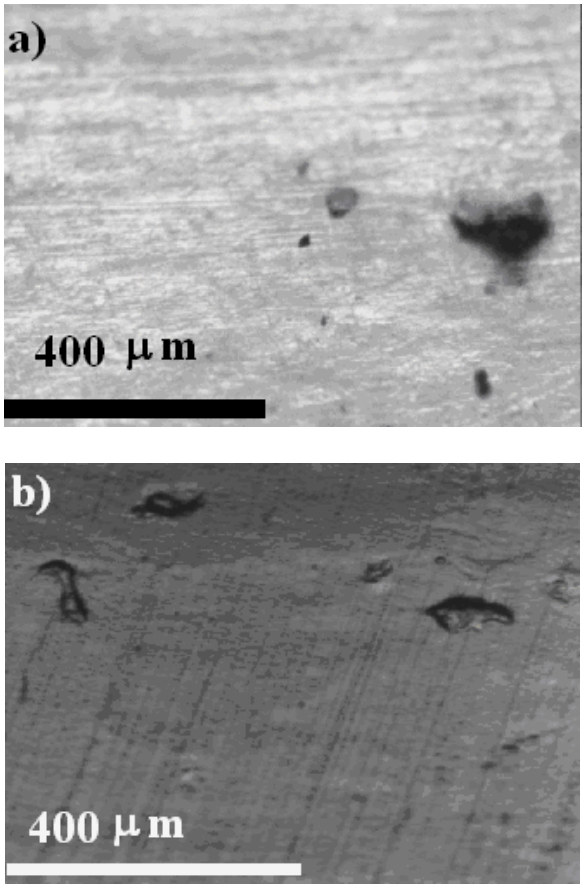

Figure 2.13 Optical micrographs used for porosity measurements of a) PA SLS, and b) PA-CB SLS.

2.4.3 Laser Absorption Behavior of the Composite

The absorption of the CO_2 laser by the Nylon-12 – carbon black material system during the SLS process resulted in the emission of visible radiation (Figure 2.14) from scanned regions of the powder bed, typically lasting for only a few seconds. A similar phenomenon has been reported in another study [102], wherein the authors irradiated carbon nanoparticles and measured the emission spectrum. Strong absorption was reported over a broad range of wavelengths. Poor conduction between the nanoparticles

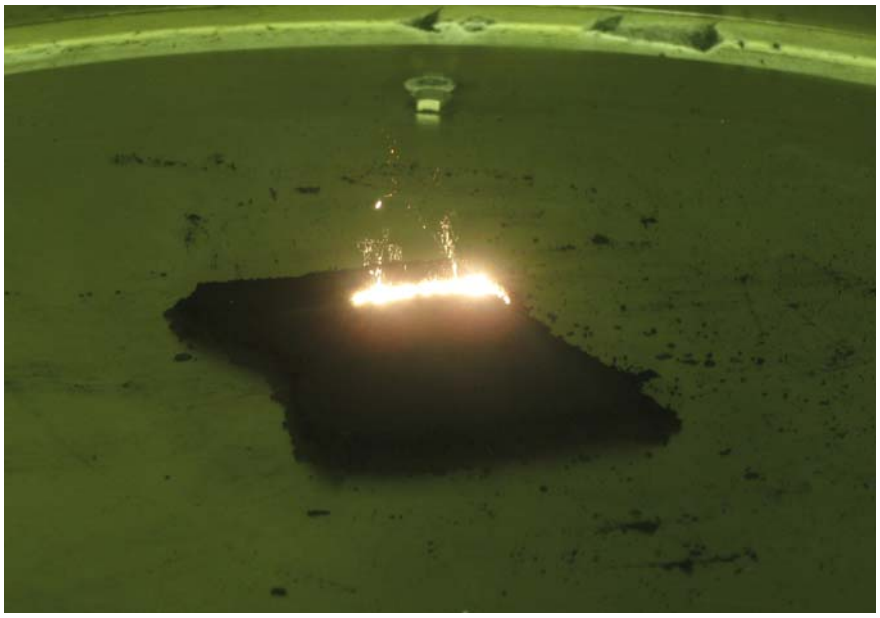

Figure 2.14 Visible radiation emitted during irradiation of carbon black by the CO_2 laser.

resulted in temperatures in excess of 3500^{o}C. It was concluded that the emitted radiation comprised primarily of blackbody radiation. The high local temperature was cited as a reason for phase transformations, evaporation and oxidation of the carbon. It has been shown that the crystalline content (graphitic content) and functional groups present on the surface of carbon nanoparticles have significant effects on the electrical conductivity of the composites. Since one of the aims of this dissertation is to investigate the electrical conductivity of carbon black-based polymer nanocomposites, a study of any possible changes to the morphology or surface chemistry of the carbon black was important. **X**-ray diffraction was used to detect changes in the graphitic content of the carbon black as a consequence of exposure to the laser.

The sieved and ball-milled carbon black (as described in section 2.1) was evenly spread (100 μm thickness) on the build platform of the Sinterstation and irradiated by the laser (3.8W, 0.762 m/s, 174^{o}C) and is shown in Figure 2.14. The position of the peak and

the area under the curve corresponding to the 002 graphitic planes (d-spacing of 0.37 nm) of irradiated and virgin carbon black were compared and are shown in Figure 2.15. No significant difference in either the position of the peak or the area under the curve was observed indicating no observable changes in the graphitic content of the carbon black as a result of laser irradiation. Moreover, XPS analysis of virgin carbon black and laser irradiated carbon black indicate no changes in the surface chemistry (Figure 2.16). The virgin carbon black and laser irradiated carbon black exhibit only one peak at approximately 285 eV which corresponds to the carbon 1s electron. A peak at approximately 532 eV corresponding to the oxygen 1s electron is not detected. This observation is significant because the presence of oxygen containing functional groups on the surface of carbon black is known to reduce its electrical conductivity [103].

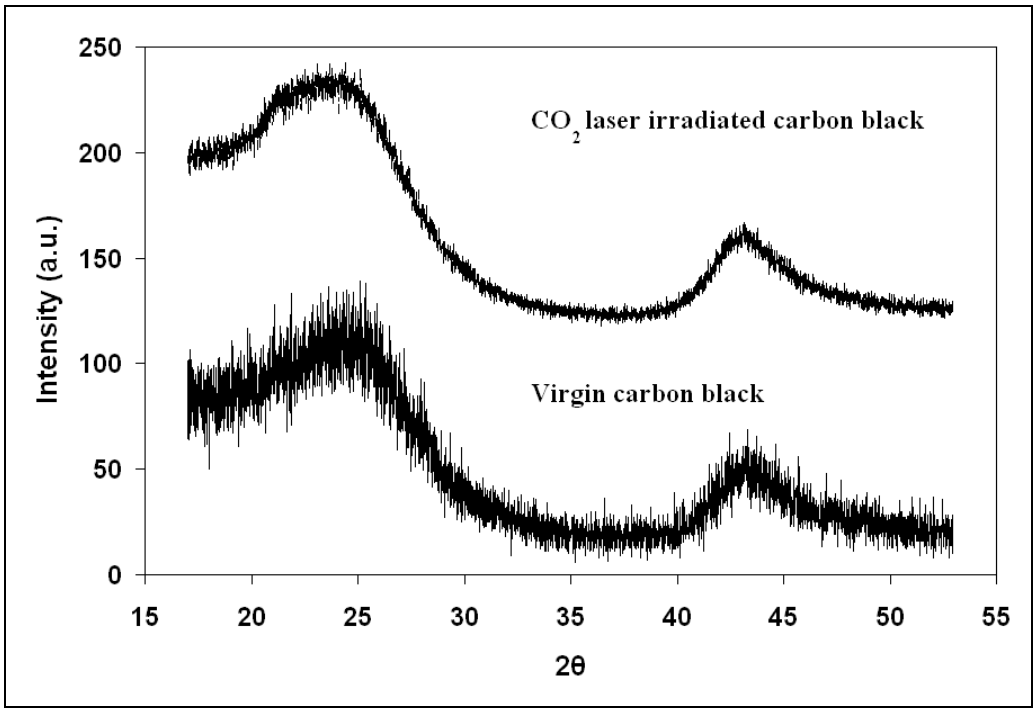

Figure 2.15 XRD patterns of virgin carbon black and irradiated carbon black.

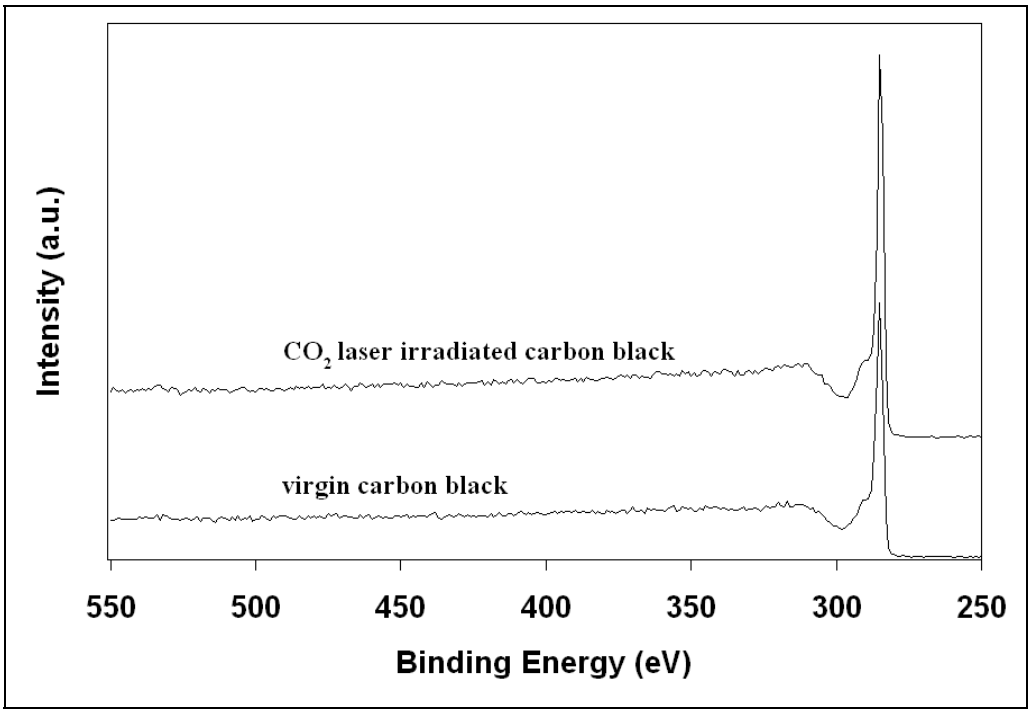

Figure 2.16 X-ray photoelectron spectrums of virgin carbon black and CO_2 laser irradiated carbon black.

The high absorption coefficient of carbon black has been used for selective laser sintering of high temperature resistant polymers [100] such as polyetherketone (PEK) and polyetheretherketone (PEEK) by blending small quantities of carbon black (0.03 wt. % to 0.1 wt. %) with the polymer. In this study, the addition of carbon black significantly enhanced the absorption behavior and facilitated laser sintering at ambient temperatures. In our study, visual inspection seemed to indicate that the intensity of the emitted visible radiation increased with laser power even while maintaining the same level of energy density. This observation is consistent with the results of earlier studies which have reported a non-linear dependence between the energy density of the laser, the intensity of the emitted radiation and the temperature of carbon nanoparticles [104, 105]. Hence, SLS experiments of the PA-4CB system were conducted at lower laser powers and scan speeds, thereby maintaining the energy densities corresponding to the optimal parameter

set (3W, 0.762 m/sec). The purpose of performing these experiments was to investigate if a lower laser power resulted in a lower porosity in these parts. Two additional parameter sets were used (2W, 0.381 m/sec and 1W, 0.203 m/sec). These parameters yielded composites with porosities comparable to those made with the optimal parameter set. However, the length scale of the porosity that might occur due to carbon black-induced degradation could be beyond the limits of the sample preparation technique being used in this study. Gas-based pycnometry is a technique that can be used to get a more accurate estimate of the porosity. Additionally, molecular weight analysis using gel permeation chromatography (GPC) could also be used to study carbon black-induced degradation of the polymer. Results from pycnometry and GPC studies are discussed in chapter 3.

2.5 Conclusions

A carbon black-filled Nylon-12 nanocomposite was successfully processed through SLS. Strong visible radiation was emitted from irradiated regions of the composite powder bed which is likely due to localized heating of the powder bed. The process parameters, namely the laser power and scan speed were optimized in order to maximize the flexural modulus. The variation in part density with respect to energy density was investigated. In the case of the neat polymer, a maximum flexural modulus of approximately 1750 MPa was achieved using a laser power of 3.08W and scan speed of 0.762 m/s and the parts were 97% dense. In the case of the nanocomposite, a maximum flexural modulus of 1450 MPa was achieved using a laser power of 3.8W and a scan speed of 0.762 m/s and the parts were 96% dense. Thermal and XRD analyses indicated that the crystallization characteristics of the polymer upon addition of the carbon black were not significantly altered. This indicates that the loss in mechanical properties upon

addition of carbon black to Nylon-12 is likely due to a weak polymer-filler interface and due to the presence of a segregated microstructure rather than differences in the crystalline morphology between the neat polymer and the nanocomposite.

CHAPTER 3 PROPERTIES OF CARBON BLACK-FILLED NYLON-12 NANOCOMPOSITES PROCESSED BY SELECTIVE LASER SINTERING AND COMPARISON WITH EXTRUSION-INJECTION MOLDING

The manufacturing technique and the processing conditions have a significant effect on the macroscopic properties of polymer nanocomposites. Unlike conventional micro-composites, the production of nanocomposites is system dependent. Hence, from a scientific and technical perspective, the study of the thermodynamics of polymer-filler interactions, filler dispersion, and the distribution is crucial. The manufacturing process greatly affects the degree of dispersion and distribution of the nano-filler in the polymer matrix, which in turn is known to be an important factor in deciding the mechanical properties of polymer nanocomposites. In the case of electrically conductive fillers, the manufacturing process has a significant effect on the percolation threshold and electrical conductivity of the composites since it can alter the orientation, dispersion, inter-particle spacing, and the filler's aspect ratio within the polymer matrix.

This chapter focuses on the effects of SLS on the microstructure and properties of a carbon black-reinforced Nylon-12 nanocomposite. This chapter also presents a comparative study of the thermo-mechanical properties and the electrical conductivity of a carbon black-reinforced Nylon-12 nanocomposite made by extrusion-injection molding, a conventional manufacturing process that was chosen mainly because of its widespread use in the polymer processing industry.

3.1 Materials and Methods

3.1.1 Materials

A blend of Nylon-12-carbon black (4 wt. %) as described in Section 2.1.2 was used for processing by SLS and extrusion-injection molding. The composite powder was not subjected to any drying procedure prior to processing. A drying procedure is particularly useful for processing polyamides due to their tendency to suffer hydrolytic degradation. However, the time scales involved in the multiple stages of the entire SLS process would make any drying procedure unfeasible. Hence, in order to mitigate any possible concerns regarding hydrolytic degradation, the powders were always stored in air-tight containers.

3.1.2 Selective Laser Sintering

The optimized process parameters as outlined in Section 2.4.1 and Table 2.1were used for fabricating test specimens in order to characterize the thermo-mechanical properties and electrical conductivity of the PA SLS and PA-4CB SLS systems.

3.1.3 Extrusion-Injection Molding

A DSM Micro 15cc Compounder (Xplore, Barrington, Illinois, USA), (vertical, co-rotating twin-screw microextruder) was employed for melt-mixing. A mixing time of 3 minutes, a screw speed of 200 rpm and a barrel temperature and feed temperature set-point of 190^{o}C were employed. A Daca micro-injector (DACA Instrumenets, Santa Barbara, California, USA) with a cylinder temperature of 190^{o}C, mold temperature of 90^{o}C and injection pressure of 110 psi was used for molding the plastic specimens. It is noted that the DSM equipment used is sufficient for screening experiments but has

limitations when attempting to relate this to a large-scale extrusion-injection molding system. For instance, the maximum allowable packing pressure during injection molding is 80psi, which is much lower than the pressure normally used in large injection molding systems. This might limit the final properties of polymers and polymer composites processed using this equipment.

Table 3.1 Notation and description of the samples used in the study

Sample ID	Description
1. PA Ex-IM	Pure nylon 12 (PA) sample made by extrusion and injection molding
2. PA-4CB Ex-IM	PA and 4wt% carbon black (CB) composite powder prepared by rotary tumbling, processed by extrusion/injection molding
3.PA-4CB Ex-IM (melt mixing)	CB pellets were directly mixed with PA in the extruder
4. PA-4CB Ex-IM (LE)	Ball milled, laser irradiated CB mixed with PA in the extruder
5. PA SLS	Neat PA processed by SLS
6. PA-4CB SLS	PA and 4wt% CB composite powder prepared by rotary tumbling, processed by SLS

Three compounding methods were investigated for producing nanocomposites by extrusion-injection molding. The motivation behind investigating the different compounding methods was to verify that the results truly reflect the differences between SLS and extrusion and are not masked by possible compounding effects. The three versions of compounding investigated were: i) composite powder prepared by rotary tumbling was fed into the extruder (PA-4CB Ex-IM); ii) carbon black pellets melt-mixed

directly with the Nylon-12 powder in the extruder (PA-4CB Ex-IM (melt mixing); and iii) ball-milled carbon black was irradiated with the CO_2 laser (3.8W, 0.762 m/s) and subsequently melt mixed with Nylon into the extruder (PA-4CB Ex-IM (LE)). The notation for the different systems used in the study and a brief description of the basic difference among them is provided in Table 3.1.

3.1.4 Thermo-mechanical Properties and Electrical Conductivity

The tensile (ASTM D638) and flexural (ASTM D790) properties of the composites were characterized using a UTS testing machine at a test speed of 2.54 mm/min and 1.27 mm/min, respectively. The impact strength (ASTM D256) was determined using a Izod pendulum test. The heat distortion temperature (ASTM D648) was measured with a TA Q800 dynamic mechanical analyzer (DMA) (TA Instruments, New Castle, Delaware, USA) at a load of 0.455 MPa and at a heating rate of 2^{o}C/min. Samples measuring approximately 5 mm X 3 mm X 12 mm were cut from flexure test specimens and were used to measure the volume resistivity by the four probe technique using a Solartron 1287 system (Solartron Analytical, Farnborough, Hampshire, United Kingdom). The resistivity was measured in the direction corresponding to the length of the flexure test specimen (5mm). The two surfaces were coated with gold using a sputter coater prior to the measurement of the electrical resistivity to ensure a good contact of the sample surface with the electrode. The linear viscoelastic properties were measured with a TA ARES® system (TA Instruments, New Castle, Delaware, USA) using a 25 mm parallel plate fixture

3.1.5 Characterization of Structure and Morphology

Fracture surfaces of the neat polymer and the composites obtained by Izod impact testing were used to study the morphology with a Zeiss Ultra 60 (Carl Zeiss, Oberkochen, Germany) scanning electron microscope (SEM) at an accelerating voltage of 5 kV- 20 kV. The structure of the carbon black was studied using a JEOL 100CX-2 (JEOL, Tokyo, Japan) transmission electron microscope (TEM) at an operating voltage of 100 kV.

The crystallinity characteristics of the neat polymer and composite were assessed through the X-ray diffraction (XRD) patterns obtained using a X'Pert Pro Alpha 1 (PANalytical, Almelo, Netherlands) diffractometer in the Bragg-Brentano geometry using a monochromatic, filtered Cu Kα1 radiation. A Seiko 220 (Seiko Instruments, Chiba, Japan) differential scanning calorimeter (DSC) was used to determine the melting temperature, crystallization temperature, the enthalpy of crystallization and the enthalpy of melting. Thin sections for transmission polarized light microscopy (PLM) were prepared using a Microm HM 355S rotary microtome (Thermo Scientific, Waltham, Massachusetts, USA).

The molecular weights of the polymer and polymer composite samples were determined using gel permeation chromatography (GPC) on a JORDI X-stream Mixed Bed Column, 250 mm X 10 mm [106]. The samples were dissolved in Hexafluoroisopropanol (HFIP)/0.01 M sodiumtrifluoroacetate (NaTFA) to a concentration of 1.25 mg/ml and left on an orbital shaker for 24 hours. The samples were subsequently filtered using 0.2μm disposable Teflon filters. The filtered samples were run in duplicate in the same solvent system. The flow rate was 1 ml/min with an injection size of 100μl of the 1.25 mg/ml solution. The eluted samples were monitored using a

Waters 410 Differential Refractometer (Waters, Milford, MA, USA) using JORDI GPC software. The raw signal data was converted to molecular weight using polymethylmethacrylate standards.

The true density and envelope density of the polymer and polymer composite samples were determined using a Geopyc 1360 and Accupyc II 1340 (Micromeritics, Norcross, Georgia, USA) respectively [107]. The true density or the skeletal density was determined using a nitrogen gas displacement technique whereas the envelope density was calculated by displacement technique using a quasi-fluid comprised of small, rigid spheres.

3.2 Results and Discussion

The section focuses on characterizing the microstructure and morphology of the various systems in order to analyze and compare the effects of SLS and extrusion-injection molding on the properties of carbon black-reinforced Nylon-12 nanocomposites.

The flexural properties and tensile properties of the six different systems are shown in Figure 3.1 and Figure 3.2 respectively. The flexural moduli and tensile moduli follow similar trends. Moreover, the flexural modulus is comparable to the tensile modulus for all systems except for the PA-4CB SLS system possibly indicating anisotropic behavior. The flexural modulus and the tensile modulus of the PA SLS system is greater than that of the PA Ex-IM system. The lower values of moduli for the PA Ex-IM system are probably a result of the low holding and packing pressures of the MicroInjector molding system. The variation in the moduli of the composite systems manufactured by SLS and extrusion-injection molding relative to those of the neat Nylon-12 systems are in contrast with each other. The tensile and flexural moduli of the three

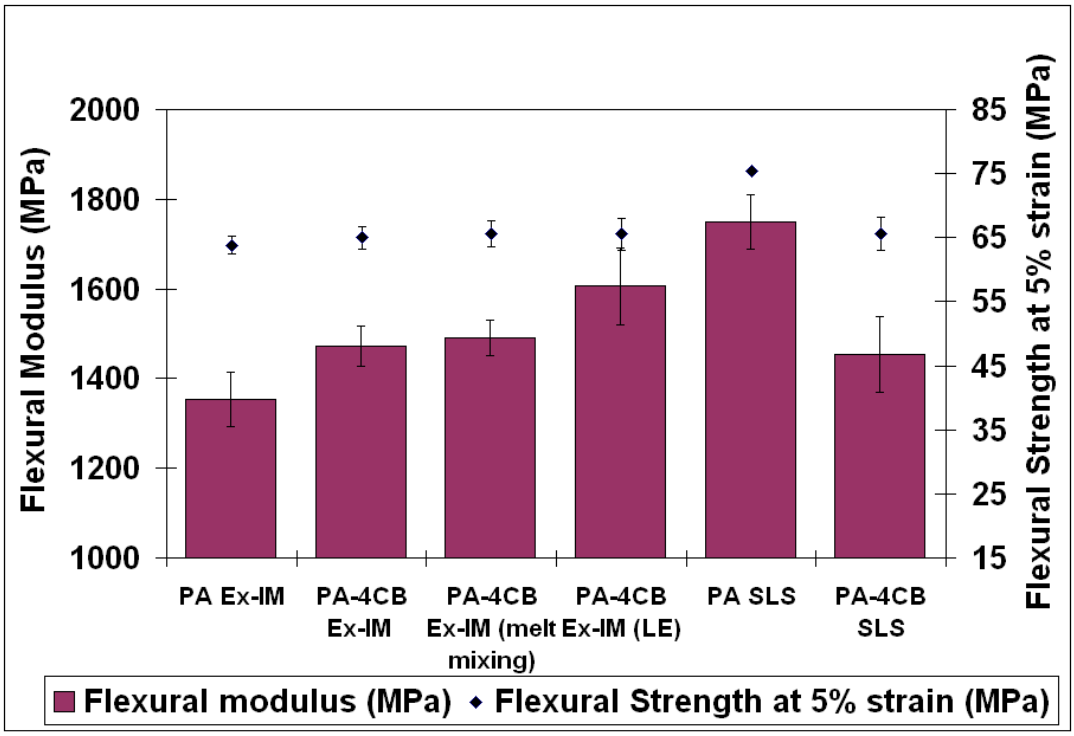

Figure 3.1 Flexural modulus and flexural strength (at 5% strain) for the six different systems.

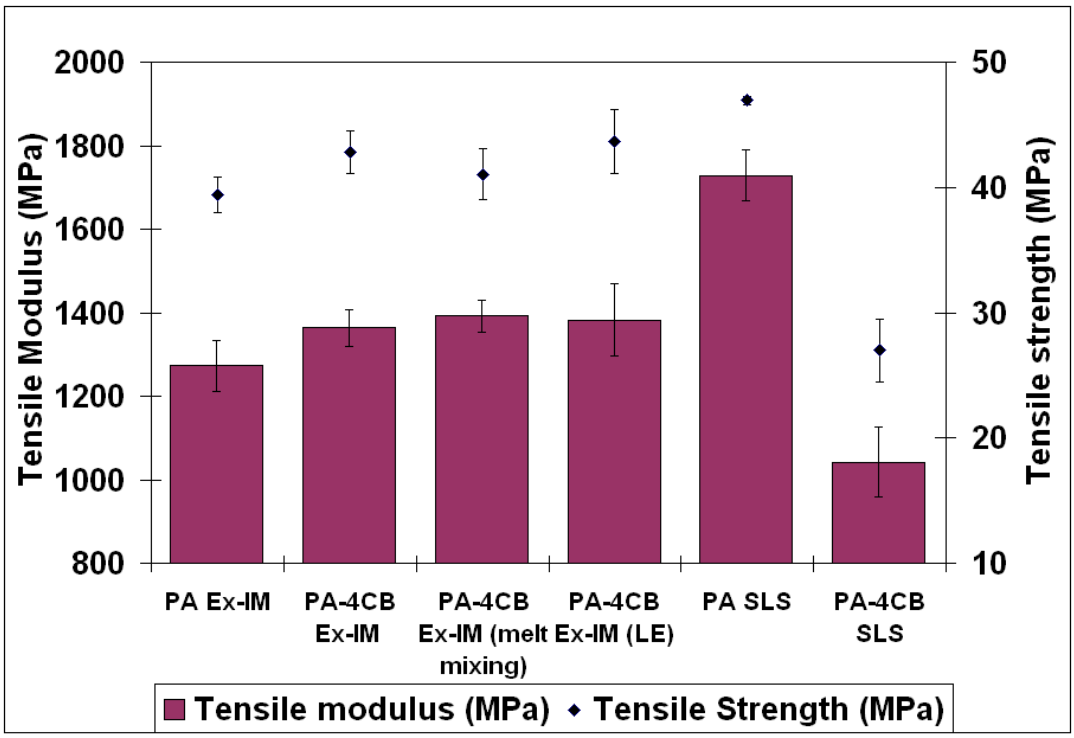

Figure 3.2 Tensile modulus and tensile strength of the six different systems.

composite systems prepared by the melt mixing method are greater than the PA Ex-IM system. However, the flexural and tensile moduli of the PA-4CB SLS system are less than those of the PA SLS system. Similar results have been obtained for low loading of nanosilica powder in Nylon11/nanosilica nanocomposites prepared by SLS [15]. Moreover, comparable values of flexural strength for all the four systems manufactured by extrusion-injection molding indicate a weak polymer-filler interaction.

The impact strength of the six systems is shown in Figure 3.3. The impact strength of the PA Ex-IM system is greater than the PA SLS system. This could be due to a difference in the size of the spherulites in the two systems. The parts made by SLS remain at an elevated temperature (approximately 173^{o}C) during the build stage (approximately one hour) for a significantly greater time than the parts made by injection molding where the temperature drops off from the melt state to room temperature in a matter of minutes. This could result in larger spherulites in the case of PA SLS system. An increase in the spherulitic size has been shown to reduce the impact strength of neat polymers [108]. The addition of carbon black to Nylon-12 results in a decrease in the impact strength of all the composite systems. However, the impact strength of the PA-4CB Ex-IM (melt mixing) and PA-4CB SLS systems is significantly lesser than that of the other two composite systems. This might be due to a poor state of dispersion of the carbon black particles in the polymer matrix.

The heat distortion temperature (HDT) of the six different systems is shown in Figure 3.4. The relative variation in the HDT of each system is similar to the variation in the flexural moduli as shown in Figure 3.1. This is an expected result since the HDT of any system is mainly affected by the flexural modulus of the part at room temperature.

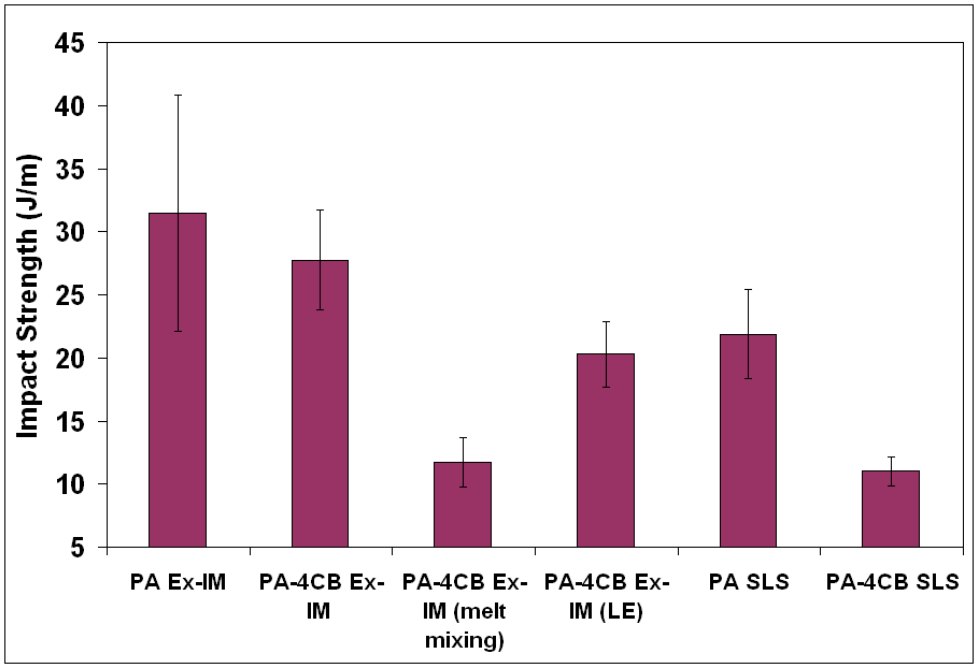

Figure 3.3 Impact strength of the six different systems.

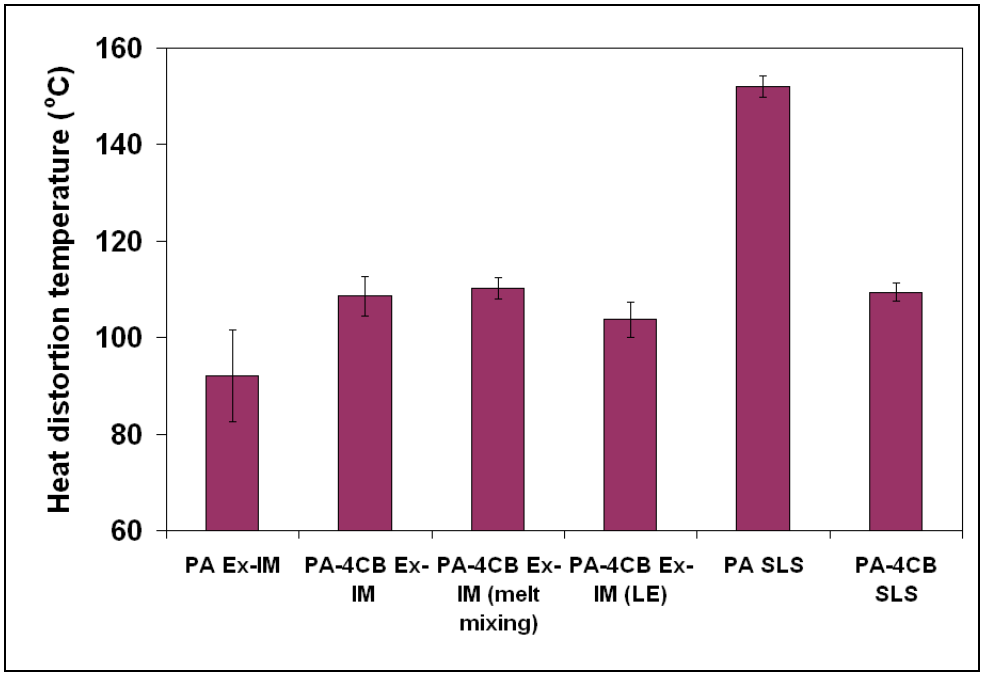

Figure 3.4 Heat distortion temperature of the six different systems.

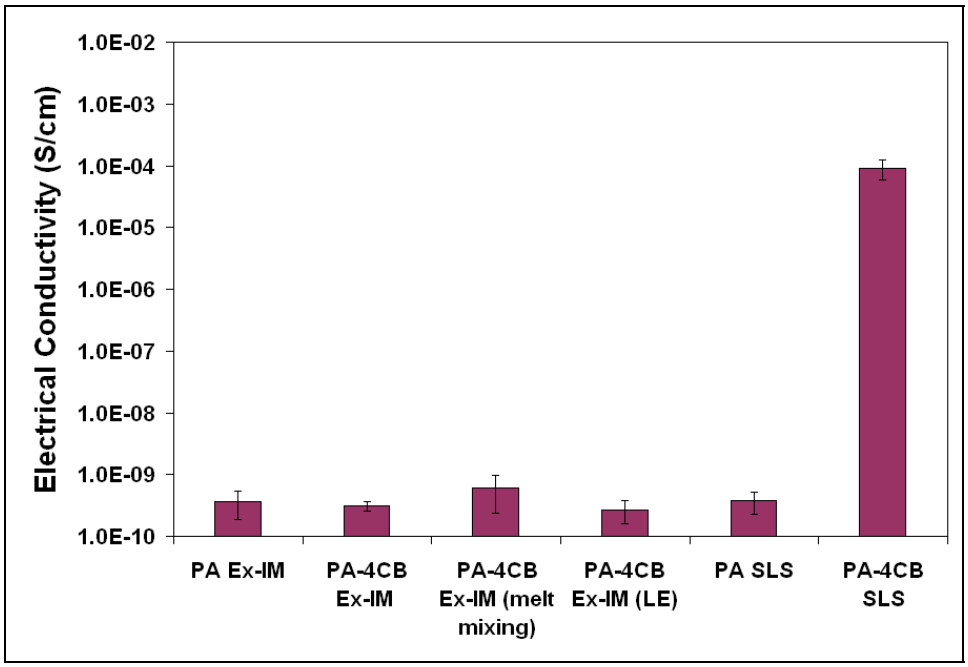

Figure 3.5 Electrical conductivity of the six systems at a AC frequency of 1 Hz.

The electrical conductivity of the six different systems is shown in Figure 3.5. It can be seen that the electrical conductivity of the PA-4CB SLS system is five orders of magnitude higher than the other five systems. The three PA-4CB systems prepared by melt mixing have similar conductivities as the neat polymer systems. This implies that percolation behavior is exhibited only by the PA-4CB SLS system. The relatively high conductivity of the PA-4CB SLS system could be due to the presence of a network of carbon black agglomerates. This network of carbon black particles could manifest itself as a segregated microstructure as shown in Figure 2.9b.

3.2.1 Molecular Weight of Nylon-12

The molecular weight and molecular weight distribution (MWD) is one of the most important properties of a polymer. The MWD has a significant bearing on the mechanical properties and the rheological properties of a polymer. An increase in the

molecular weight of the polymer is known to result in an increase in the modulus, strength, and elongation at break of polymeric parts. These observations have been attributed to an increase in long-range entanglements of the polymer [109]. The study of the molecular weight of Nylon-12 is particularly necessary for this dissertation which aims to compare and analyze the effects of the extrusion-injection molding process and the SLS process on the properties of polymer nanocomposites. Firstly, the polyamide group of polymers are known to undergo solid state polymerization reactions when placed at elevated temperatures for lengthy durations [110] which can result in the cross-linking of chains [111]. The re-use of a batch of polymer powder can aggravate this issue. This phenomenon is of particular importance to the SLS process because an increase in the molecular weight of the polymer can result in a significant increase in its viscosity and consequently affect the mechanical properties and dimensional accuracy of the parts [112]. Hence, in order to minimize the effects of any possible increase in the molecular weight of Nylon-12 due to re-use in the SLS process, parts made only from a fresh batch of powder were used for property characterization. Secondly, investigation of the molecular weight of the PA-4CB SLS system could offer insights into possible local heating (and the resulting pyrolysis and chain scission) due to the irradiation of the carbon black by the infra-red laser. Lastly, due to their hygroscopic nature, polyamides tend to absorb high levels of moisture quickly. Presence of low levels of water during processing can result in a reaction between water and the amide group resulting in the breaking of bonds, lowering of the molecular weight and deterioration of the properties of the polymer. Absorption of moisture after processing can affect the mechanical properties and the electrical conductivity. The absorption of moisture can be a very serious issue

during the processing of certain polyamides such as Nylon 6 which can have an equilibrium moisture content of 3 wt. % [113]. The equilibrium moisture content for the Nylon-12 used in this dissertation is 0.5 wt. % [88] which was verified by measuring the change in the weight of a small quantity of the powder after drying at 80^{o}C under a pressure of approximately 60mm of mercury (1 atmosphere = 760 mm of mercury) for five hours.

Table 3.2 Molecular weight and poly-dispersity index as determined using GPC

Sample ID	M_n	M_w	M_z	PDI
PA powder	7049	18151	38645	2.57
PA SLS	9940	36342	81831	3.66
PA-4CB SLS	10071	37895	83185	3.76
PA Ex-IM	7211	19706	42331	2.73
PA-4CB Ex-IM	7857	22713	48328	2.89

The number-averaged molecular weight (M_n), the weight-averaged molecular weight (M_w), the z-averaged molecular weight (M_z) and the poly-dispersity index (PDI) of the various systems as determined by GPC is shown in Table 3.2. Firstly, the average molecular weights and the PDI of the SLS-processed systems witness a significant increase as compared to the unused powder indicating the occurrence of solid state polymerization. Secondly, the average molecular weights and the PDI of the PA SLS system and PA-4CB SLS system are comparable, indicating no deleterious effects on the molecular weight of the polymer due to carbon black-induced localized heating in SLS. Lastly, the average molecular weights of the PA Ex-IM and PA-4CB Ex-IM systems are marginally greater than those of the Nylon-12 powder indicating no evidence of hydrolytic degradation. A broader MWD did not result in enhanced values of modulus

and strength (as seen in Figure 3.1 and Figure 3.2). This observation might be attributed to two likely reasons. First, changes in the MWD of the polymer are known to result in enhanced mechanical properties only above a critical value of the MW [109]. The MW of the polymer powder used in this dissertation might be below this critical value for Nylon-12. Second, deleterious effects due to differences in other aspects of the microstructure and morphology such as the crystallization behavior of the polymer, the presence of porosity, and the state of dispersion of carbon black could be suppressing any possible increase in the mechanical properties due to a wider MWD.

3.2.2 Crystallization Behavior of Nylon-12

Nylon-12 is a semi-crystalline polymer that consists of crystalline and amorphous domains within a superstructure of spherulites. The final mechanical properties depend on the volume fraction of the crystalline domains as well as their size and structure. Nylon-12 undergoes crystalline transitions and so far, four polymorphs have been detected: α, α', γ, and γ'. The most commonly obtained crystal from the melt at atmospheric pressure is the γ-form. The predominant reflections (XRD) of each of the polymorphs and their corresponding d-spacings are listed in Table 3.3.

Table 3.3 Principal reflections and corresponding d-spacings of the Nylon-12 polymorphs

Crystal form	Reflections (^{o})	d-spacing (nm)
α [114]	22.774	0.390
	20.157	0.440
α' [115]	20.353	0.436
	21.018	0.422
γ [116]	21.128	0.420
γ' [116]	21.128	0.420

The effects of the addition of carbon black and the effects of the processing technique on the crystalline state of Nylon-12 were investigated using XRD, DSC and PLM. XRD patterns yielded information about the types of crystals present in the samples and the width of the crystalline lamellae (along the direction perpendicular to the reflection plane), which was estimated using the Debye-Scherrer equation:

$$L_T = \frac{K\lambda}{\beta \cos\theta} \tag{3.1}$$

where L_T is the lamella thickness, K is the crystal shape factor which was be taken as 0.9 [1], λ is the wavelength of the x-ray radiation (0.154 nm), β is the full width at half maximum and θ is the peak position of the XRD pattern. XRD patterns of the Nylon-12 powder and the PA SLS, PA Ex-IM, PA-4CB SLS and PA-4CB Ex-IM systems are shown in Figure 3.6. The predominant reflections and their corresponding d-spacings are tabulated in Table 3.4.

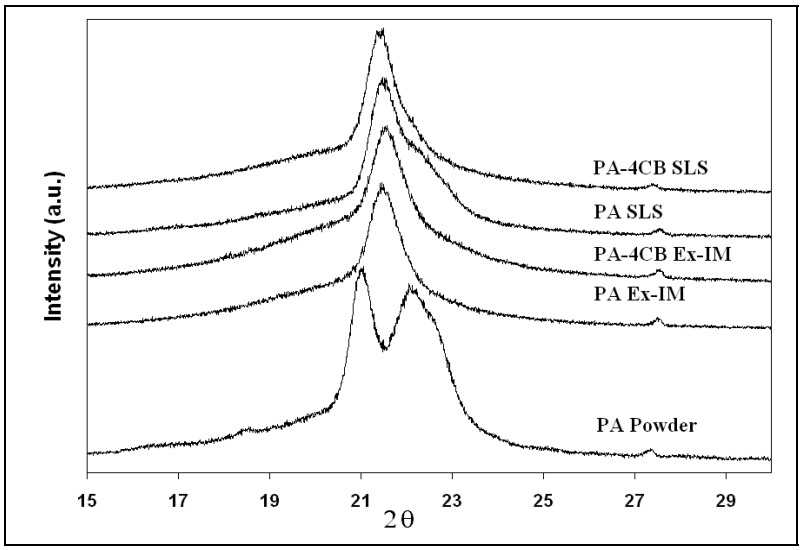

Figure 3.6 XRD patterns of the Nylon-12 powder and samples manufactured by SLS and extrusion-injection molding.

Table 3.4 Principal reflections, corresponding d-spacings and the average lamella thickness for various systems investigated by XRD

Sample ID	2θ	d-spacing (nm)	Avg. Lamella thickness (nm)
PA powder	20.973	0.423	14.475 ± 1.215
	22.023	0.403	8.235 ± 0.04
PA Ex-IM	21.529	0.412	12.453 ± 2.860
PA SLS	21.495	0.413	10.562 ± 0.283
PA-4CB Ex-IM	21.282	0.417	11.381 ± 0.821
PA-4CB SLS	21.468	0.413	12.735 ± 1.394

The XRD pattern of the Nylon-12 powder has two strong reflections at 20.973^{o} and 22.023^{o} (d-spacing of 4.23 nm and 4.03 nm, respectively). Moreover, the Nylon-12 powder exhibits only one melting peak with a relatively high enthalpy of melting (relative to the enthalpy of melting for the other systems listed in Table 3.5). This indicates the presence of the α-form crystal in the Nylon-12 powder. It is important to note that the d-spacings of the α-form crystal listed in Table 3.3 correspond to a perfectly defined crystal [114]. Large variations in the d-spacings of the α-form crystal of Nylon-12 have been reported in literature. This can probably be attributed to the fact that the α-form crystal is generated under conditions of high temperature and pressure. Moreover, earlier studies have shown that an increase in the content of the α-form crystal results in an increase in the enthalpy of melting [111].

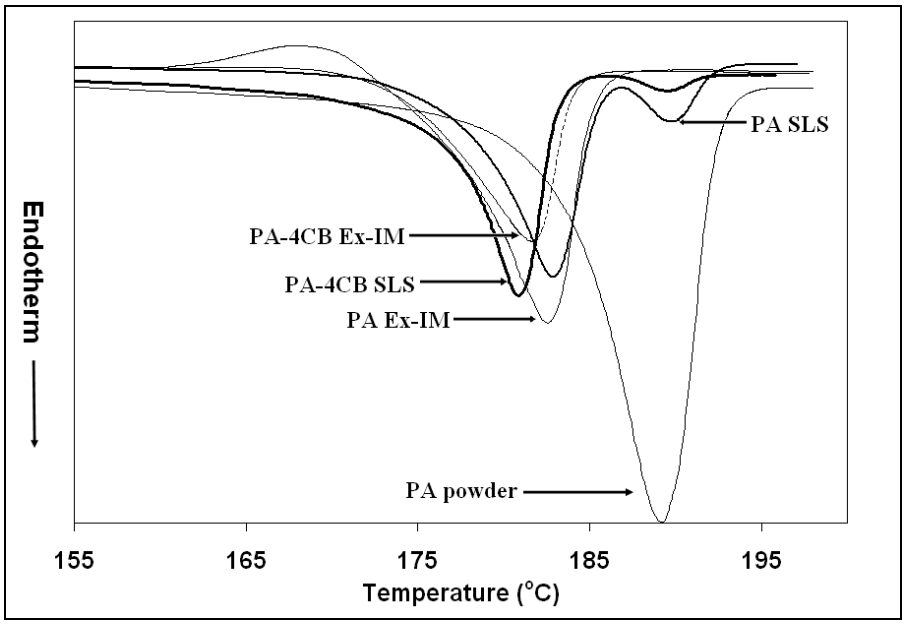

Figure 3.7 Melting endotherms of the Nylon-12 powder and systems processed by SLS and extrusion-injection molding.

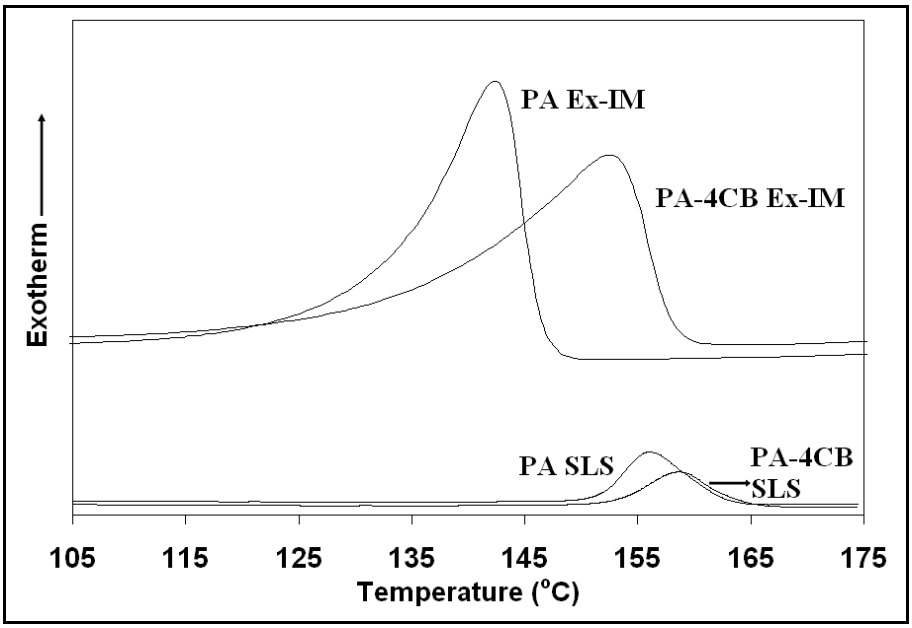

Figure 3.8 Crystallization exotherms for systems processed by SLS and extrusion-injection molding.

DSC was used to measure the degree of crystallinity, crystallization temperature, melting temperature, enthalpy of crystallization and the enthalpy of melting. The degree of crystallinity was calculated using the following equation:

$$\chi = \frac{1}{1 - wt\%} \frac{\Delta H_F}{\Delta H_C} \tag{3.2}$$

where χ denotes the degree of crystallinity, *wt. %* corresponds to the weight fraction of carbon black, ΔH_F is the enthalpy of melting of the sample and ΔH_C is the theoretical enthalpy of melting for 100% crystalline Nylon-12. ΔH_C for the γ-form is 209.2 J/g [111]. The melting endotherms and crystallization exotherms of the various systems are shown in Figure 3.7 and Figure 3.8. The melting endotherm for each system was obtained by heating a sample weighing between 5-10 mg at 5°C/min from 25°C to 195°C. The cooling exotherms were subsequently obtained by varying the cooling rate based on the system being investigated. The cooling rates for the injection molded samples and the SLS-processed samples are summarized in Table 3.6. The reason behind varying the cooling rate was to simulate the differences in cooling rates in injection molding and SLS. The results from the DSC analyses of three samples per system are summarized in Table 3.5 and Table 3.6.

Table 3.5 Range of melting and degree of crystallinity for various systems

Sample ID	ΔH_F of 1st melting peak(J/g)	ΔH_F of 2ndt melting peak (J/g)	χ_c (%)
PA powder	87.40	N/A	N/A
PA SLS	42.03	5.26	22.6 ± 2.0
PA Ex-IM	53.29	N/A	25.5 ± 0.5
PA-4CB SLS	40.85	1.23	21.0 ± 1.1
PA-4CB Ex-IM	43.73	N/A	21.8 ± 1.6

Table 3.6 Range of crystallization and the enthalpy of crystallization for various systems

Sample ID	Cooling rate (°C/min)	T_{crsyt} range (°C)	ΔH of crystallization (J/g)
PA SLS	2	165.2 - 148.8	44.7 ± 0.8
PA-4CB SLS	2	166.3 - 150.4	44.6 ± 0.9
PA Ex-IM	30	154.7 - 106.7	51.8 ± 1.1
PA-4CB Ex-IM	30	167.2 - 101.2	49.6 ± 1.2

The XRD pattern of the PA Ex-IM system exhibits only one strong reflection. This corresponds to the γ-form crystal. The single reflection in the XRD pattern agrees well with the presence of a single melting peak of PA Ex-IM. This is in contrast with the melting curve and XRD pattern of the PA SLS system. As discussed in section 2.4.1, the presence of two melting peaks for PA SLS and a small bulge in its XRD pattern corresponds to trace amounts of the original α-form crystal that remain unmelted in the final part. The presence of these unmelted particle cores can be visualized (particularly in the large spherulites) by comparing the transmitted light micrographs in Figure 3.10a (un-polarized light) and Figure 3.10b (polarized light). Figure 3.9b and Figure 3.10b also indicate differences in size distribution of the spherulites. The PA Ex-IM system has a narrower size distribution of spherulites with the majority lying in the range of 5μm-10μm. In contrast, the spherulites in the PA SLS system have a wider size distribution. This indicates that the size distribution of the spherulites in the PA SLS system is likely similar to the particle size distribution of the original Nylon-12 powder and that the relative variation in spherulitic size along the depth of the part would be lesser for SLS processed parts than injection molded parts [1]. It is also important to note that the lamellar thickness (Table 3.4) as well as the degree of crystallinity (Table 3.5) is comparable for the Ex-IM systems and the SLS-processed systems. In the case of the SLS-processed systems, the areas under the two melting peaks were summed up prior to calculating the degree of crystallinity. This is not entirely accurate due to the presence of two crystal forms. However, this procedure is the best approximation in the absence of the theoretical enthalpy of melting for the α-form crystal.

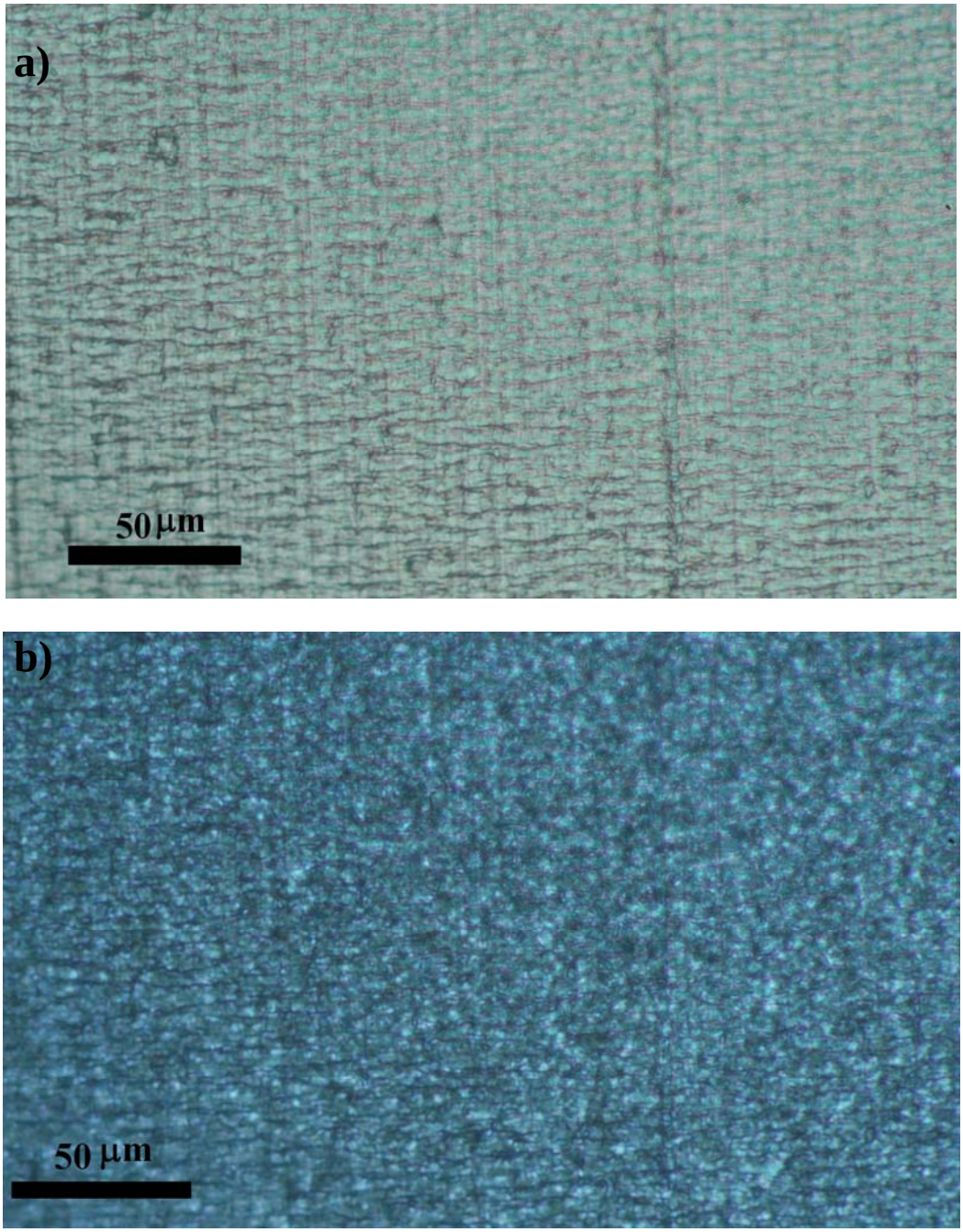

Figure 3.9Transmission optical micrographs of a) PA Ex-IM in un-polarized light, and b) PA Ex-IM in polarized light.

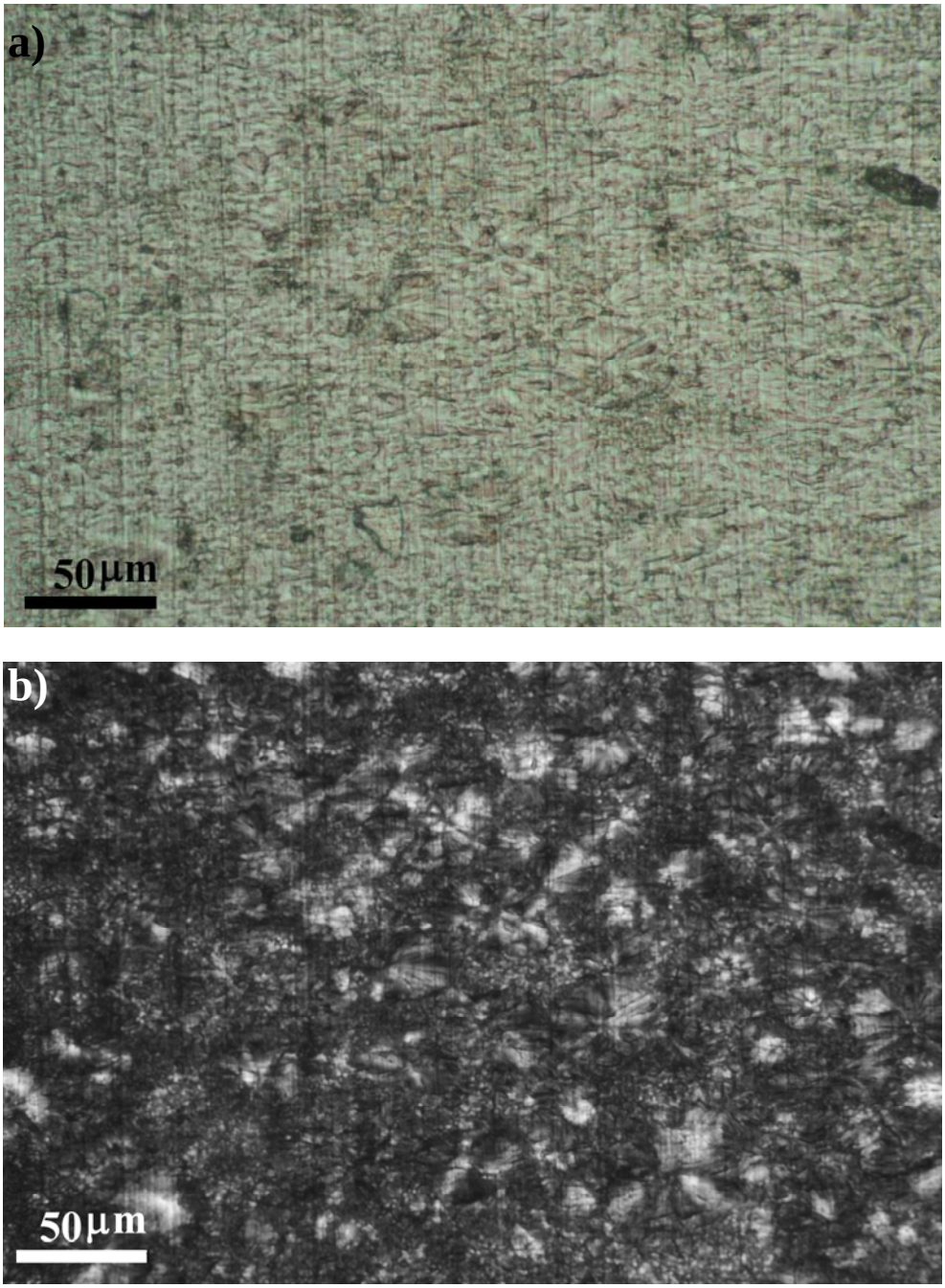

Figure 3.10 Transmission optical micrographs of a) PA SLS in un-polarized light, and b) PA SLS in polarized light.

Transmitted light micrographs of the PA-4CB SLS and PA-4CB Ex-IM systems are shown in Figure 3.11 and Figure 3.12. The PA-4CB Ex-IM system has a homogenous distribution of the carbon black relative to the PA-4CB SLS system which has an

extremely segregated structure. A 4μm thick sample of the PA-4CB Ex-IM system had very low transmittance to visible light. In contrast, a 4μm thick sample of the PA-4CB SLS system had good transmittance but very poor sample integrity. This can be attributed to the presence of carbon black rich channels (approximately 20 μm in dimension) in the PA-4CB SLS system. Hence, micrographs of the PA-4CB SLS system in Figure 3.11 were obtained from samples that were approximately 25μm in thickness. The cooling exotherms of the injection-molded and SLS-processed systems are shown in Figure 3.8. The crystallization temperature (defined as the temperature at which crystallization commences) for the PA-4CB Ex-IM system is approximately 13^{o}C (Table 3.6) higher than that of the PA Ex-IM system whereas it is almost the same for the SLS processed systems. This indicates that carbon black likely acts as a nucleating agent only in the Ex-IM system and not in the SLS-processed system. This is in agreement with the micrographs in Figure 3.12. The carbon black agglomerates are broken down (in the extruder) and more uniformly distributed in the Ex-IM system than in the SLS-processed system. Numerous, well dispersed carbon black particles acting as individual nucleating agents would result in several (but smaller) spherulites in the Ex-IM system. This offers an explanation for the fact that almost no contrast was achievable under polarized light for the PA-4CB Ex-IM system with a 20X objective lens. In contrast, relatively larger spherulites were visible for the PA-4CB SLS system. However, due to the relatively high sample thickness, it is difficult to clearly visualize the spherulites.

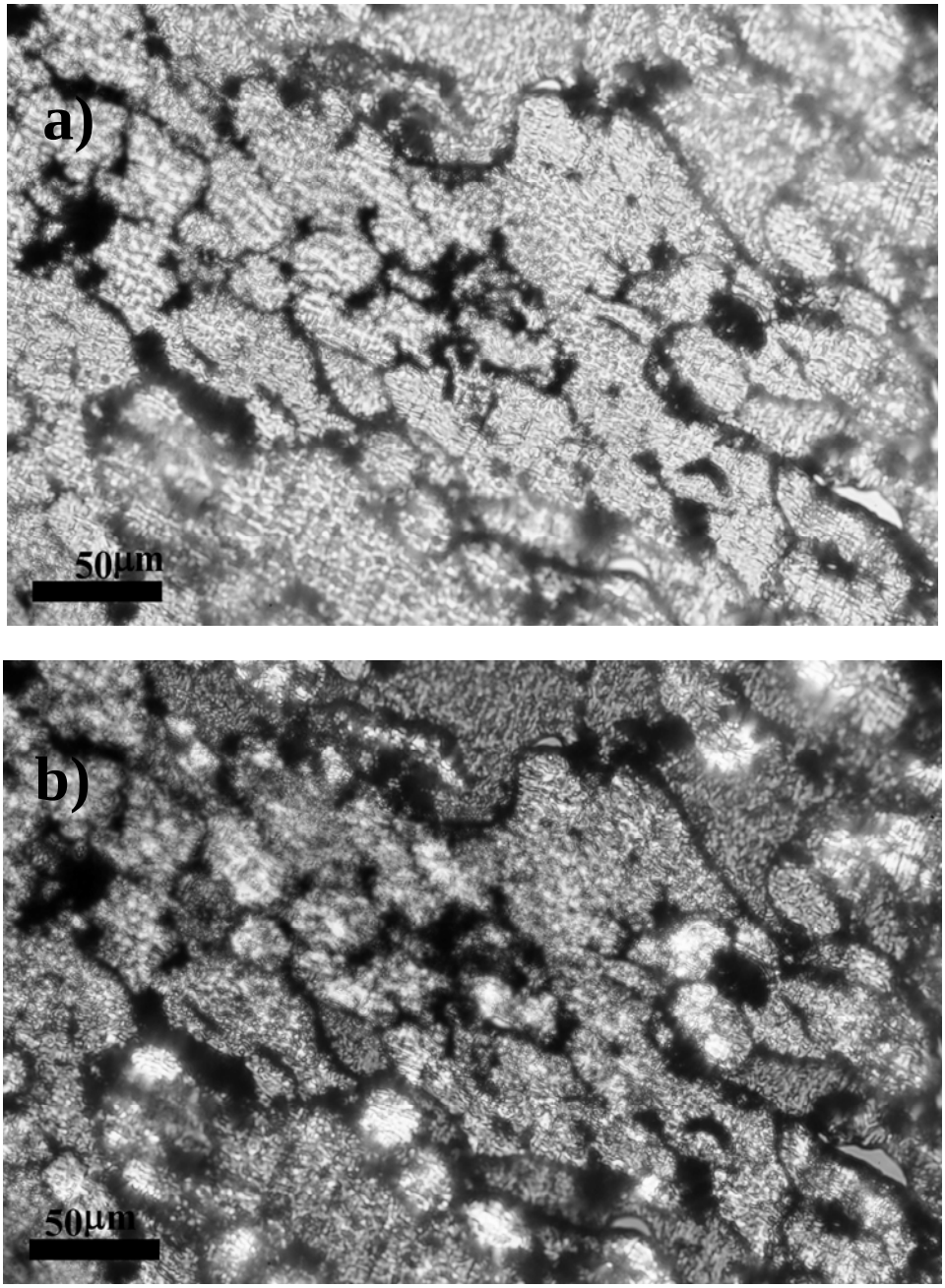

Figure 3.11 Transmission optical micrographs of a) PA-4CB SLS in un-polarized light, b) PA-4CB SLS in polarized light,

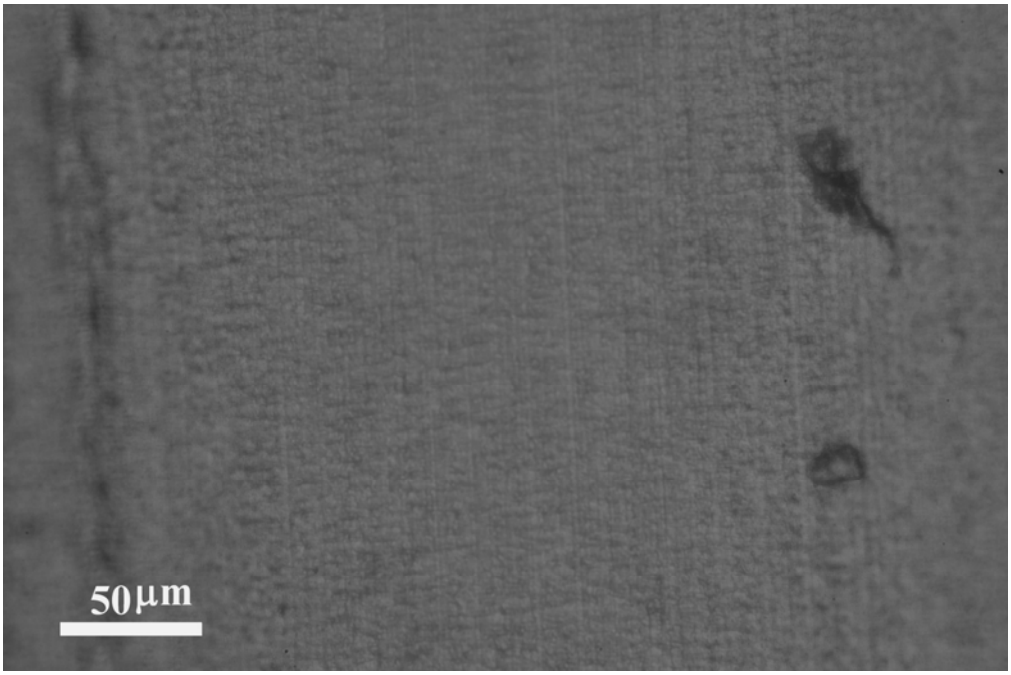

Figure 3.12 Transmission optical micrographs of PA-4CB Ex-IM in un-polarized light.

3.2.3 State of dispersion of carbon black

The state of dispersion refers to the extent to which the carbon black agglomerates are broken down to the level of primary aggregates and how well they are uniformly distributed throughout the polymer matrix. The dispersion and distribution of carbon black plays a major role in determining the final properties of the composite. Incomplete dispersion resulting in even a low content of relatively large, unbroken agglomerates can have deleterious effects on certain mechanical properties such as impact strength, tensile strength and elongation at break [103]. The state of dispersion is strongly dependent on the manufacturing process, the processing conditions and the properties of the material system.

The agglomeration of carbon black occurs due to attractive forces that exist on its surfaces. These forces vary widely in magnitude and create particle structures of varying

strength. As described earlier in Section 2.1.2, carbon black in its powdery form exists as primary aggregates that are loosely held together in the form of agglomerates. The predominant bonding mechanisms within the agglomerates in decreasing order of magnitude are: solid bridges, liquid bridge forces, Van der Waals forces, and electrostatic forces [90]. Solid bridge forces have their origins in permanent chemical bonds between two particles and are the most difficult to break. Liquid bridge forces are a result of small quantities of liquid in interstitial pores of the adjacent particles. The stability and the strength of the bridge depend on the surface tension, the viscosity of the liquid and the distance between the two particles. The size of the pores (which is determined by the structure and morphology of the carbon black and the size of the primary particle) and the wettability (which is determined by the functional groups on the surface of carbon black) play important roles in the dispersion of the carbon black. High structure carbon blacks, with a relatively more open structure are easier to break down than low structure carbon blacks [103]. Moreover, a carbon black with surface functionalization (such as carboxylic acid groups and hydroxyl groups) would have greater interaction with the amide group in the Nylon-12 (via hydrogen bonding) and consequently be easier to disperse than a carbon black with no oxygen containing groups on its surface.

In addition to the properties of the material system, the manufacturing process plays a very important role in the dispersion of carbon black. Most manufacturing processes employ external loads that result in an internal stress field and a hydrodynamic flow field within the polymer composite melt. The duration of this stress field and its ability to overcome the inter-aggregate forces of attraction determine the extent to which the carbon black agglomerates get broken down and get uniformly distributed.

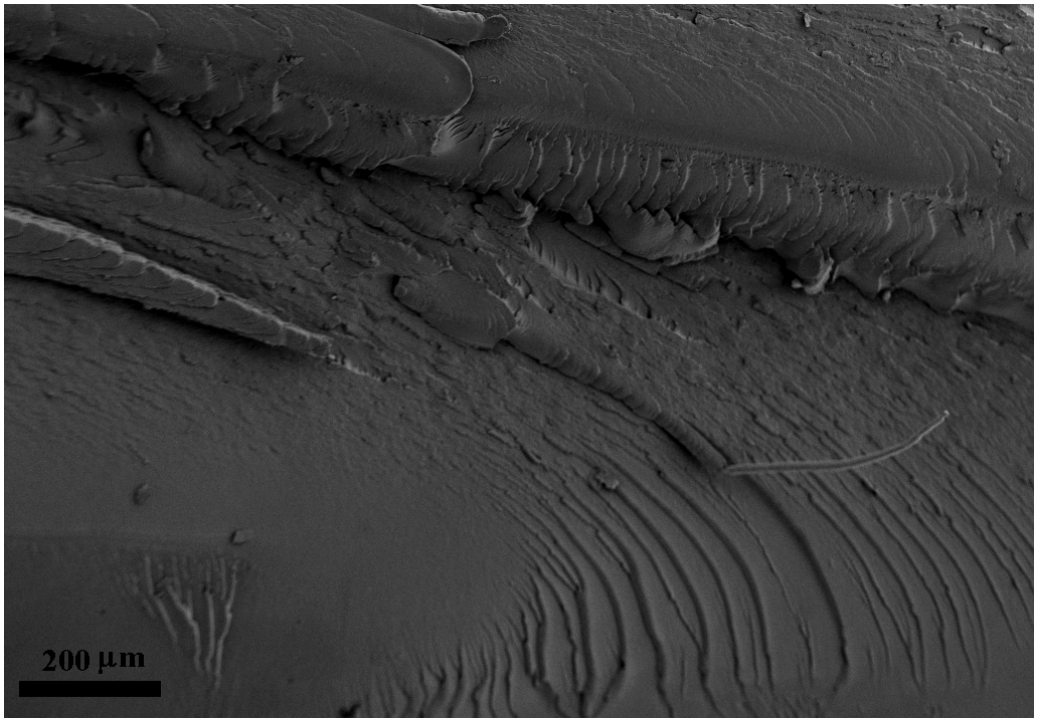

Figure 3.13 Low magnification SEM image of the fracture surface of PA-4CB Ex-IM.

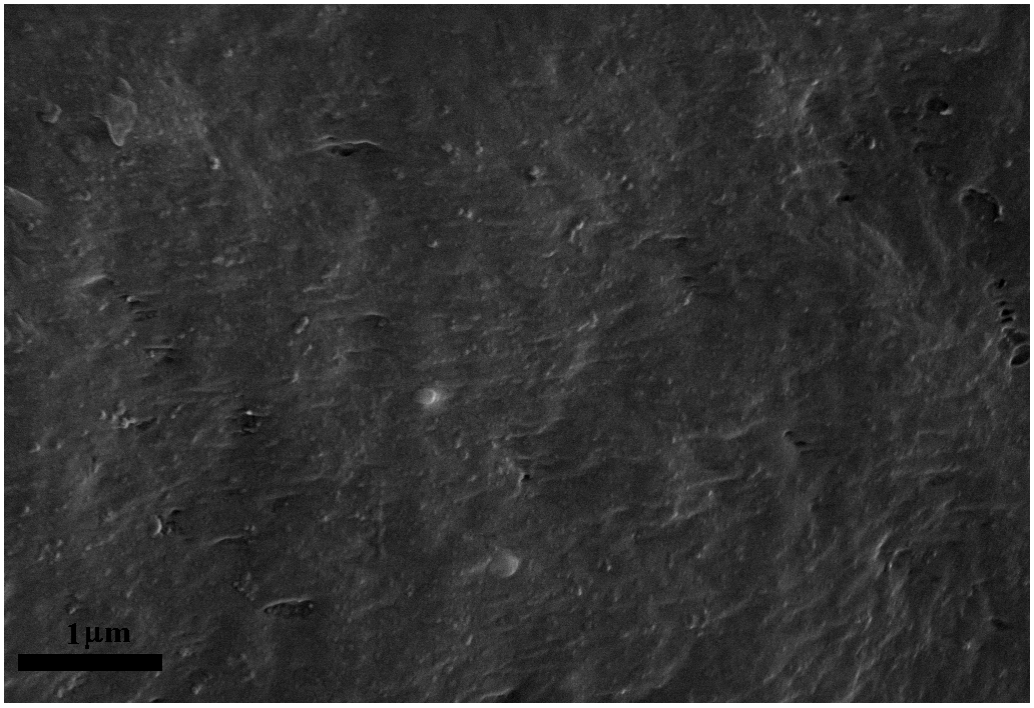

Figure 3.14 High magnification SEM image of the fracture surface of PA-4CB Ex-IM.

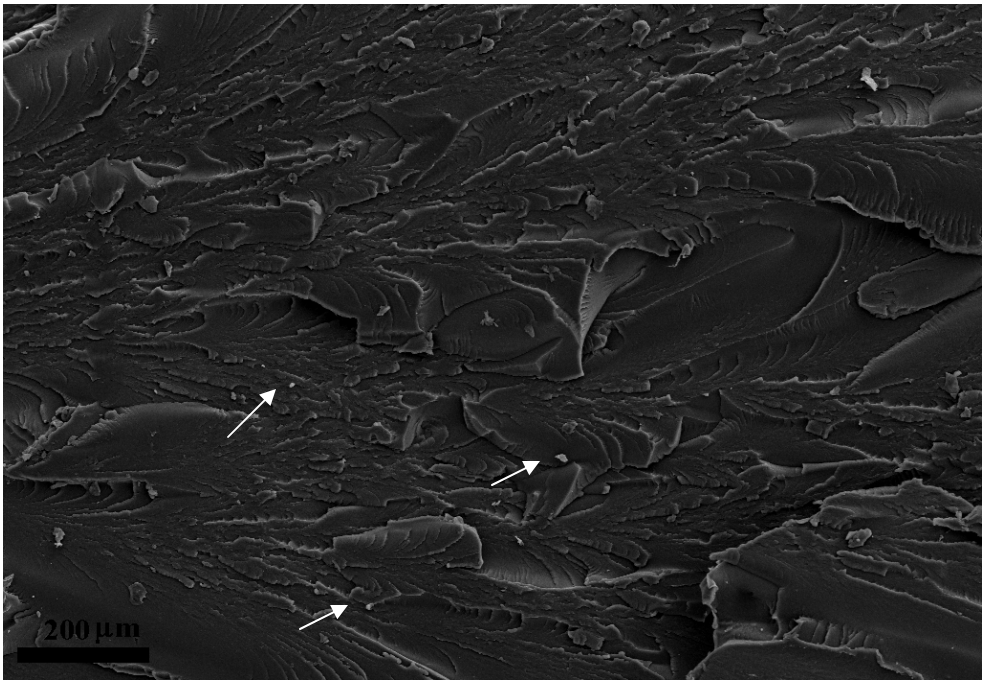

Figure 3.15 Low magnification SEM image of the fracture surface of PA-4CB Ex-IM (melt mixing) indicating the presence of agglomerates of carbon black.

SEM images of the fracture surfaces of the PA-4CB SLS and PA-4CB Ex-IM are shown in Figure 2.9b and Figure 3.13 which represent very different microstructures obtained from the same composite powder. The composite powder (refer to Figure 2.4b) consisted of agglomerates of carbon black (primarily <5μm) adhering to the surface of the Nylon-12 powder surface. The effect of the SLS process on these agglomerates is in sharp contrast with that of the extrusion-injection molding process. The SLS process, being solely driven by the reduction of surface energy of the polymer is unable to overcome the inter-agglomerate attractive forces and results in a mottled microstructure with alternating regions (order of 10μm) of polymer and carbon black whereas the shear forces in the extruder disperse the agglomerates into aggregates (<100 nm) and distribute them randomly within the polymer matrix. For a given set of process parameters during the extrusion process (screw speed, temperature and mixing time), the extent of

dispersion of the agglomerates depends on their initial dimensions and the mechanism by which they are incorporated into the polymer melt. This explains the presence of several agglomerates (approximately <20μm as seen in Figure 3.15) for the PA-4CB Ex-IM (melt mixing) system which involved the incorporation of millimeter sized carbon black pellets into the extruder as opposed to the use of the composite powder for the PA-4CB Ex-IM system.

3.2.4 Porosity

The results from the pycnometry analysis of the PA SLS, PA-4CB SLS, PA Ex-IM and PA-4CB Ex-IM systems are shown in Table 3.7. Pycnometry analysis of the PA SLS and PA-4CB SLS systems was intended to complement the results from the procedure outlined in Section 2.3. The envelope density was calculated by a displacement technique using a quasi-fluid comprised of small, rigid spheres approximately 25 μm in diameter. Hence all the porosity and surface features (which are smaller than the sphere diameter) would be included in the sample's volume. This is of importance for SLS-processed parts which typically have high surface roughness due to the presence of incompletely melted powder particles. The true density was calculated using a nitrogen gas displacement technique. The porosity of the sample was calculated using the following relation:

$$\text{Percent porosity} = 1 - \frac{\rho_e}{\rho_d} \tag{3.3}$$

where ρ_d and ρ_e are the true density and the envelope density respectively. The samples that were used for pycnometry were created by cutting flexure test specimens along the width with a razor blade. The surfaces created by cutting the flexure test specimens were

polished using P1200 and P2400 grade sandpaper for 15 minutes. Additionally, in order to account for porosity due to surface roughness, the remaining four surfaces of the PA SLS and PA-4CB SLS samples were also polished using the above procedure and were denoted as PA SLS mod and PA-4CB SLS mod.

Table 3.7 Envelope density, true density and percent porosity measurements

Sample ID	Envelope density (g/cc)	True density (g/cc)	Percent porosity (%)
PA SLS	0.953	1.019	6.517
PA SLS Mod.	1.028	1.021	~0
PA-4CB SLS	0.949	1.045	9.142
PA-4CB SLS Mod.	0.923	1.039	11.167
PA Ex-IM	0.982	1.022	3.914
PA-4CB Ex-IM	0.991	1.042	4.885

Results from the pycnometry analysis indicate that the PA Ex-IM and PA-4CB Ex-IM had porosities less than 5%. Additionally, the PA SLS mod had a true density lower than the envelope density. Since this is not physically possible, such results signify near full density and are usually attributed to the ability of some polymers to absorb low molecular weight gases such as nitrogen. It is also important to note that PA SLS had a porosity of approximately 6.5%. Since PA SLS mod was nearly fully dense, the porosity of PA SLS can be attributed almost entirely to the surface roughness that is typical of SLS-processed parts. In comparison, the PA-4CB SLS had a porosity of approximately 9.14%. Assuming that the porosity due to surface roughness would be the same for PA-4CB SLS and PA SLS, an internal porosity of approximately 3% could be expected for PA-4CB SLS mod. However, pycnometry analysis yielded an unexpectedly high result of 11.17% which is greater than the value of 4% as determined by the method outlined in

section 2.3. The result of pycnometric analysis is likely due to the porosity present in the carbon black rich domains of the PA-4CB SLS system which cannot be determined using the method outlined earlier. Hence, based on the results presented in Table 3.7, the PA-4CB SLS system has a porosity of approximately 10 % which is predominantly present in the carbon black rich domains.

3.2.5 Viscoelastic Properties

Rheological properties of polymers and polymer composite systems are important from the application and processing point of view. The study of linear viscoelastic properties of polymer composites can offer insights into the microstructure of the material as well as the state of dispersion and distribution of the reinforcing material. Dynamic measurements offer valuable information regarding the dynamics of structures formed by particles in a viscoelastic medium. The linear viscoelastic regimes of each of the six samples were identified by performing a strain sweep test at a frequency of 1 Hz. The rheological properties of the SLS-processed systems and the extrusion-injection molded systems were measured at 194^{o}C and 185^{o}C, respectively. These temperatures were chosen on the basis of completion of melting for each of the systems as shown in Figure 3.7. The storage modulus was monitored as a function of strain. The range of strains in which the storage modulus remained constant was identified as the linear regime. It can be observed that the PA-4CB SLS system alone had a much narrower linear regime. The strain amplitude at which a linear response was obtained for the PA-4CB SLS system (~ 0.1%) was two orders of magnitude lower than the other five systems (~ 10 %). Since the region of linear viscoelasticity is very sensitive to the presence of fillers at low frequencies [1], the results can be explained by differences in the state of

dispersion of the CB particles or the presence of a network of CB particles in the PA-4CB SLS system that significantly add to the non-linearity of the response.

The linear viscoelastic response of the six systems as represented by the viscosity and the storage modulus (G') are shown in Figure 3.16 and Figure 3.17 respectively. A monotonically increasing trend similar to that of the storage modulus is observed for the loss modulus (G"). The storage and loss moduli are known to represent the elastic and viscous responses of the system, respectively. The linear viscoelastic properties of polymers are known to be more sensitive to the presence of fillers at low frequencies. The extent of dispersion of carbon black, the strength of the polymer-carbon black interaction, and the state of the polymer melt present within an agglomerate effects the viscoelastic properties of the polymer composite melt. Highly agglomerated systems which are usually the result of the lack of an external force necessary to overcome the inter-agglomerate attractive forces are known to have a high viscosity [103]. Moreover, the size of the agglomerate (which affects the state of polymer melt within the agglomerate: pendular, funicular or capillary) affects its strength and consequently the viscoelastic properties of the polymer composite melt [117]. The viscosity and the storage modulus of the PA-4CB SLS systems as shown in Figure 3.16 and Figure 3.17 are significantly greater than those of the extrusion-injection molded systems. Hence, it can be inferred that the level of agglomeration is significantly greater in the PA-4CB SLS system than the other composite systems. The presence of a network of carbon black particles cannot be inferred from these results alone. An investigation of the viscoelastic properties of composites with increasing loading of carbon black would be necessary [91].

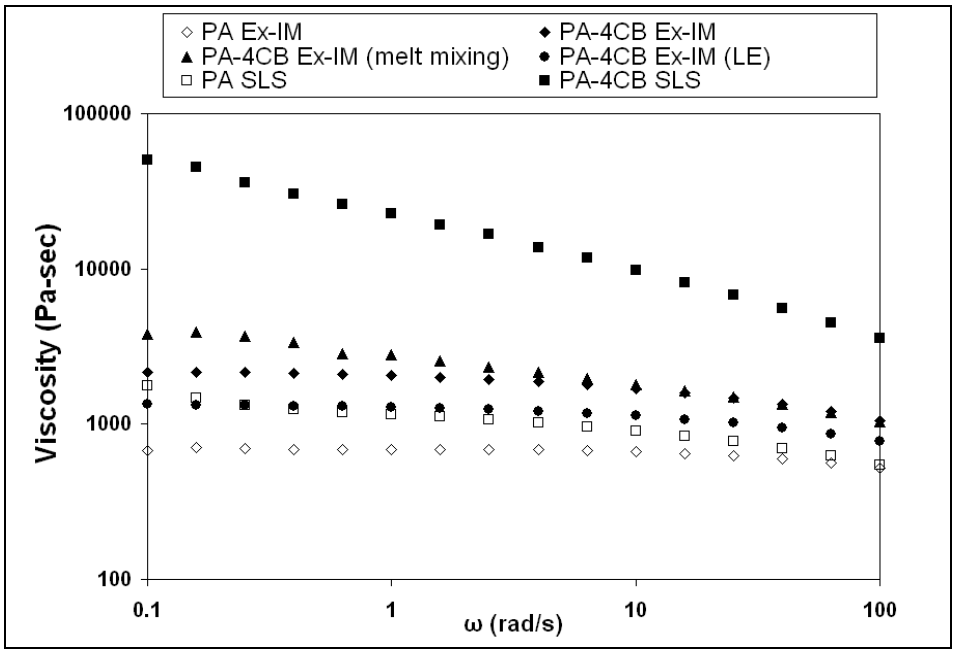

Figure 3.16 Frequency dependence of the viscosity of the various systems.

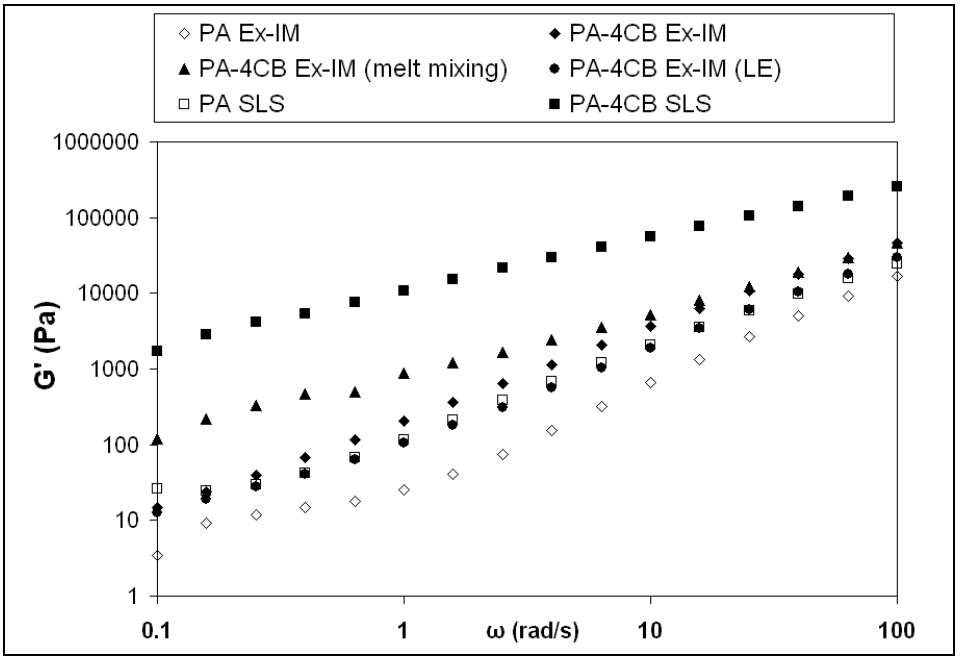

Figure 3.17 Frequency dependence of the storage modulus of the various systems.

The variation of G' and G" for the PA-4CB SLS and PA-4CB Ex-IM systems is shown in Figure 3.18. The moduli for the remaining four systems follow similar trends as

that of the PA-4CB Ex-IM system and have therefore been omitted for the sake of clarity. An important point to be noted is that G" > G' for the PA-4CB Ex-IM system (and similarly for the other four systems) throughout the entire range of frequencies investigated. This denotes a liquid-like viscoelastic behavior. However, only the PA-4CB SLS system exhibits a deviation from this behavior. An intersection of the G' and G" curves is observed at high frequencies. Since the response at high frequencies reflects short-range motions of the polymer chains, an observation that G' > G" indicates that the chains are getting constricted. Similar observations have been made for intercalated clay systems [118]. The Nylon-12 chains can get constricted in the interstitial voids of the carbon black agglomerates. The PA-4CB Ex-IM system which has relatively well dispersed carbon black would have a lower fraction of voids than the highly agglomerated PA-4CB SLS system. This could be a possible explanation for G' being greater than G" at high frequencies for the PA-4CB SLS system.

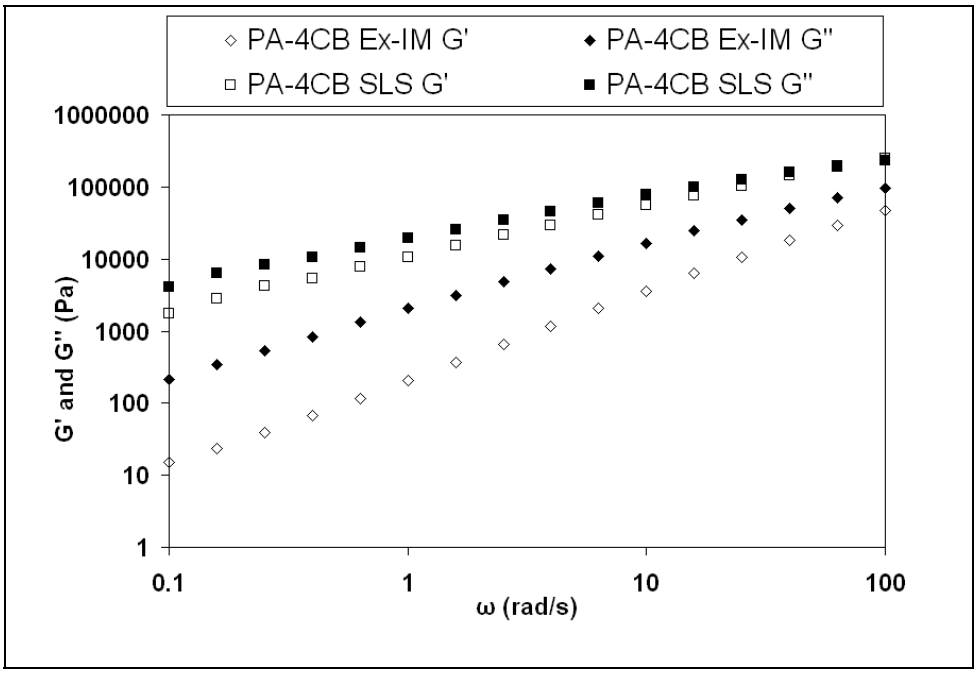

Figure 3.18 Variation of storage modulus and loss modulus with respect to frequency for the PA-4CB SLS and the PA-4CB Ex-IM systems.

3.2.6 Electrical Conductivity

The impedance spectrum of the various systems was measured over frequencies ranging between 0.1 Hz – 100,000 Hz. The impedance was used to calculate the conductivity by using the dimensions of the sample. The variation in the electrical conductivity of the PA SLS and PA-4CB SLS systems with respect to the frequency of the AC voltage is shown in Figure 3.19. The variation in conductivity for the other four systems was similar to that of the PA SLS system and has therefore been omitted for the sake of clarity. It can be seen that the electrical conductivity of the PA-4CB SLS system at low frequencies is approximately five orders of magnitude higher than that of the other systems. Additionally, the conductivity of the PA-4CB SLS system is invariant over the range of frequencies investigated whereas the conductivity of the other five systems increases with increasing frequencies.

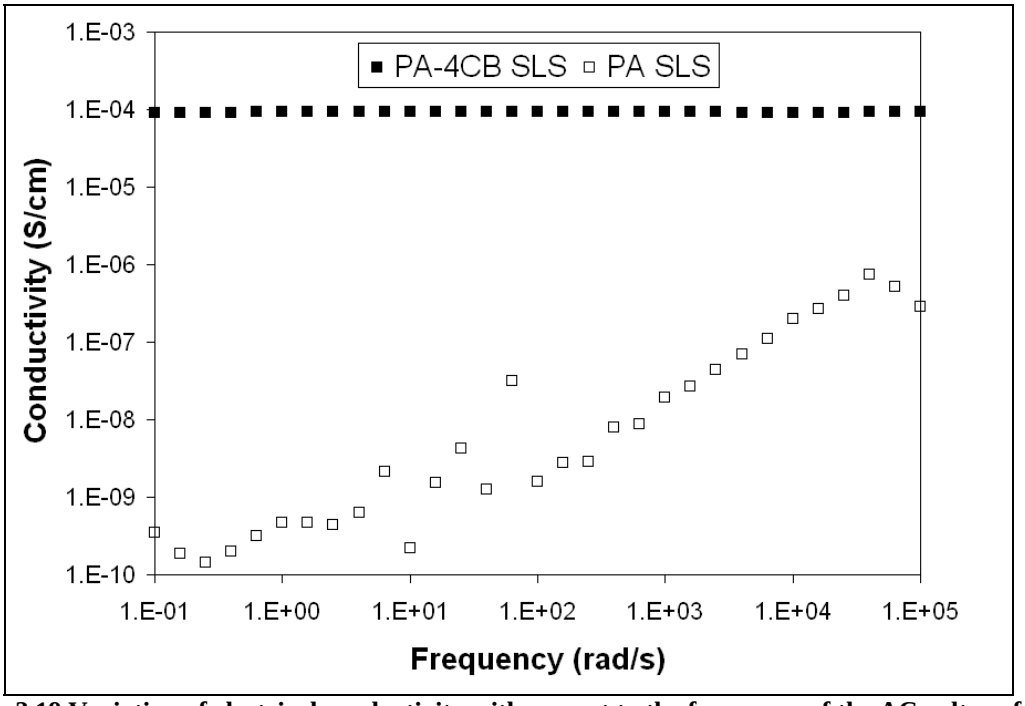

Figure 3.19 Variation of electrical conductivity with respect to the frequency of the AC voltage for the PA SLS and PA-4CB SLS systems.

The results of the impedance spectroscopy for the PA-4CB SLS can be correlated with its microstructure. The relatively higher conductivity and the frequency independence indicate the presence of a network of carbon black particles which are in intimate contact with each other in the PA-4CB SLS system. Transmission optical microscopy of thin sections (Figure 3.11a) and SEM imaging of the fracture surface (Figure 2.9b) of the PA-4CB SLS system indicate the presence of a segregated structure. However, neither of the two techniques give a good perspective of the extent of the network. In order to simulate the process of network formation, a small quantity of the composite powder (approximately 20 mg) was spread evenly into a thin layer on a piece of aluminum foil and placed on a hot stage at 210^{o}C. SEM images of these samples at various time steps are shown in Figure 3.20. Figure 3.20c presents a relatively large field of view (with no pores unlike the fracture surface) of the segregated structure. Though Figure 3.20c does not contain a network that spans the entire field of view, it is important to note that this image would correspond to a single layer in the SLS process. The superposition of multiple layers would increase the probability of the formation of a network of carbon black particles. Moreover, the nature of segregated structure does not suggest the presence of a spatial limit on the extent of network formation.

Similar to the PA-4CB SLS system, the conductivity of the PA-4CB Ex-IM system can also be related to its microstructure. The variation of the impedance with respect to the frequency of the AC voltage exhibits a typical behavior of a system containing conductive particles dispersed (that are not in contact with each other) in an insulating medium. A simplistic representation of such a system is shown in Figure 3.21**.** Carbon black being a conductive particle is represented by a resistor (R_c). The Nylon-12

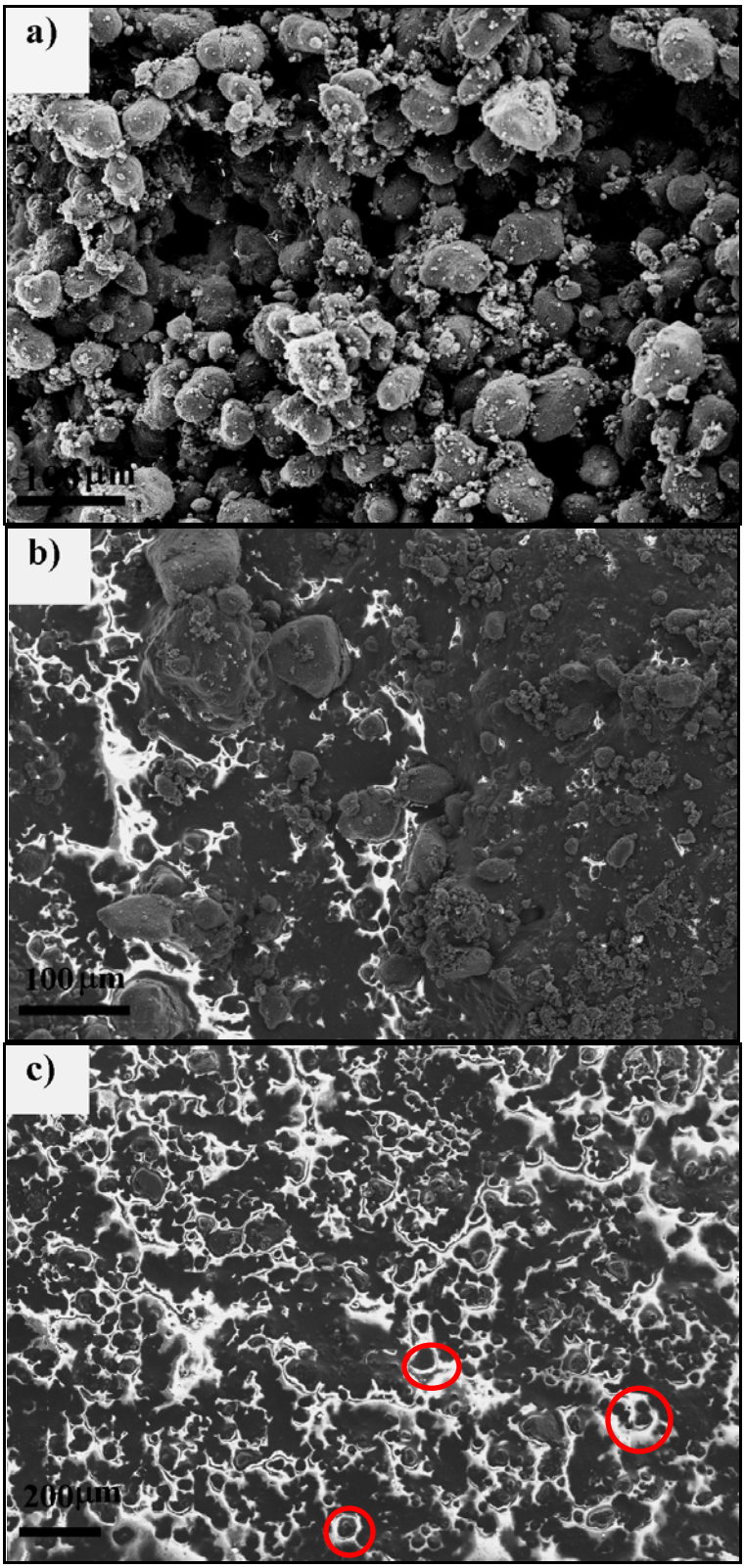

Figure 3.20 SEM images of the composite powder placed on a hot stage at 210°C at the following time steps a) 1 minute, b) 10 minutes, and c) 20 minutes (circled areas correspond to some regions of the microstructure that contain polymer entirely surrounded by carbon black).

matrix being a dielectric material is represented as a capacitor (C_p) and resistor (R_p) in parallel. The value of this capacitance and resistance would depend on the dimension of the polymeric layer between the two carbon black aggregates. At low frequencies, the charge prefers to flow through the polymeric resistor since the impedance due to the polymeric capacitor is relatively higher (since impedance due to a capacitor is inversely proportional to its frequency [119]). However, at high frequencies the impedance due to the capacitor is lower than the polymeric resistance and the charge prefers to flow through the polymeric capacitance. Moreover, since the net impedance of the polymer reduces with increasing frequency, the net impedance of the composite material also reduces with an increase in frequency. The fact that no frequency dependence was observed for the PA-4CB SLS system can be explained by the presence of a network of carbon black agglomerates which are in intimate contact with each other. In such a scenario the resistance of the carbon black agglomerates (which is determined by their structure) is the main contributor to the overall resistance.

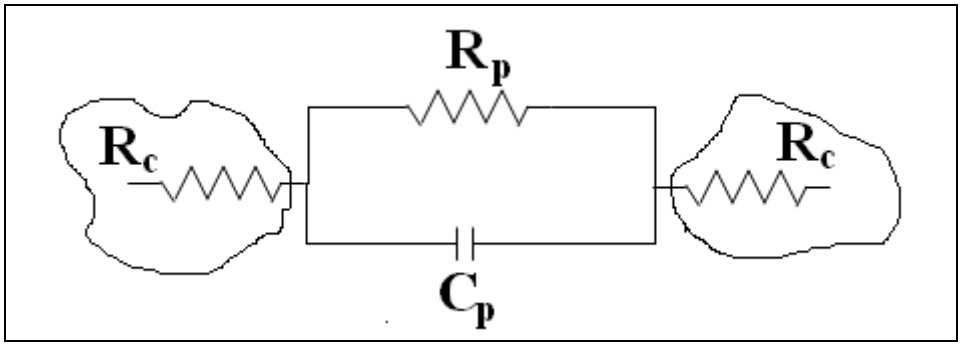

Figure 3.21 Schematic RC representation of an electrically insulating material.

3.2.7 Summary

The state of dispersion of carbon black in Nylon-12-carbon black composites manufactured by SLS and extrusion-injection molding has shown to be an important

factor that affects the final properties. The state of dispersion is greatly dependent on the manufacturing process and the processing conditions. This sub-section summarizes and compares the effects of the SLS process and the extrusion-injection molding process on the microstructure and properties of a Nylon-12-carbon black composite.

The effects of extrusion and injection molding on the microstructure and properties of a carbon black-polymer composite are well documented and have been the subject of many studies. Hence, a brief summary will be provided with the objective of setting the background for the analysis of the SLS process. The first stage of dispersion of carbon black in a polymer melt is the “incorporation” stage which witnesses the diffusion of the polymer chains into the voids of the agglomerates and is accompanied by an increase in the density. The following stage is the “dispersion” stage when the shear forces break down the agglomerates. The third stage comprises the random distribution of the broken down agglomerates/aggregates within the polymer melt. The stages overlap with each other but their relative importance varies with time. The extent of dispersion and distribution depend upon the temperature of the melt, the screw speed, the duration of mixing, and the size distribution of the carbon black agglomerates at the commencement of mixing. During the injection molding stage, the mold temperature, injection speed, injection pressure and holding pressure have a significant effect on the microstructure and properties of the final part. The carbon black acts as a nucleating agent and results in smaller spherulites than those present in the PA Ex-IM system. The use of a MicroInjector with a relatively low packing and holding pressure could be the reason behind PA Ex-IM having an elastic modulus lower than its rated properties [88]**.** The low

pressures could manifest themselves as flow marks on the fracture surfaces as seen in Figure 3.22.

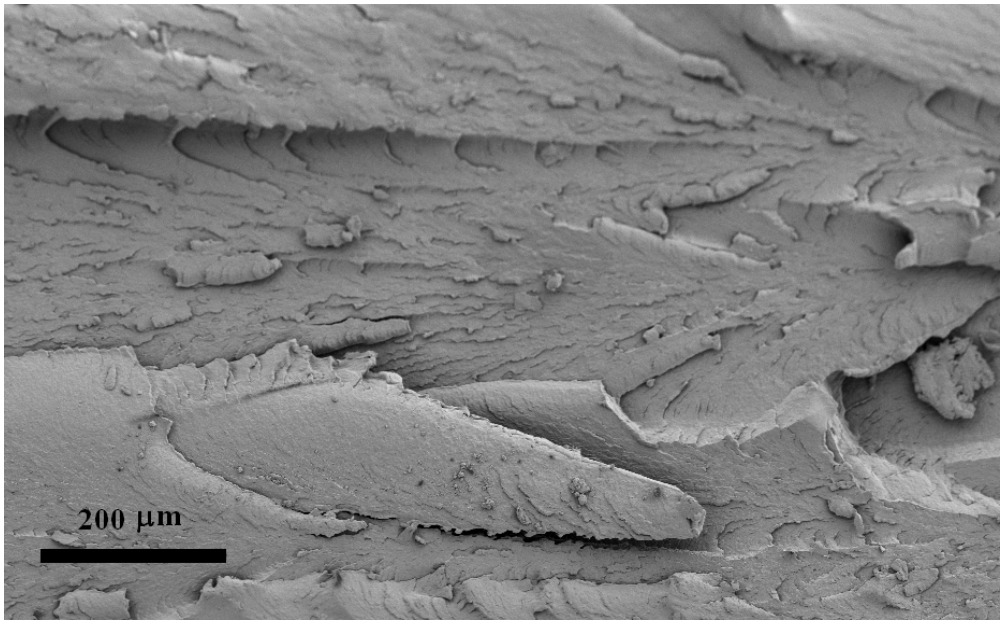

Figure 3.22 SEM image of the fracture surface of PA Ex-IM.

The flexural and tensile moduli of the composite systems manufactured by extrusion-injection molding are greater than those of the PA Ex-IM system. This can be attributed to better dispersion of the carbon black agglomerates as compared to SLS. However, the flexural strength and tensile strength of all the four extrusion-injection molded systems are comparable, indicating weak adhesion between the carbon black and polymer. The presence of relatively large agglomerates in the PA-4CB Ex-IM (melt mixing) system does not have a deleterious effect on its elastic modulus but significantly lowers the impact strength. These results are consistent with earlier studies [103] which have found that the presence of even a few relatively large agglomerates of carbon black can significantly lower mechanical properties such as impact strength and elongation at break.

The effects of the SLS process on the Nylon-12-carbon black composite powder are in sharp contrast with that of the extrusion-injection molding process. The SLS process induces re-agglomeration of the carbon black agglomerates. The re-agglomeration of nanoparticles of carbon in polymer melts and solutions have been studied earlier [50, 120]. The re-agglomeration occurred due to Brownian motion (under conditions of shear at high frequency) or was facilitated by an electric field. However, the length scales and time scales involved in the SLS-processing of a polymer nanocomposite powder seem to indicate that Brownian motion cannot be the mechanism of re-agglomeration. Instead, re-agglomeration appears to be mainly driven by liquid bridge forces between adjacent agglomerates. The presence of polymer in the interstitial voids can be inferred from the relatively high viscosity (Figure 3.16) and by the observation of storage modulus being greater than the loss modulus at high frequencies (Figure 3.18) for the PA-4CB SLS system.

A schematic of the process is shown in Figure 3.23. Upon irradiation by the CO_2 laser, the polymer melt begins to diffuse into the interstitial voids of the agglomerates. The kinetics of diffusion would depend upon the dimension of the voids, the average molecular weight of the polymer, the molten residence time of the melt, and the wettability of the carbon black particles by the polymer. The liquid bridge forces facilitate the re-organization of the polymer and the carbon black agglomerates and form a segregated microstructure. A similar spatial re-organization of nanoparticles by the polymer melt has been reported earlier [121]. Regions of polymer surrounded entirely by carbon black (circled in Figure 3.20c) could be weak spots and be responsible for the presence of voids on the fracture surface of the PA-4CB SLS system as seen in Figure

2.9b. The loading of the carbon black would determine if this segregated structure would form a network. In the absence of carbon black acting as a nucleating agent (refer to section 4.2.2) the nature of crystallization of the domains of polymer would be similar to that of the SLS processing of the neat polymer.

The SLS process has similarities with the process of compression molding. In order to compare the microstructure and mechanical properties of parts made by compression molding, the composite powder was used to fabricate flexure test specimens at a pressure of 1100 psi, a mold temperature of 210^{o}C and a pressing time of 20 minutes. The resulting part had a flexural modulus of 1375 MPa and an elongation at break of approximately 4.16 %. It is important to note that only one specimen was tested (ASTM standards require a minimum of 5 specimens). SEM imaging of the fracture surface (Figure 3.24) indicated the presence of several voids (order of 100μm) as a result of incomplete consolidation of the polymer and the presence of a segregated microstructure similar to the PA-4CB SLS system. An increase in the pressure would result in more complete consolidation and greater penetration of the melt into the segregated carbon black agglomerates resulting in a further increase in the flexural modulus. However, it is unlikely that a significant increase in the pressure would prevent the formation of a segregated microstructure.

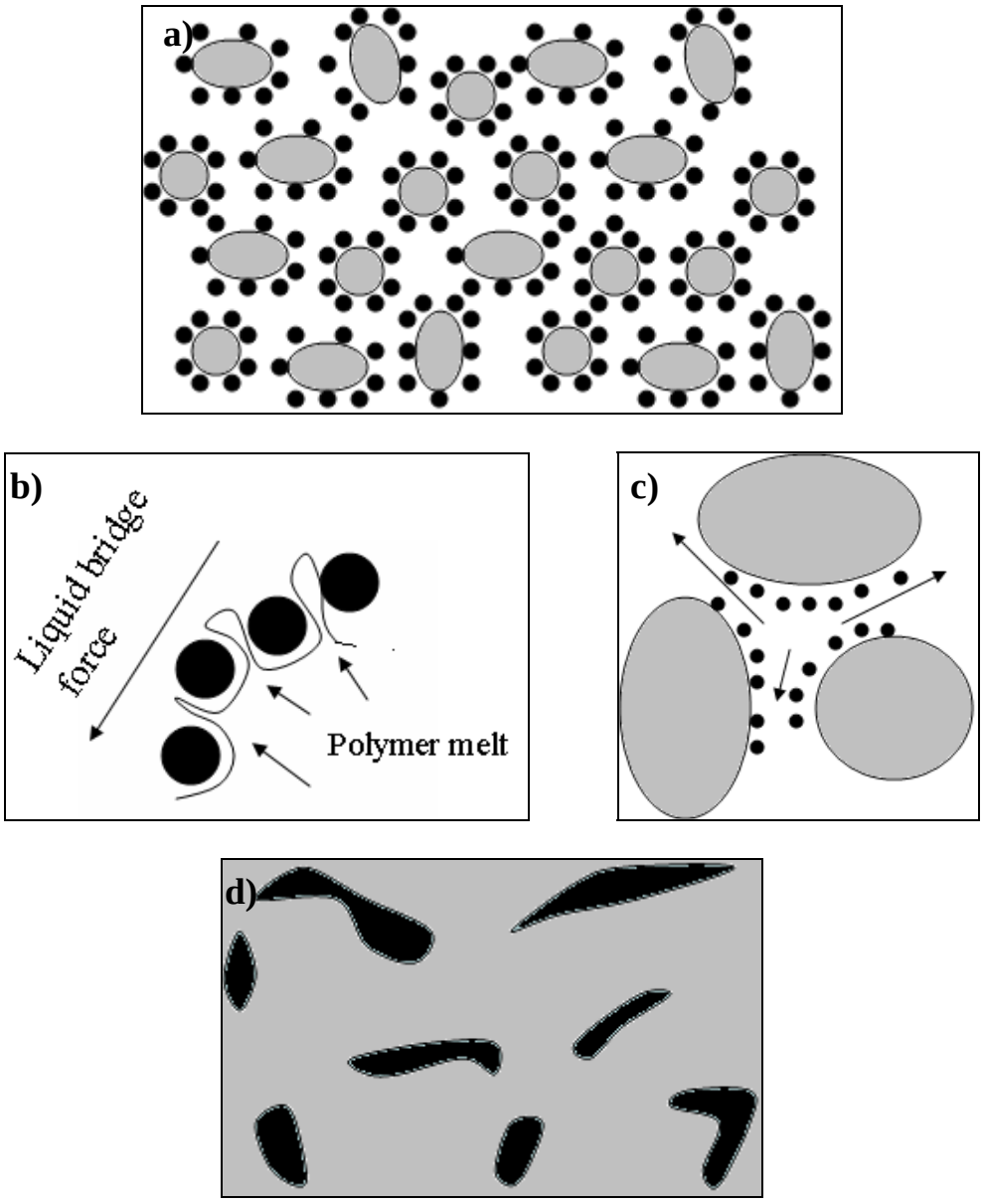

Figure 3.23 Schematic representation of the SLS processing of a polymer nanocomposite powder blend a) composite powder prior to irradiation by CO_2 (grey areas correspond to polymer particles and black areas correspond to carbon black agglomerates), b) Upon irradiation by laser, polymer melt infiltration into interstitial voids of carbon black, c)re-agglomeration of carbon black, and d)formation of segregated microstructure.

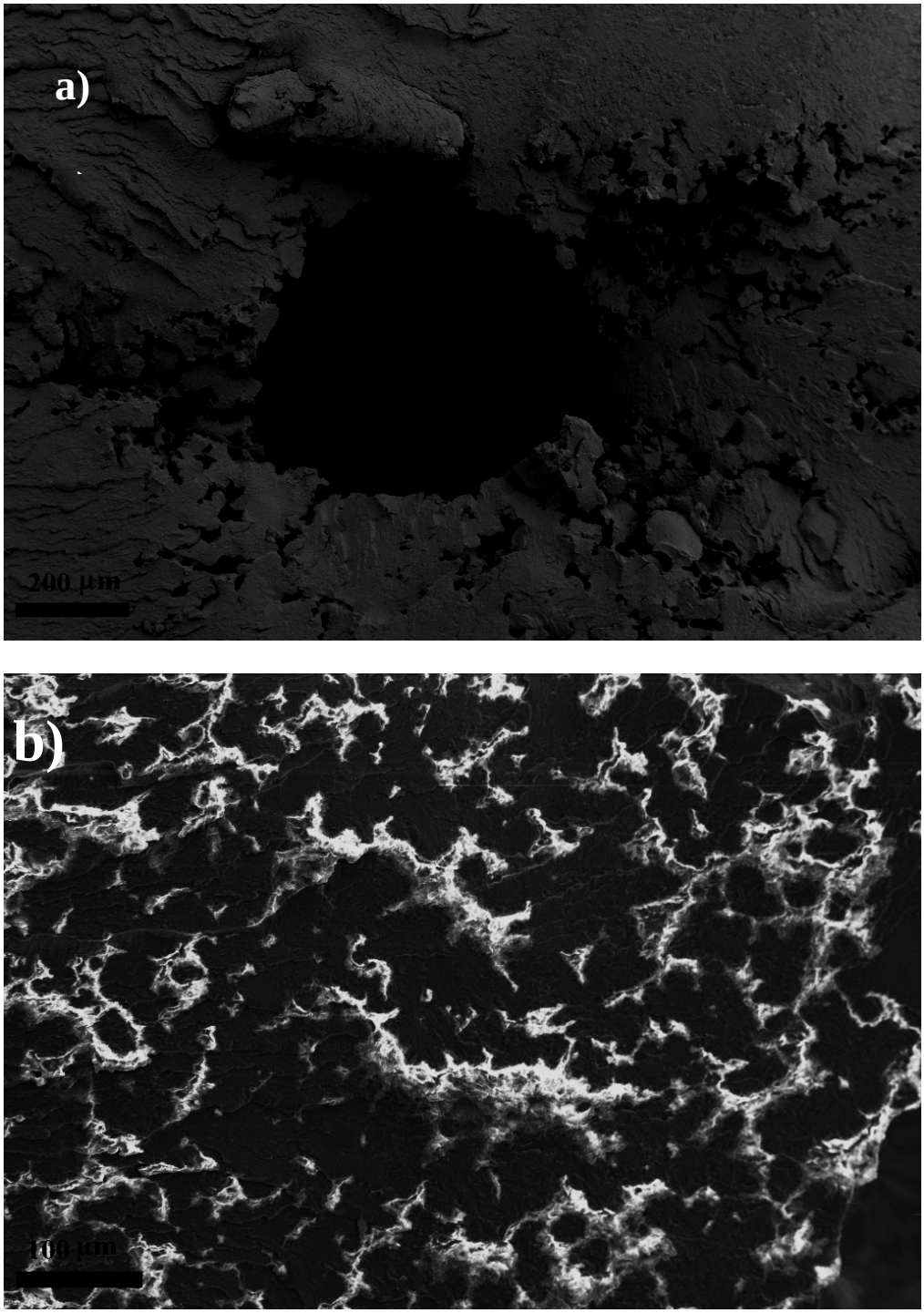

Figure 3.24 SEM images of the fracture surface of compression molded flexure test specimen at 210°C and 1100 psi.

In sum, the formation of a segregated microstructure containing micron-sized domains of low density agglomerates is the principal reason for the elastic moduli of the PA-4CB SLS system being lower than that of the PA SLS system. The presence of

agglomerates is also responsible for the relatively low impact strength of the PA-4CB SLS. It is also important to note that the tensile modulus of the PA-4CB SLS system is lower than the flexural modulus. This could be an indication of imperfect bonding between successive layers in the SLS process which could be exacerbated in the presence of a porous nano-filler. Defects arising due to imperfect bonding between successive layers could be of relatively lower significance in flexure testing (for the mode of loading of parts schematically represented in Figure 3.25) than in tensile testing.

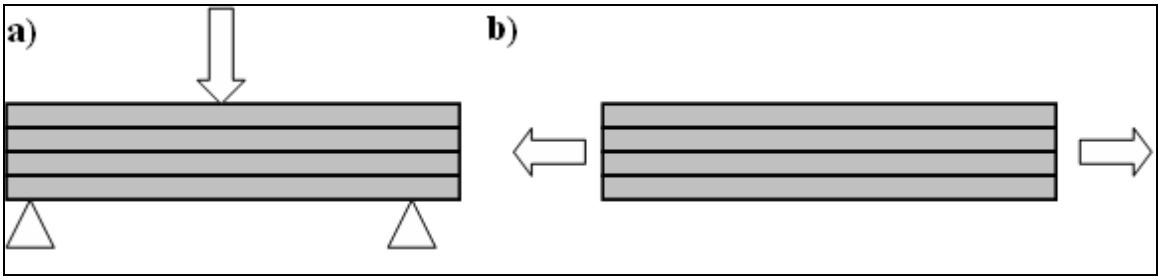

Figure 3.25 Schematic representation of mode of loading in, a) flexure specimen and, b) tensile specimen manufactured by SLS. Each layer in the diagram corresponds to a layer in the SLS process.

3.3 Conclusions

This chapter focused on investigating the thermo-mechanical properties and electrical conductivity of a carbon black-filled Nylon-12 nanocomposite processed by SLS. The properties, microstructure and morphology of parts manufactured by SLS were compared with those made by extrusion-injection molding. The effects of the microstructure, crystalline morphology, porosity and changes in the molecular weight of the polymer on the properties of the composite were studied. The segregated microstructure in the PA-4CB SLS system, containing alternating domains of Nylon-12 and carbon black, was found to have the greatest effect on the mechanical properties and

the electrical conductivity of the composite. The initial size distribution of the carbon black agglomerates and the polymer particles dictates the size and shape of these individual domains. Moreover, results from the porosity analysis indicated that the inherent porous nature of carbon black agglomerates and the presence of this segregated microstructure necessitate a pycnometry-based method to determine part densities. The extrusion process resulted in the breakdown and more uniform distribution of the carbon black agglomerates. The greater extent of dispersion was the reason for enhanced mechanical properties and lower electrical conductivity of the PA-4CB Ex-IM system. This is of significance because extruded pellets of nanocomposites can be cryogenically milled into powders that can processed by SLS. SLS-manufactured nanocomposites obtained from such powders can be expected to have a greater elastic modulus than the neat polymer. The addition of carbon black to Nylon-12 did not change the crystal form or the degree of crystallinity. Moreover, carbon black served as a nucleating agent only in the case of the composites manufactured by extrusion-injection molding.

CHAPTER 4 SLS PROCESS MODELING

The SLS process employs thermal energy to selectively consolidate regions of a powder bed. Models of varying complexity have been developed to study the effects of the SLS parameters on the sintering process. The earliest models that were developed by Sun [122] and Nelson [123] employed a one-dimensional (1-D) thermal conduction model coupled with an empirically derived sintering rate equation to study the effects of the SLS process parameters on the sintering depth and changes in the density of amorphous polymers during laser sintering. The 1-D model was also modified to study thermal degradation of the polymeric binder during the laser sintering of composite materials [124]. Subsequently, two-dimensional (2-D) and three-dimensional (3-D) models were developed to study the temperature evolution and changes in density within parts built using amorphous polymers. Recently, the empirical sintering law was extended to Nylon-12 and Nylon-12-glass bead composites and the predicted densities were compared with experimental results [125, 126]. A 3-D model might appear to be necessary to accurately model the SLS process. However, earlier studies [127] have shown that a 1-D approximation is valid when the non-dimensional parameter N, as defined below in equation 4.1 is significantly greater than 3.9.

$$N = \frac{S\omega}{\alpha_d} \tag{4.1}$$

where S is the laser scan speed, ω is the beam radius and α_d is the thermal diffusivity of the powder bed. A beam diameter of approximately 400 μm, scan speeds in the range of 0.762 m/s – 1.524 m/s and a thermal diffusivity of 6.2×10^{-8} m^2/s for Nylon-12 [125] yield

a value greater than 2000 for the parameter N. The approximation remains valid even in the case of the Nylon-12/carbon black (4 wt. %) nanocomposite. Hence, this chapter focuses on a 1-D thermal model coupled with sintering-induced densification and thermal degradation of the polymer. The objective of this chapter is to apply and validate the methodology developed by Childs et al [126] to study the densification of a Nylon-12/carbon black nanocomposite during the SLS process and to correlate theoretical predictions of the density with experimental measurements.

4.1 Theoretical background

This sub-section provides a brief summary of the theoretical background of the modeling methodology used in this study. A more detailed description can be found elsewhere [12, 124, 125]. The unsteady 1-D energy balance equation is given by the following:

$$\rho(T)C_p(T)\frac{\partial T}{\partial t} = \frac{\partial}{\partial z}\left(k\frac{\partial T}{\partial z}\right) + G(z,t) \tag{4.2}$$

The boundary conditions are:

$$-k\frac{\partial T}{\partial z} = \alpha < I > -h\left(T - T_{amb}\right); \qquad z = 0, t \le \tau \tag{4.3}$$

$$-k\frac{\partial T}{\partial z} = -h\left(T - T_{amb}\right); \qquad z = 0; t > \tau$$

$$\frac{\partial T}{\partial z} = 0 \quad ; \quad z = z_{bottom}, t > 0$$

where $\rho(T)$ is the powder bed density, $T(z,t)$ is the temperature at a depth z below the powder bed surface and at time t, $<I>$ is the average energy input from the laser beam, α is the absorptivity of the powder bed, k is the effective thermal conductivity, $C_p(T)$ is the

effective heat capacity, τ corresponds to the duration that a certain region of the powder bed is exposed to the laser beam, *h* is the combined radiative and convective heat transfer coefficient, and T_{amb} is the ambient temperature in the SLS process chamber. The term *G(z,t)* represents a heat sink/source due to phase change and thermal degradation of the semi-crystalline polymer. The boundary conditions shown in equation 4.3 account for the flux from the laser, energy losses at the powder bed surface due to convection and radiation and an assumption of zero heat loss at the bottom of the simulated powder bed.

Table 4.1 Summary of thermal property data used for the simulations

Nylon-12		
Material property	Value	Reference
Thermal conductivity	0.25 W/m-K	[88]
Specific heat	(460+7.8T) J/Kg-K	[126]
Absorptivity	0.8	[125]
Emissivity	0.8	[125]
Material density	1020 Kg/m^3	[88]
Powder density	480 Kg/m^3	Tap density
Carbon black		
Thermal conductivity	0.05 W/m-K	[128]
Specific heat	650 J/Kg-K	[128]
Absorptivity	1	[102]
Emissivity	1	[102]
Material density	1800 Kg/m^3	[129]
Powder density	80 Kg/m^3	Tap density

The laser beam was modeled as a circular energy source with a Gaussian intensity profile and a 1/e^2 radius ω, as given by:

$$I(r) = \frac{2P}{\pi\omega^2}\exp\left(-\frac{2r^2}{\omega^2}\right) \tag{4.4}$$

where P is the laser power and r is the radial distance from the center of the beam. During the laser sintering process, any given point on the surface of the powder bed may receive

more than one energy pulse as the laser scans successive lines in a raster pattern. This is determined by the laser scan spacing as well as the radius of the laser beam. In this study (with a beam diameter of 400 μm and a scan spacing of 150 μm), the model was developed in a manner such that any point on the surface of the powder bed would receive distinct energy pulses from three adjacent scan lines. This process is schematically depicted in Figure 4.1.

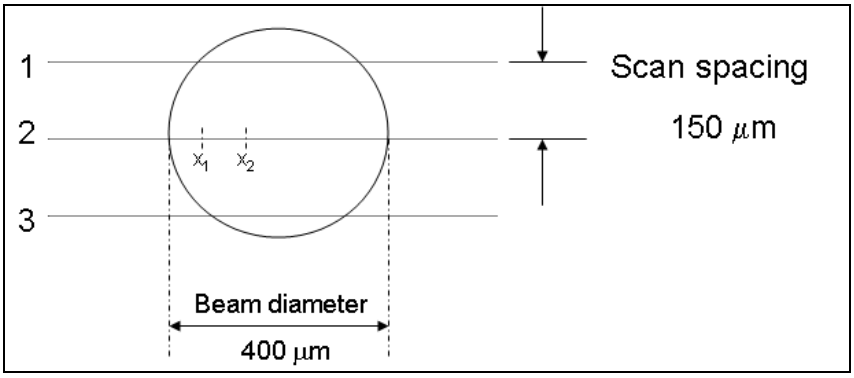

Figure 4.1 Schematic representation of a point on the surface of the powder bed receiving multiple energy pulses from three adjacent scan lines (x_1 and x_2 denote two points along a particular scan line).

The schematic representation shown above can be used to calculate the average intensity (<I>)of the beam between points x_1 and x_2 as follows:

$$< I >= \frac{\int_{x_1}^{x_2} \frac{2P}{\pi\omega^2} \exp\left(-\frac{2r^2}{\omega^2}\right) dx}{\int_{x_1}^{x_2} dx} = \frac{P}{\pi\omega|x_1 - x_2|}\sqrt{\frac{\pi}{2}}\frac{erf\left(\sqrt{2}x_2/\omega\right) - erf\left(\sqrt{2}x_1/\omega\right)}{\exp\left(2H^2/\omega^2\right)} \quad (4.5)$$

where H is the hatch spacing of the laser, taken to be 151.4 μm (6 mils). The distance $|x_1 - x_2|$ is determined by the laser scan speed and Δt, the time step of the simulation. In

order to ensure an accurate description of the transient temperature response, Δt in the simulation has to be chosen such that $|x_1 - x_2| << \omega$.

The thermal conductivity, specific heat and the density are functions of temperature and porosity of the powder bed and were calculated at every time step of the simulation. The material properties used in this study are listed in Table 4.1.The effective specific heat and thermal conductivity of the composite were calculated as the weight average of the individual specific heats (and thermal conductivities) of the component phase (in this case, the Nylon-12 and the carbon black). Since the weight fraction of air is negligible, the specific heat of the powder bed is the same as that of the fully dense material. The thermal conductivity of the powder bed was determined by using the Yagi and Kunni equation [130] as shown below:

$$k_{powder} = \frac{\beta(1-\varepsilon)k_{eff}}{1+\varphi\frac{k_g}{k_{eff}}} \tag{4.6}$$

where β=1, φ=0.034 [124] and k_g is the thermal conductivity of the gas within the powder bed (in this study, the gas is nitrogen) used for environment control in the SLS machine. The Yagi-Kunni equation accounts for the effective thermal conductivity of the composite, the void fraction, the shape of the powders and the effects of the surrounding gas. The density of the powder bed was related to the density of the fully dense material using the following relation:

$$\rho = \rho_{eff}(1-\varepsilon) \tag{4.7}$$

where ε is the porosity of the powder bed. During the SLS process, the density of the powder bed changes due to sintering as well as thermal degradation. A change in the porosity of the powder bed during a time step Δt is given by:

$$\varepsilon_{new} = \varepsilon_{old}(1 - s\Delta t) \tag{4.8}$$

where s is the sintering rate determined by the following relation:

$$s = A_s \exp\left(-\frac{E_s}{RT} - \beta X\right) \tag{4.9}$$

where A_s is the Arrhenius rate constant for sintering, E_s is the activation energy, R is the universal gas constant, T is the temperature and β and X are factors that account for the phase change during melting and solidification [126]. The use of these factors lends validity to the assumption that the latent heat L is neither absorbed nor released during melting or solidification and has its basis in a temperature recovery method [131]. The factor X is assigned a value of 1 until commencement of melting and is linearly reduced to a value of 0 upon completion of melting.

The change in density due to thermal degradation of the polymer was handled in a manner similar to that of sintering induced densification as described above in equations 4.8-4.9. Linear kinetics were assumed and the change in density of the powder bed during a time step Δt was determined using the following relation:

$$\rho_{new} = \rho_{old}(1 - k\Delta t) \tag{4.10}$$

where k is the rate determined by the following relation:

$$k = A_d \exp\left(-\frac{E_d}{RT}\right) \tag{4.11}$$

where A_d is the Arrhenius rate constant for thermal degradation, E_d is the activation energy, and R and T are as described above. Moreover, the model assumed that the term G(z,t) in equation 4.2 is effectively zero for the energy densities employed in this study. This implies that most of the energy from the laser is used to heat the powder bed.

The initial values for A_s, E_s and β (equation 4.9) for neat Nylon-12 were obtained from the results of earlier studies [125, 126] and are shown in Table 4.2. Subsequently, the parameters of neat Nylon-12 were varied in accordance with the results of the sensitivity analysis performed by Childs et al [126] in order for the results of the model to match the experimental results of porosity obtained in this study. The parameters for the Nylon-12/carbon black system were varied according to the procedure outlined in the study by Childs et al in which the authors successfully tested the assumption that the addition of a filler to a polymer would change only the rate constant (A_s) and not the activation energy (E_s) for sintering. However, this may not be true for all material systems. Badrinarayan reported an increase in activation energy of approximately 20% for a polymethylmethacrylate (PMMA)-silicon carbide (25 vol. %) system over the neat PMMA system [132]. The aim of this model is to test this assumption for the Nylon-12/carbon black (4wt. % corresponding to 20 vol. %) system. The rate constant of the filled system was varied from that of the neat Nylon-12 system in an inverse proportion to the melt viscosities of the two systems. The ratio of the filled system to the unfilled was determined by using the Mooney equation which has been shown to describe the viscosity of a wide range of suspensions [133].

$$\ln\left(\frac{\eta}{\eta_1}\right) = \frac{k_E \phi}{1 - \phi/\phi_m} \tag{4.12}$$

where η and η_1 correspond to the viscosity of the filled and un-filled systems, ϕ corresponds to the volume fraction of the filler (20 % in this case), ϕ_m is the theoretical maximum volume fraction (taken to be 0.60) and k_E (taken to be 2.5) is the Einstein co-efficient [133].

4.2 Computer implementation

The model described above was implemented using the PDE toolbox in MATLAB®. The simulation code is listed in Appendix A. The code was designed to handle multiple layers using the procedure outlined by Vail [124]. It allowed for all necessary data to be input prior to execution. A time step of 25 μs was sufficient to accurately capture the transient temperature response. A powder bed depth of 1016 μm (40 mils) was sufficient to satisfy the Neumann boundary condition at the bottom. A schematic diagram of the simulated powder bed is shown in Figure 4.2**.** The top-most node point in Figure 4.2 lies within a scan area as shown in Figure 4.3. Upon completion of scanning of one layer, a delay time of 30 seconds was provided prior to the commencement of scanning on the next layer to realistically represent the time taken to deliver a new layer of powder on top of a previously processed layer. The simulated powder bed of 1016 μm (40 mils) (equivalent to ten layers in the SLS process conducted with 101.6 μm (4 mils) thick layers) was discretized into one hundred node points (each node point is equivalent to 10.16 μm (0.4 mils) of the powder bed). Henceforth in this chapter, all results pertaining to porosity (or density) will represent average values for one layer in the SLS process (10 node points in the simulation).

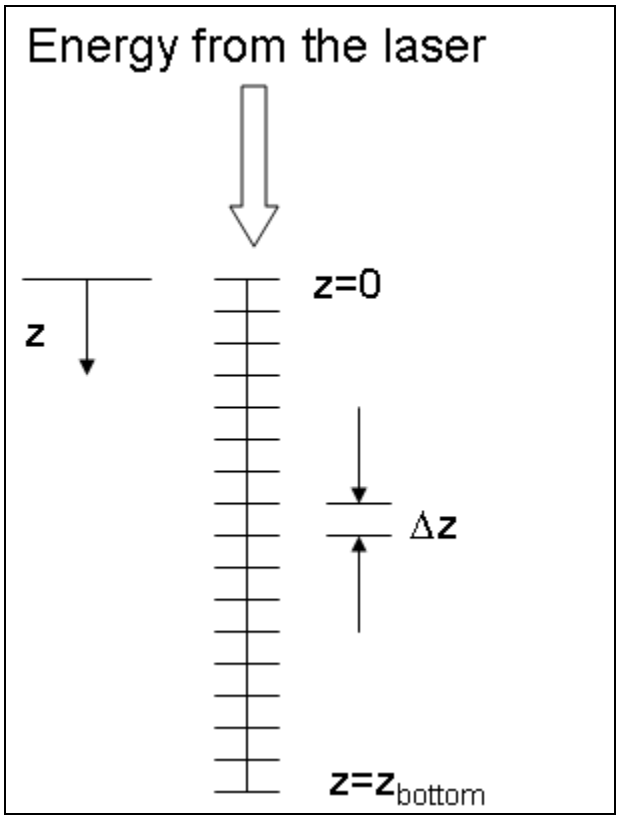

Figure 4.2 Schematic representation of the simulated powder bed.

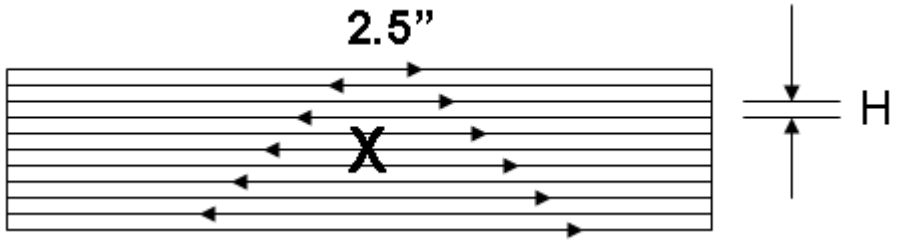

Figure 4.3 Schematic diagram of scanned area in the simulation (‘X” corresponds to the top-most node point in the simulated powder bed) illustrating raster scanning with spacing (H = 152.4 μm) and vector length of 2.5”.

4.3 Results and Discussion

4.3.1 Determination of Rate Constants

The rate constants A_s, E_s and β in equation 4.9 can be obtained by performing isothermal sintering experiments as outlined by Nelson [123]. However, in the absence of

a sintering cell, the initial choice of parameters was made by referring to the results of earlier studies [125, 126] which were obtained by fitting the results of their model to experimentally obtained values of part density. A similar approach was followed in this study. The sensitivity analysis performed by Childs [126] indicated that the activation energy E_s and the choice of the parameter β had a greater effect on the simulated part density than the rate constant A_s. In this study, the effects of varying E_s and β (from the initial choice [125, 126] as shown in Table 4.2) on the simulated density of the top layer of a Nylon-12 part fabricated with a laser power of 3.08W and scan speed of 0.762 m/s (the optimal parameter set for the PA SLS system) were studied. The criteria for the final choice of E_s and β were as follows:

a) Depth of sintering should not exceed two layers for a laser power of 3.08W and scan speed of 0.762 m/s.

b) A laser power of 3.08W and scan speed of 0.762 m/s should result in complete densification of the top-most layer in the Nylon-12 system, as has been experimentally determined. A constraint on the number of layers permitted to achieve complete densification was not placed.

The choice of E_s determined the extent of densification of the top layer prior to the commencement of the next layer whereas the parameter β was found to have a significant effect on the depth of sintering because it controls the extent of retardation of the polymer as it undergoes melting/crystallization. Decreasing the value of β was found to increase the depth of sintering irrespective of the choice of E_s. The effect of varying E_s and β on the predicted density of the top layer is shown in Figure 4.4. The effect of β on the powder bed density for an activation energy of 98.5 kJ/mol is shown in Figure 4.5. It

can be seen that a choice of β less than 6 resulted in significant densification beyond three layers. Based on these initial results, the choice of E_s and β were finalized and are listed in Table 4.2. The results of multi-layer simulations using values of E_s and β listed below indicated a negligible increase in densification beyond the first layer as shown in Figure 4.6. This implies that a significant degree of densification within a given layer occurs prior to the delivery of the subsequent layer in the SLS process. Hence, all results of predicted part densities that are reported in this chapter were obtained from single layer simulations.

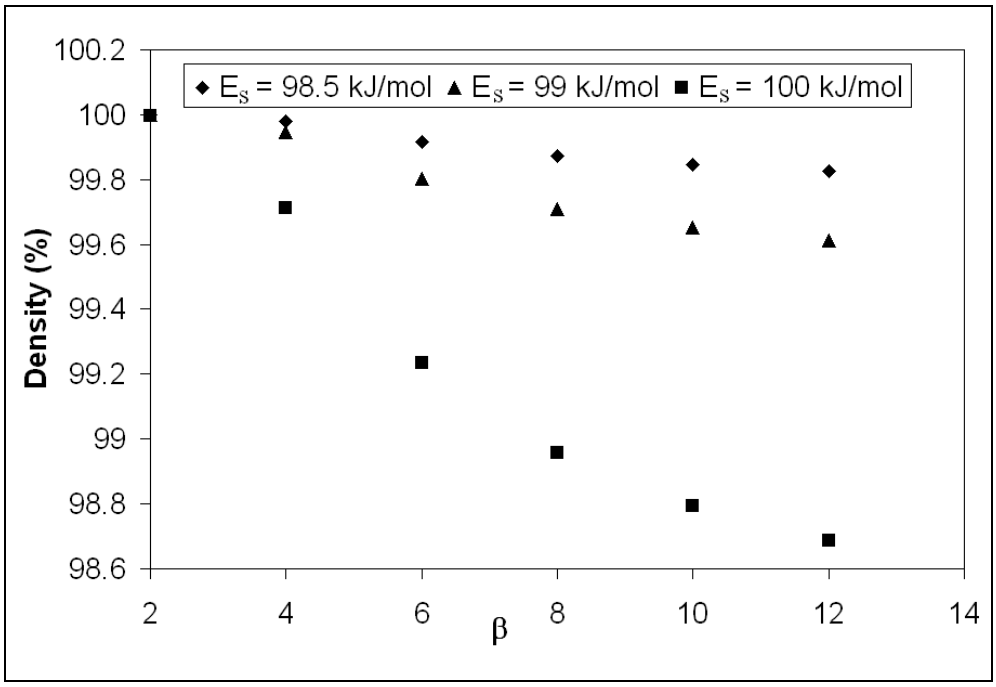

Figure 4.4 Variation of predicted average density of the top layer (for PA SLS as a function of β for different activation energies (E_s) for sintering) at a laser power of 3.08 W and scan speed of 0.762 m/s.

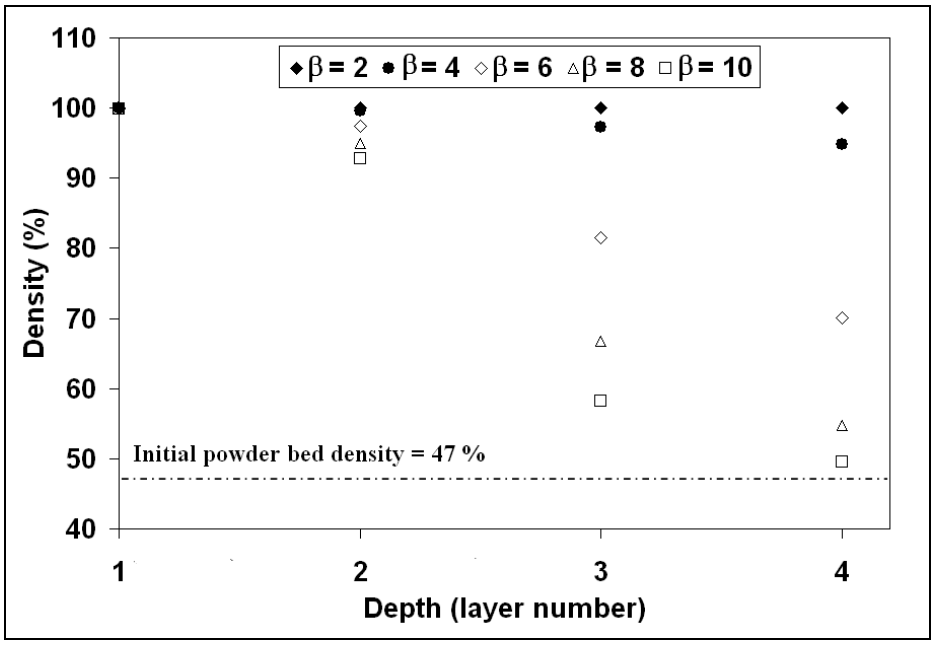

Figure 4.5 Predicted average density as a function of depth from the powder bed surface for the PA SLS model (for different values of β at a laser power of 3.08 W, scan speed of 0.762 m/s, and activation energy of 98.5 kJ/mol) prior to commencement of scanning of the second layer in the SLS process. Values on the x-axis denote the layer number (each 101.6 μm in the SLS process) from the top of the powder bed.

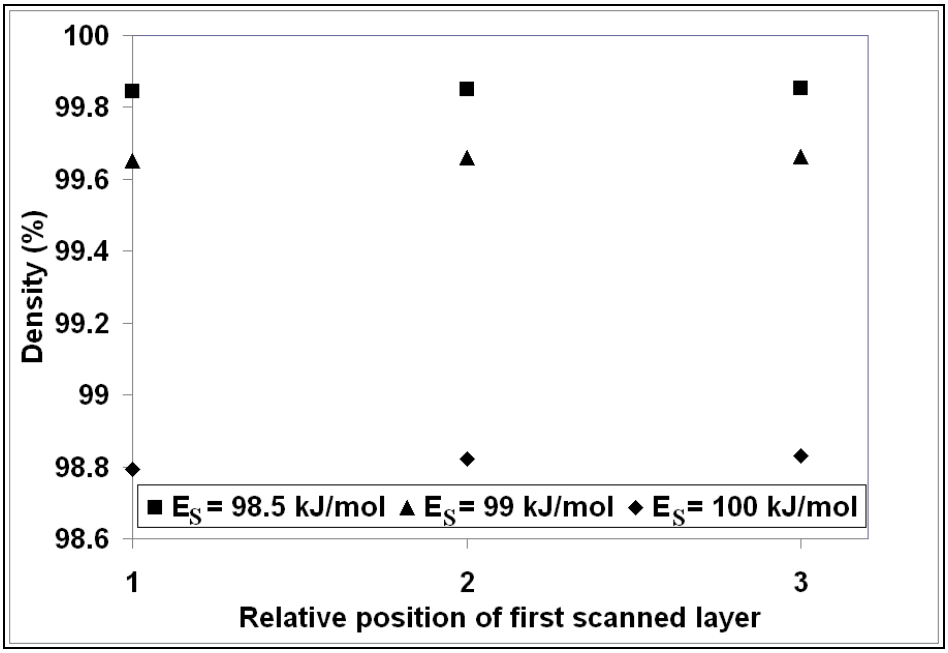

Figure 4.6 Predicted average density of the first scanned layer as a function of its position from the top of the powder bed (for various activation energies for sintering (PA SLS) at a laser powder of 3.08 W and scan speed of 0.762 m/s). Values on the x-axis denote the relative position (in layers) of the first scanned layer with respect to the top of the powder bed in a multi-layer simulation.

The rate constants A_d and the activation energy E_d (in equation 4.11) for the thermal degradation of the neat Nylon-12 powder and the composite powder were calculated by performing isothermal degradation studies as outlined by Vail [124] using a Seiko TG/DTA 320 system in a nitrogen atmosphere. The initial rate of normalized weight loss at each given temperature (300°C to 500°C, in steps of 50°C) was plotted against the inverse of the temperature as shown in Figure 4.7 to yield the constants in equation 4.11.

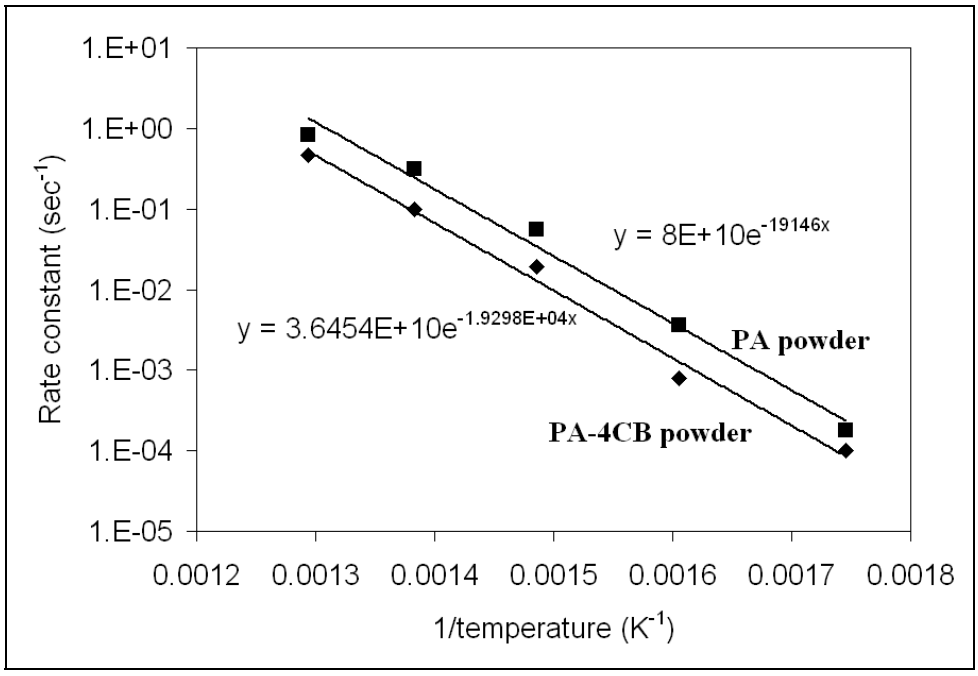

Figure 4.7 Thermal decomposition rate constants for neat PA powder and PA-4CB powder.

Table 4.2 Summary of the constants in the rate equations for sintering and thermal degradation

Value	PA SLS	PA-4CB SLS	Childs [126]	Sun [125]
A_s (s^{-1})	5 x 10^{11}	2.36 x 10^{11}	5 x 10^{11}	5 x 10^{11}
E_s (kJ/mol)	98.5	98.5	103	149.66
β	10	10	10	8
A_d (s^{-1})	8 x 10^{10}	3.64 x 10^{10}	N/A	N/A
E_d/R (K)	19298	19146	N/A	N/A

4.3.2 Dependence of Part Density on Energy Density of the Laser

The variation of the predicted part density with respect to entire range of energy densities (refer to Table 2.1 and Table 2.2) employed in this study for the PA SLS and PA-4CB SLS systems are shown in Figure 4.8. It should be noted that those combinations of laser powers and scan speeds that gave identical energy densities yielded comparable values of predicted part density and have therefore been omitted in Figure 4.8. The differential absorption of the laser in Nylon-12 and carbon black was not considered while performing the simulations for the PA-4CB SLS system. This could be an important phenomenon that affects the thermal degradation of Nylon-12 and is discussed in the following sub-section.

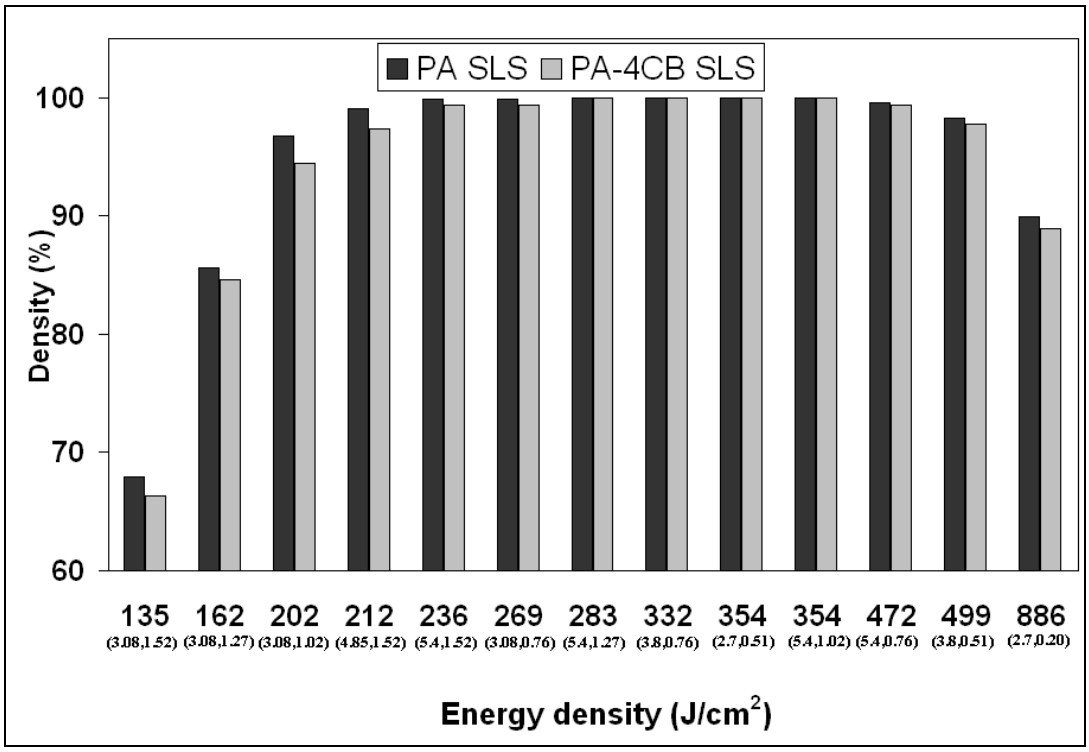

Figure 4.8 Variation in predicted average density (as a percentage of theoretical density) of the top layer for the PA SLS and PA-4CB SLS systems with respect to the energy density of the laser beam. Numbers within brackets on the x-axis denote laser power in watts and scan speed in m/s.

The results of part densities for the PA SLS system are in reasonably good agreement with the experimental results of the variation of flexural modulus as shown in Figure 2.6a as well as the expected trend as shown in Figure 2.11. The significantly lower values of flexural modulus for energy densities lesser than 269 J/cm^2 (3.08W, 0.762 m/s) are a direct consequence of incomplete densification. As the energy density increases beyond 269 J/cm^2, the density remains constant at a maximum value of nearly 100 % and subsequently begins to drop due to thermal degradation. The maximum predicted value of thermal degradation in the PA SLS system (for the range of parameters investigated and given in Table 2.1) is around 0.5 % corresponding to an energy density of 472 J/cm^2 (5.4W, 0.762 m/s).

The variation in predicted part density of the PA-4CB SLS system follows the same trend as that of the PA SLS system The relatively lower predicted part densities (at the lower end of the spectrum) are a consequence of the lower sintering rate for the PA-4CB SLS system. The relatively greater extents of predicted thermal degradation (at the upper end of the spectrum) are a consequence of higher temperatures in the powder bed which is a result of a lower effective thermal conductivity and a lower specific heat for the composite powder in comparison with that of the Nylon-12 powder.

The predicted part densities for the PA-4CB SLS system shown in Figure 4.8 are greater than the experimentally determined values of part density as shown in Figure 2.12. The sample preparation technique creating artifacts on the surface of the specimen could be a reason for the relatively lower densities. Another likely reason for this observation is that the model for the PA-4CB SLS system considered effective material properties and did not account for differential absorption of the energy from the laser

beam as well as the differences in thermo-physical properties of Nylon-12 and carbon black. The model described above treats the PA-4CB composite powder as a homogenous material and does not take into consideration the discrete temperature spikes that a Nylon-12 particle would experience on its surface due to carbon black-induced localized heating. The following subsection studies this phenomenon by suitably modifying the model described above.

4.3.3 Effect of Carbon Black on Thermal Degradation of the Polymer

The objective of this subsection is to investigate the magnitude of the temperature spike that a Nylon-12 particle would experience on its surface due to carbon black-induced localized heating. The objective was achieved by modifying the model described above and is schematically represented in Figure 4.9. It is compared with the models that were used to study the PA SLS and PA-4CB SLS systems. The modified model consisted of carbon black only on the top-most node point of the discretized powder bed with Nylon-12 powder present on all underlying node points.

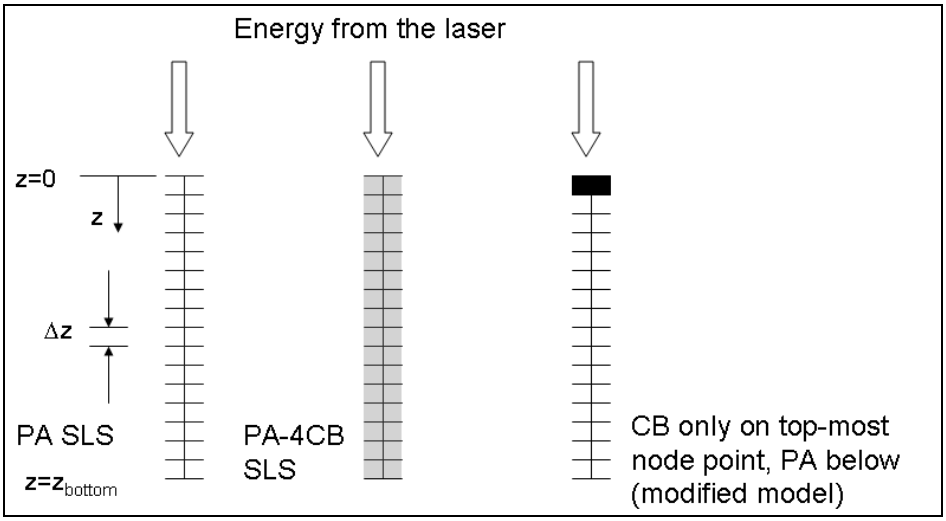

Figure 4.9 Schematic diagram of the modified model in comparison with the PA SLS and PA-4CB SLS models used to study the effect of carbon black-induced localized heating on thermal degradation of Nylon-12.

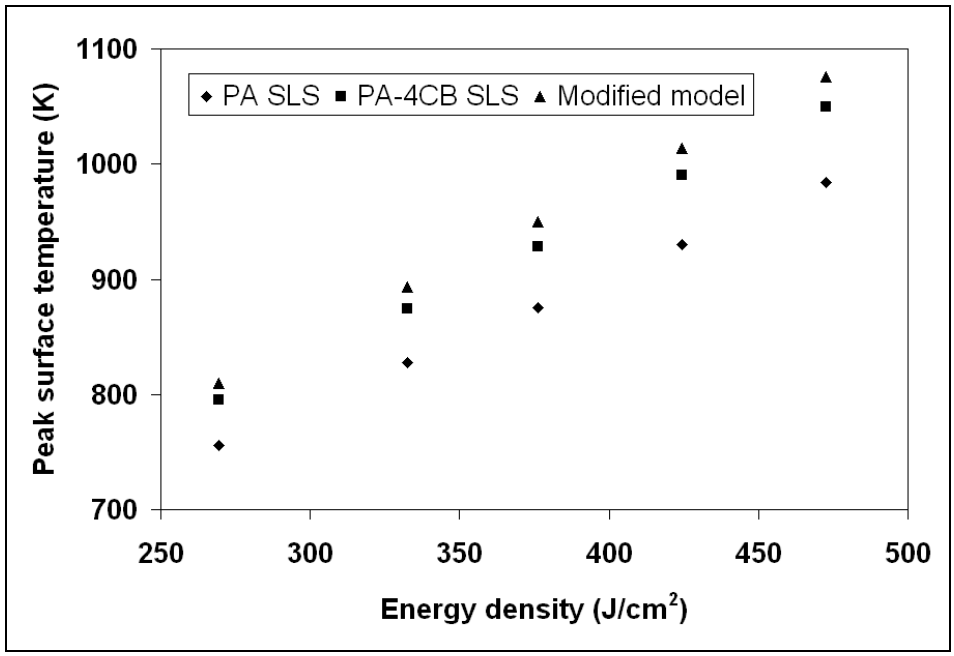

Figure 4.10 Variation in predicted peak surface temperatures in the modified model, PA SLS model, and PA-4CB SLS model with respect to the energy density.

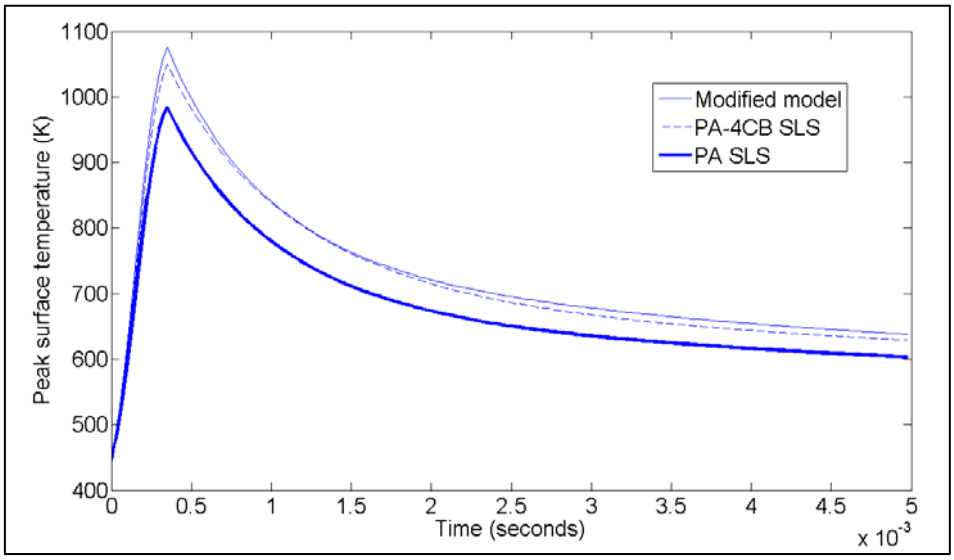

Figure 4.11 Variation in predicted surface temperatures in the modified model, PA SLS model, and PA-4CB SLS model at an energy density of 472 J/cm^2.

The variation in the predicted peak surface temperatures for the PA SLS system, PA-4CB SLS system, and the modified system with respect to energy density is shown in Figure 4.10. The predicted surface temperature at an energy density of 472 J/cm^2 is shown in Figure 4.11. It can be seen that for a given energy density, the modified system

and the PA SLS system experienced the highest and lowest peak surface temperatures, respectively. Higher temperatures can be attributed to a lower thermal conductivity, a lower specific heat, and a higher absorptivity of the material.

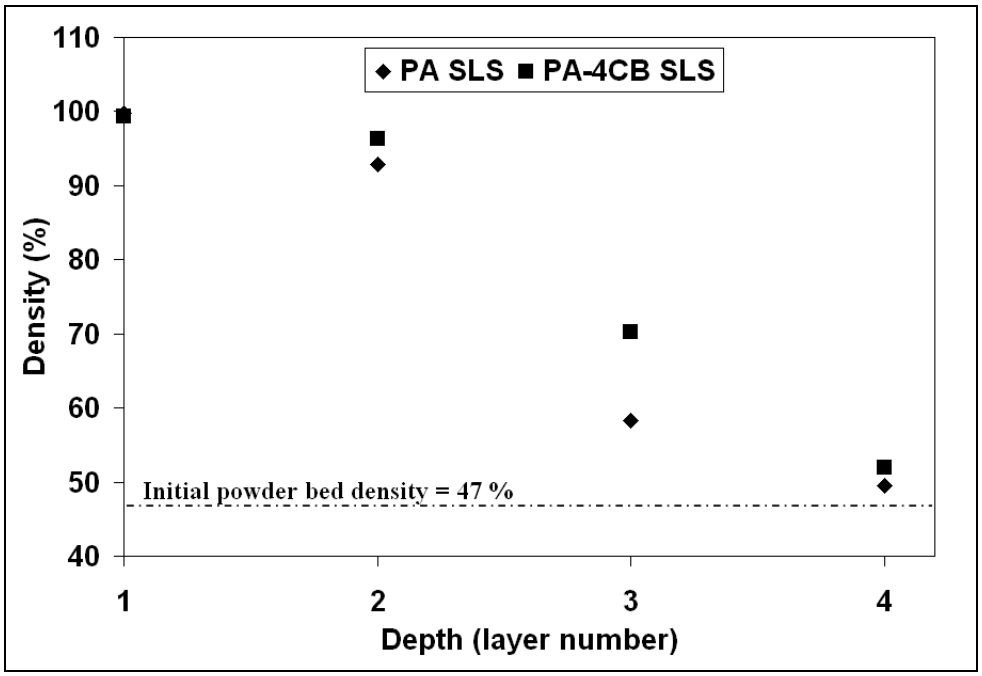

Figure 4.12 Predicted average density as a function of depth from the powder bed surface for the PA SLS and PA-4CB SLS systems (for different values of β at a laser power of 3.08 W, scan speed of 0.762 m/s, and activation energy of 98.5 kJ/mol) prior to commencement of scanning of the second layer in the SLS process. Values on the x-axis denote the layer number (each 101.6 μm in the SLS process) from the top of the powder bed.

The higher predicted surface temperature for the PA-4CB SLS system resulted in a higher predicted depth of sintering as shown in Figure 4.12, and as was experimentally observed. It should also be noted that the model for the modified system predicted a peak surface temperature that was approximately 50-100 K (for the range of energy densities considered) higher than that of the PA SLS system. Hence, during the SLS processing of the PA-4CB powder, the Nylon-12 particle would experience discrete temperature spikes on its surface whose magnitude can be determined using the modified model described

above. Moreover, the kinetic rate equation for thermal degradation due to carbon black-induced localized heating might be different from the model described above. The modified model represents an extreme case wherein all the carbon black particles are located in a thin layer at the top. This scenario is expected to predict the highest possible temperatures where the composite powder is completely desegregated. A more realistic depiction of the processing of the PA-4CB SLS system would require a 2-D or 3-D model that accounts for a heterogeneous material distribution with distinct thermo-physical properties.

4.4 Conclusions

A 1-D thermal model coupled with a sintering rate equation and a thermal degradation rate equation was implemented for the PA SLS and PA-4CB SLS systems. An empirical method of calculating the constants in the sintering rate equation that has been developed in earlier studies was successfully applied in this model. The results of the model can be used to estimate a window of optimal process parameters for the SLS-processing of polymer nanocomposites. Moreover, a model that considered the effective material properties of the PA-4CB SLS system did not predict a significant increase in the thermal degradation of the polymer. The predicted part densities for the PA-4CB SLS system were greater than experimentally determined values of part density. This is likely due to artifacts that could have been created on the surface of the sample during sample preparation. The creation of artifacts could have been exacerbated in the case of the PA-4CB SLS system due to the presence of a segregated microstructure as well as thermal degradation due to carbon black-induced localized heating. Additionally, the phenomenon of carbon black-induced localized heating was investigated. The presence of

carbon black on the surface of Nylon-12 resulted in higher surface temperatures. Carbon black-induced localized heating would result in discrete temperature spikes whose magnitude was estimated by the model.

CHAPTER 5 CONCLUSIONS

This chapter concludes the dissertation. Section 5.1 provides a summary of the dissertation. The scientific and technical contributions of this research are outlined in section 5.2. Finally, section 5.3 discusses potential areas of future research.

5.1 Summary of the Dissertation

The objective of this dissertation was to investigate the fundamental scientific and engineering aspects of processing an electrically conductive polymer nanocomposite (ECPC) by SLS. This objective was achieved through a systematic investigation of the processing and properties of a carbon black-filled electrically conductive Nylon-12 nanocomposite manufactured by SLS. In addition to the processing of an ECPC, the results of this research have provided valuable insights into the processing of polymer nanocomposites by SLS.

Chapter 2 demonstrates the successful processing of a carbon black-filled Nylon-12 nanocomposite by SLS. The laser power and the scan speed were optimized in order to maximize the flexural modulus of the parts. The flexural modulus of the nanocomposite was found to be lower than that of the neat polymer. The microstructure and porosity of parts made by different energy densities of the laser were investigated by optical microscopy and scanning electron microscopy. A segregated microstructure containing carbon black-rich regions was detected and was the likely reason for the lower flexural modulus for the nanocomposite.

The absorption of the CO_2 laser by the carbon black resulted in the emission of visible radiation that appeared to be more sensitive to the laser power than the energy

density. This thermal radiation from the scanned regions of the powder bed increased the depth of sintering and reduced the dimensional accuracy of the PA-4CB SLS parts at high energy densities relative to that of the PA SLS parts.

Chapter 3 focused on characterizing the microstructure and morphology of the PA-4CB SLS system in order to relate its thermo-mechanical properties and electrical conductivity to the SLS process. A comparative study of the properties, microstructure and morphology of a carbon black-reinforced Nylon-12 nanocomposite made by extrusion-injection molding was also presented. The effects of the microstructure, crystallization behavior, porosity and changes in the molecular weight of the polymer on the properties of the nanocomposites were studied. Results from the porosity analysis demonstrated the necessity for a pycnometry-based method to determine the part densities of the PA-4CB SLS system due to the segregated microstructure and inherent porous nature of carbon black. The addition of carbon black did not significantly alter the crystallization behavior of Nylon-12 in the SLS process. The segregated microstructure containing alternating domains of Nylon-12 and carbon black was found to have the greatest effect on the mechanical properties and the electrical conductivity of the composite. The dimension and structure of these domains is dictated by the size distributions of the polymer particles and the agglomerates of carbon black present in the composite powder. Hence, the preparation technique employed for the feedstock composite powder can be optimized in order to achieve the required properties for the manufactured composite based on its intended use.

Chapter 4 implemented a one-dimensional thermal model coupled with a sintering rate equation and a thermal degradation model to study the variation in part densities of

the PA SLS and PA-4CB SLS systems with respect to the energy density. The results of the model showed good agreement with the experimental results. Moreover, the model was modified to study the effects of carbon black-induced localized heating on the density of the PA-4CB SLS system. The addition of carbon black resulted in higher local temperatures which increased the depth of sintering but did not increase the extent of thermal degradation of the polymer for the range of energy densities investigated in this dissertation.

5.2 Contributions

The contributions of this dissertation can be divided into the following categories:

1. Contributions to the fundamental knowledge of SLS-processing of polymer nanocomposites.
2. Technical contributions.

5.2.1 Contribution to Fundamental Knowledge

This dissertation has offered new insights into the SLS-processing of a rotary-tumbled polymer nanocomposite powder blend. The SLS-processing of a polymer nanocomposite powder blend resulted in the formation of a segregated microstructure that was shown to have the greatest effect on the properties of the manufactured parts. The properties of SLS-processed polymer nanocomposites can be varied by varying the structure of the nanofiller, the strength of interaction between the filler and the polymer and the size distribution of the polymer powder and agglomerates of the nanoparticles. Moreover, the results from this research are also useful in understanding the properties of

polymer nanocomposites manufactured by the SLS-processing of powders obtained by cryogenic milling of extruded polymer nanocomposite pellets.

5.2.2 Technical Contributions

This dissertation employed SLS to manufacture an electrically conductive polymer composite with a relatively low percolation threshold of less than 4 wt. % of carbon black. This was attributed to the formation of a segregated microstructure that aided the formation of a network of carbon black particles.

A heat transfer model was developed to study the effects of carbon black-induced localized heating on the densification and thermal degradation of Nylon-12. This model complements the experimental results of earlier studies and can be modified for the SLS-processing of other polymers.

5.3 Future Work

Based on the work done in this dissertation, several recommendations for future work can be made. First, the effect of varying the loading of carbon black on the microstructure and properties of SLS-processed polymer nanocomposites can be studied. Second, the SLS-processing of surface-functionalized nanoparticle-polymer powder blends can be investigated in order to study the effect of polymer-nanoparticle interaction on the microstructure and properties of the nanocomposites. Third, the properties of hybrid polymer composites containing multiple fillers (nanofillers and conventional micron-sized fillers) can be investigated. Finally, the heat transfer model can be modified into a more comprehensive 3-D model that accounts for a heterogeneous material distribution.

APPENDIX A MATLAB CODE

Appendix A presents the MATLAB code that was written to study the variation in the density of the polymer with respect to the energy density during the SLS process. The theoretical background for this model is presented in chapter 4. This code consists of the script “heat_conduction.m”, which is the main body of the code. It solves the model described in chapter 4 by calling the following functions: “pdex.m”, which defines the differential equation; “pdexic.m”, which defines the initial conditions, and “pdexbc.m” which defines the boundary conditions.

heat_conduction.m

```
clear
clc

global xmin xmax tmin tmax x_ndiv t_ndiv u counter I

%------------INPUT PARAMETERS----------------------------------%

scan_vector_length = 2.5; %inch
part_width = 0.5; %inch
scan_spacing = 150 ; %micron
scan_speed = 60; %inch/sec
delta_t = 2.5e-5;    % sec
beam_dia = 400; % micron
laser_power = 3; % watt
I_o = 2*4*laser_power/(pi*(beam_dia*1e-6)^2); % Peak irradiance assuming Gaussian
beam

n_layers = 1;

n_deltat = round(scan_vector_length/(scan_speed*delta_t)); %number of time steps per
scan line
n_beam_1=ceil(264.60e-6/(scan_speed*0.0254*delta_t));
n_beam_2=ceil(400.00e-6/(scan_speed*0.0254*delta_t));
```

```
n_beam_3=ceil(264.60e-6/(scan_speed*0.0254*delta_t));

time_rem = 30; % seconds (time after 3 irradiations until beginning of next layer)
delta_t_rem=0.10;
n_deltat_rem = time_rem/delta_t_rem;

%-------DEFINING SPATIAL AND TIME DOMAINS----------------------%
xmin = 0;
xmax = 40e-3*0.0254;     % 40 mils in meters
x_ndiv = 100;            % Number of nodes
tmin = 0;
tmax = delta_t;
t_ndiv = 5;

m = 0;
x = linspace(xmin,xmax,x_ndiv);
t = linspace(tmin,tmax,t_ndiv);

%------------------------------------------------------------------%

%------INITIALIZING MATERIAL PROPERTIES------------------%
global density porosity K spec_heat T_air temp_bed_setpoint
wt = 0;   % weight fraction of carbon black
vol = 0;  % initial volumer fraction of carbon black
init_density = 480; %tap density of the Nylon-12 powder bed in kg/m3
max_density = 1020; % Material density of Nylon-12
init_porosity = (max_density-init_density)/max_density;
density=init_density*ones(1,x_ndiv);
porosity=init_porosity*ones(1,x_ndiv);
porosity_degrad = zeros(1,x_ndiv);

k_eff=0.25*(1-vol)+0.05*vol;    %effective thermal conductivity
C_p=3946*(1-wt)+650*wt;         % effective specific heat
spec_heat = C_p*ones(1,x_ndiv);
K_yk = k_eff/(1+(0.034*0.0358/k_eff));
K=(1-porosity)*K_yk;             %thermal conductivity of the powder bed
T_air = 173.5 + 273;             %Kelvin
temp_bed_setpoint = 173.5 + 273;  %Kelvin

n_time_steps = round(3*n_deltat+n_deltat_rem);
surf_temp=zeros(1,n_layers*n_time_steps);
time=zeros(1,n_layers*n_time_steps);
temp=zeros(n_layers*n_time_steps,x_ndiv);
bed_porosity=zeros(n_layers*n_time_steps,x_ndiv);
bed_porosity_degrad=zeros(n_layers*n_time_steps,x_ndiv);
```

```
%--------constants in the sintering rate equation----------%
E_s=98.5e3;
beta=8;
A_s=(5e11);

%--------constants for the kinetic equation for thermal degradation----%
A_d=8e10;
E_d=1.9149e4;


surf_temp(1)=temp_bed_setpoint;
time(1)=0;
temp(1,:)=temp_bed_setpoint;
bed_porosity(1,:)=porosity;
bed_porosity_degrad(1,:)=porosity_degrad;
%-----------------------------------------------------------%

for k = 1:n_layers
   % -------FIRST SCAN LINE WITH IRRADIATION BY LASER-------------
   mid_nodes = floor(n_beam_1/2);
   delta_x=264/(n_beam_1);

   if mod(n_beam_1,2)==1
      for a=1:mid_nodes+1
         x_coord(round(mid_nodes+3/2-(2*a-1)/2))=delta_x*(2*a-1)/2;
         x_coord(round(mid_nodes+3/2+(2*a-1)/2))=-delta_x*(2*a-1)/2;
      end
   else
      x_coord(mid_nodes+1)=0;
      for a=1:mid_nodes
         x_coord(mid_nodes+1-a)=a*delta_x;
         x_coord(mid_nodes+1+a)=-a*delta_x;
      end
   end

   for counter = 1+(k-1)*n_time_steps:n_beam_1+(k-1)*n_time_steps

I=I_o*(beam_dia/2)/(2*delta_x)*sqrt(pi/2)*1/exp(2*scan_spacing^2/(beam_dia/2)^2)*ab
s((erf(sqrt(2)*2*x_coord(counter-(k-1)*n_time_steps+1)/beam_dia)-
erf(sqrt(2)*2*x_coord(counter-(k-1)*n_time_steps)/beam_dia)));
      sol = pdepe(m,@pdex,@pdexic,@pdexbc,x,t);
      u = sol(:,:,1);
      surf_temp(counter+1)=u(end,1);
      time(counter+1)=(counter-(k-1)*n_time_steps)*delta_t + (k-
1)*(3*n_deltat*delta_t+n_deltat_rem*delta_t_rem);
```

```
      temp(counter+1,:)=u(end,:);
      for i=1:x_ndiv
         if u(end,i)>=(273+194)
            k_s=A_s*exp(-E_s/(8.314*(u(end,i))));
            spec_heat(i)=(460+7.8*u(end,i))*(1-wt)+650*wt;
         else
            k_s=A_s*exp(-E_s/(8.314*(u(end,i)))-beta*(1-4370/87400*(u(end,i)-
(174+273))));
            spec_heat(i)=C_p;
         end
         k_d = A_d*exp(-E_d/u(end,i));
         porosity(i)=porosity(i)*(1-k_s*delta_t);

         if porosity(i)<0
            porosity(i)=0;
         end
         porosity_degrad(i)=1-(1-porosity_degrad(i))*(1-k_d*delta_t);
      end
      bed_porosity(counter+1,:)=porosity;
      bed_porosity_degrad(counter+1,:)=porosity_degrad;
      K=(1-porosity)*K_yk;
      density=(1-porosity)*max_density;
      counter
   end

   for counter = n_beam_1+1+(k-1)*n_time_steps:n_deltat+(k-1)*n_time_steps
      I=0;
      sol = pdepe(m,@pdex,@pdexic,@pdexbc,x,t);
      u = sol(:,:,1);
      surf_temp(counter+1)=u(end,1);
      time(counter+1)=(counter-(k-1)*n_time_steps)*delta_t + (k-
1)*(3*n_deltat*delta_t+n_deltat_rem*delta_t_rem);
      temp(counter+1,:)=u(end,:);
      for i=1:x_ndiv
         if u(end,i)>=(273+194)
            k_s=A_s*exp(-E_s/(8.314*(u(end,i))));
            spec_heat(i)=(460+7.8*u(end,i))*(1-wt)+650*wt;
         else
            k_s=A_s*exp(-E_s/(8.314*(u(end,i)))-beta*(1-4370/87400*(u(end,i)-
(174+273))));
            spec_heat(i)=C_p;
         end
         k_d = A_d*exp(-E_d/u(end,i));
         porosity(i)=porosity(i)*(1-k_s*delta_t);
         if porosity(i)<0
            porosity(i)=0;
```

```
            end
            porosity_degrad(i)=1-(1-porosity_degrad(i))*(1-k_d*delta_t);
        end
        bed_porosity(counter+1,:)=porosity;
        bed_porosity_degrad(counter+1,:)=porosity_degrad;
        K=(1-porosity)*K_yk;
        density=(1-porosity)*max_density;
        counter
    end

    % -------SECOND SCAN LINE WITH IRRADIATION BY LASER----------
    mid_nodes = floor(n_beam_2/2);
    delta_x=400/(n_beam_2);
    if mod(n_beam_2,2)==1
        for a=1:mid_nodes+1
            x_coord(round(mid_nodes+3/2-(2*a-1)/2))=delta_x*(2*a-1)/2;
            x_coord(round(mid_nodes+3/2+(2*a-1)/2))=-delta_x*(2*a-1)/2;
        end
    else
        x_coord(mid_nodes+1)=0;
        for a=1:mid_nodes
            x_coord(mid_nodes+1-a)=a*delta_x;
            x_coord(mid_nodes+1+a)=-a*delta_x;
        end
    end
    for counter = n_deltat+1+(k-1)*n_time_steps:n_deltat+n_beam_2+(k-1)*n_time_steps

I=I_o*(beam_dia/2)/(2*delta_x)*sqrt(pi/2)*1/exp(2*scan_spacing^2/(beam_dia/2)^2)*ab
s((erf(sqrt(2)*2*x_coord(counter-n_deltat-(k-1)*n_time_steps+1)/beam_dia)-
erf(sqrt(2)*2*x_coord(counter-n_deltat-(k-1)*n_time_steps)/beam_dia)));
        sol = pdepe(m,@pdex,@pdexic,@pdexbc,x,t);
        u = sol(:,:,1);
        surf_temp(counter+1)=u(end,1);
        time(counter+1)=(counter-(k-1)*n_time_steps)*delta_t + (k-
1)*(3*n_deltat*delta_t+n_deltat_rem*delta_t_rem);
        temp(counter+1,:)=u(end,:);
        for i=1:x_ndiv
            if u(end,i)>=(273+194)
                k_s=A_s*exp(-E_s/(8.314*(u(end,i))));
                spec_heat(i)=(460+7.8*u(end,i))*(1-wt)+650*wt;
            else
                k_s=A_s*exp(-E_s/(8.314*(u(end,i)))-beta*(1-4370/87400*(u(end,i)-
(174+273))));
                spec_heat(i)=C_p;
            end
            k_d = A_d*exp(-E_d/u(end,i));
```

```
        porosity(i)=porosity(i)*(1-k_s*delta_t);
        if porosity(i)<0
           porosity(i)=0;
        end
        porosity_degrad(i)=1-(1-porosity_degrad(i))*(1-k_d*delta_t);
     end
     bed_porosity(counter+1,:)=porosity;
     bed_porosity_degrad(counter+1,:)=porosity_degrad;
     K=(1-porosity)*K_yk;
     density=(1-porosity)*max_density;
     counter
  end

  for counter = n_deltat+n_beam_2+1+(k-1)*n_time_steps:2*n_deltat+(k-
1)*n_time_steps
     I=0;
     sol = pdepe(m,@pdex,@pdexic,@pdexbc,x,t);
     u = sol(:,:,1);
     surf_temp(counter+1)=u(end,1);
     time(counter+1)=(counter-(k-1)*n_time_steps)*delta_t + (k-
1)*(3*n_deltat*delta_t+n_deltat_rem*delta_t_rem);
     temp(counter+1,:)=u(end,:);
     for i=1:x_ndiv
        if u(end,i)>=(273+194)
           k_s=A_s*exp(-E_s/(8.314*(u(end,i))));
           spec_heat(i)=(460+7.8*u(end,i))*(1-wt)+650*wt;
        else
           k_s=A_s*exp(-E_s/(8.314*(u(end,i)))-beta*(1-4370/87400*(u(end,i)-
(174+273))));
           spec_heat(i)=C_p;
        end
        k_d = A_d*exp(-E_d/u(end,i));
        porosity(i)=porosity(i)*(1-k_s*delta_t);
        if porosity(i)<0
           porosity(i)=0;
        end
        porosity_degrad(i)=1-(1-porosity_degrad(i))*(1-k_d*delta_t);
     end
     bed_porosity(counter+1,:)=porosity;
     bed_porosity_degrad(counter+1,:)=porosity_degrad;
     K=(1-porosity)*K_yk;
     density=(1-porosity)*max_density;
     counter
  end

  % -------THIRD SCAN LINE WITH IRRADIATION BY LASER----------
```

```
   mid_nodes = floor(n_beam_3/2);
   delta_x=264/(n_beam_3);
   if mod(n_beam_3,2)==1
      for a=1:mid_nodes+1
         x_coord(round(mid_nodes+3/2-(2*a-1)/2))=delta_x*(2*a-1)/2;
         x_coord(round(mid_nodes+3/2+(2*a-1)/2))=-delta_x*(2*a-1)/2;
      end
   else
      x_coord(mid_nodes+1)=0;
      for a=1:mid_nodes
         x_coord(mid_nodes+1-a)=a*delta_x;
         x_coord(mid_nodes+1+a)=-a*delta_x;
      end
   end

   for counter = 2*n_deltat+1+(k-1)*n_time_steps:2*n_deltat+n_beam_3+(k-
1)*n_time_steps

I=I_o*(beam_dia/2)/(2*delta_x)*sqrt(pi/2)*1/exp(2*scan_spacing^2/(beam_dia/2)^2)*ab
s((erf(sqrt(2)*2*x_coord(counter-2*n_deltat-(k-1)*n_time_steps+1)/beam_dia)-
erf(sqrt(2)*2*x_coord(counter-2*n_deltat-(k-1)*n_time_steps)/beam_dia)));
      sol = pdepe(m,@pdex,@pdexic,@pdexbc,x,t);
      u = sol(:,:,1);
      surf_temp(counter+1)=u(end,1);
      time(counter+1)=(counter-(k-1)*n_time_steps)*delta_t + (k-
1)*(3*n_deltat*delta_t+n_deltat_rem*delta_t_rem);
      temp(counter+1,:)=u(end,:);
      for i=1:x_ndiv
         if u(end,i)>=(273+194)
            k_s=A_s*exp(-E_s/(8.314*(u(end,i))));
            spec_heat(i)=(460+7.8*u(end,i))*(1-wt)+650*wt;
         else
            k_s=A_s*exp(-E_s/(8.314*(u(end,i)))-beta*(1-4370/87400*(u(end,i)-
(174+273))));
            spec_heat(i)=C_p;
         end
         k_d = A_d*exp(-E_d/u(end,i));
         porosity(i)=porosity(i)*(1-k_s*delta_t);
         if porosity(i)<0
            porosity(i)=0;
         end
         porosity_degrad(i)=1-(1-porosity_degrad(i))*(1-k_d*delta_t);
      end
      bed_porosity(counter+1,:)=porosity;
      bed_porosity_degrad(counter+1,:)=porosity_degrad;
      K=(1-porosity)*K_yk;
```

```
    density=(1-porosity)*max_density;
    counter
  end

  for counter = 2*n_deltat+n_beam_3+1+(k-1)*n_time_steps:3*n_deltat+(k-
1)*n_time_steps
    I=0;
    sol = pdepe(m,@pdex,@pdexic,@pdexbc,x,t);
    u = sol(:,:,1);
    surf_temp(counter+1)=u(end,1);
    time(counter+1)=(counter-(k-1)*n_time_steps)*delta_t + (k-
1)*(3*n_deltat*delta_t+n_deltat_rem*delta_t_rem);
    temp(counter+1,:)=u(end,:);
    for i=1:x_ndiv
      if u(end,i)>=(273+194)
        k_s=A_s*exp(-E_s/(8.314*(u(end,i))));
        spec_heat(i)=(460+7.8*u(end,i))*(1-wt)+650*wt;
      else
        k_s=A_s*exp(-E_s/(8.314*(u(end,i)))-beta*(1-4370/87400*(u(end,i)-
(174+273))));
        spec_heat(i)=C_p;
      end
      k_d = A_d*exp(-E_d/u(end,i));
      porosity(i)=porosity(i)*(1-k_s*delta_t);
      if porosity(i)<0
        porosity(i)=0;
      end
      porosity_degrad(i)=1-(1-porosity_degrad(i))*(1-k_d*delta_t);
    end
    bed_porosity(counter+1,:)=porosity;
    bed_porosity_degrad(counter+1,:)=porosity_degrad;
    K=(1-porosity)*K_yk;
    density=(1-porosity)*max_density;
    counter
  end

  tmin = 0;
  tmax = delta_t_rem;
  t_ndiv = 5;
  t = linspace(tmin,tmax,t_ndiv);

  for counter = 3*n_deltat+1+(k-1)*n_time_steps:n_time_steps+(k-1)*n_time_steps
    I=0;
    sol = pdepe(m,@pdex,@pdexic,@pdexbc,x,t);
    u = sol(:,:,1);
    surf_temp(counter+1)=u(end,1);
```

```
      time(counter+1)=time(3*n_deltat+(k-1)*n_time_steps)+(counter-3*n_deltat-(k-
1)*n_time_steps)*delta_t_rem;
      temp(counter+1,:)=u(end,:);
      for i=1:x_ndiv
         if u(end,i)>=(273+194)
            k_s=A_s*exp(-E_s/(8.314*(u(end,i))));
            spec_heat(i)=(460+7.8*u(end,i))*(1-wt)+650*wt;
         else
            k_s=A_s*exp(-E_s/(8.314*(u(end,i)))-beta*(1-4370/87400*(u(end,i)-
(174+273))));
            spec_heat(i)=C_p;
         end
         k_d=A_d*exp(-E_d/u(end,i));
         porosity(i)=porosity(i)*(1-k_s*delta_t_rem);
         if porosity(i)<0
            porosity(i)=0;
         end
         porosity_degrad(i)=1-(1-porosity_degrad(i))*(1-k_d*delta_t_rem);
      end
      bed_porosity(counter+1,:)=porosity;
      bed_porosity_degrad(counter+1,:)=porosity_degrad;
      K=(1-porosity)*K_yk;
      density=(1-porosity)*max_density;
      counter
   end

   if k<n_layers
      porosity(11:100)=porosity(1:90);
      porosity_degrad(11:100)=porosity_degrad(1:90);
      K(11:100)=K(1:90);
      u(end,11:100)=u(end,1:90);

      porosity(1:10)=init_porosity;
      porosity_degrad(1:10)=0;
      K(1:10)=(1-init_porosity)*K_yk;
      u(end,1:10)=temp_bed_setpoint;
   end

   tmin = 0;
   tmax = delta_t;
   t_ndiv = 5;
   t = linspace(tmin,tmax,t_ndiv);
end

y=zeros(1,n_layers);
x_axis=1:n_layers;
```

```
for l=1:n_layers
   y(l)=mean(bed_porosity(l*n_time_steps+1,((l-1)*10+1):(l*10)));
end

disp('DONE!!!');
```

pdex.m

```
function [c,f,s] = pdex(x,t,u,dudx)

%--------function to define the PDE -------%

global xmin xmax x_ndiv density spec_heat K

flag = round(x/((xmax-xmin)/(x_ndiv-1)) + 1);

c = density(flag)*spec_heat(flag);
f = K(flag)*dudx;
s = 0;
```

pdexic.m

```
function u0 = pdexic(x)

%-------------function to define the initial conditions-----%

global xmin xmax x_ndiv u counter temp_bed_setpoint
if counter ==1
   u0 = temp_bed_setpoint;
else
   flag = round(x/((xmax-xmin)/(x_ndiv-1)) + 1);
   u0 = u(end,flag);
end
```

pdexbc.m

```
function [pl,ql,pr,qr] = pdexbc(xl,ul,xr,ur,t)

%-----function to define the boundary conditions-------%

global u T_air counter temp_bed_setpoint I

Gr_Pr = 1e6;     % Grashof Prandtl number
```

```
if Gr_Pr>1e5 & Gr_Pr<2e7
   a = 0.54;
   b = 0.25;
else
   a = 0.14;
   b = 0.33;
end

h_c = a*(Gr_Pr)^b;
h_r=0;
if counter==1
   if temp_bed_setpoint>T_air
      h_r = 5.67e-8*(0.85*temp_bed_setpoint^4-0.10*T_air^4)/(temp_bed_setpoint-
T_air) ;
   end
   h = h_c + h_r;  %Composite heat transfer coefficient with radiative and convective
heat transfer
   pl =-0.85*I + h*(temp_bed_setpoint-T_air);
else
   if u(end,1)>T_air
      h_r = 5.67e-8*(0.85*u(end,1)^4-0.10*T_air^4)/(u(end,1)-T_air);
   end
   h = h_c + h_r;
   pl =  -0.85*I + h*(u(end,1)-T_air); %
end


ql = -1;
pr = 0;
qr = -1;
```

REFERENCES

[1] Bhattacharya, S.N., Gupta, R.K., and Kamal, M.R., *Polymeric Nanocomposites: Theory and Practice*. 2008: Hanser.

[2] Guo, S., Zhang, C., Wang, W., Liu, T., Tjiu, W.C., He, C., and Zhang, W.-D., *Preparation and characterization of polyurethane/multiwalled carbon nanotube composites.* Polymers and Polymer Composites, 2008. **16**(8): p. 501-507.

[3] Bryning, M.B., Islam, M.F., Kikkawa, J.M., and Yodh, A.G., *Very low conductivity threshold in bulk isotropic single-walled carbon nanotube-epoxy composites.* Advanced Materials, 2005. **17**(9): p. 1186-1191.

[4] Zhang, W., Dehghani-Sanij, A.A., and Blackburn, R.S., *Carbon based conductive polymer composites.* Journal of Materials Science, 2007. **42**(10): p. 3408-3418.

[5] Hwang, J., Muth, J., and Ghosh, T., *Electrical and mechanical properties of carbon-black-filled, electrospun nanocomposite fiber webs.* Journal of Applied Polymer Science, 2007. **104**(4): p. 2410-2417.

[6] Tiwari, M.K., Yarin, A.L., and Megaridis, C.M., *Electrospun fibrous nanocomposites as permeable, flexible strain sensors.* Journal of Applied Physics, 2008. **103**(4): p. 044305-1.

[7] Gul, V.E., *Structure and Properties of Conducting Polymer Composites*. 1996, Utrecht: VSP.

[8] Huang, J.-C., *Carbon black filled conducting polymers and polymer blends.* Advances in Polymer Technology, 2002. **21**(4): p. 299-313.

[9] Cembrola, R.J., *Relationship of carbon black dispersion to electrical resistivity and vulcanizate physical properties.* Polymer Engineering and Science, 1982. **22**(10): p. 601-609.

[10] Agari, Y., Ueda, A., and Nagai, S., *Thermal conductivities of composites in several types of dispersion systems.* Journal of Applied Polymer Science, 1991. **42**(6): p. 1665-1669.

[11] Yui, H., Wu, G., Sano, H., Sumita, M., and Kino, K., *Morphology and electrical conductivity of injection-molded polypropylene/carbon black composites with addition of high-density polyethylene.* Polymer, 2006. **47**(10): p. 3599-3608.

[12] Beaman, J.J., Barlow, J.W., Bourell, D.L., Crawford, R.H., Marcus, H.L., and McAlea, K.P., *Solid freeform fabrication: A New Direction in Manufacturing* 1997, Dordrecht: Kluwer Academic Publishers.

[13] Deckard, C.R., *Selective Laser Sintering*, Doctoral dissertation in Mechanical Engineering, 1988, University of Texas, Austin

[14] Kai, C.C. and Fai, L.K., *Rapid Prototyping: Principles and Applications in Manufacturing*. 1997: John Wiley & Sons.

[15] Chung, H. and Das, S., *Functionally graded Nylon-11/silica nanocomposites produced by selective laser sintering.* Materials Science and Engineering A, 2008. **487**: p. 251-257.

[16] Chung, H. and Das, S., *Processing and properties of glass bead particulate-filled functionally graded Nylon-11 composites produced by selective laser sintering.* Materials Science and Engineering A, 2006. **437**(2): p. 226-234.

[17] Williams, J.M., Adewunmi, A., Schek, R.M., Flanagan, C.L., Krebsbach, P.H., Feinberg, S.E., Hollister, S.J., and Das, S., *Bone tissue engineering using polycaprolactone scaffolds fabricated via selective laser sintering.* Biomaterials, 2005. **26**(23): p. 4817-4827.

[18] Hao, L., Savalani, M.M., Zhang, Y., Tanner, K.E., Heath, R.J., and Harris, R.A., *Characterization of selective laser sintered-hydroxyapatite-based biocomposite structures for bone replacement.* Proceedings of the Royal Society of London, Series A (Mathematical, Physical and Engineering Sciences), 2007. **463**(2084): p. 1857-69.

[19] Popov, V.K., Evseev, A.V., Antonov, E.N., Bagratashvili, V.N., Konovalov, A.N., Panchenko, V.Y., Barry, J.J.A., Whitaker, M.J., and Howdle, S.M., *Laser technologies for fabricating individual implants and matrices for tissue engineering.* Journal of Optical Technology, 2007. **74**(9): p. 636-40.

[20] Leong, K.F., Wiria, F.E., Chua, C.K., and Li, S.H., *Characterization of a poly-ε-caprolactone polymeric drug delivery device built by selective laser sintering.* Bio-Medical Materials and Engineering, 2007. **17**(3): p. 147-157.

[21] Kruth, J.P., Wang, X., Laoui, T., and Froyen, L., *Lasers and materials in selective laser sintering.* Assembly Automation, 2003. **23**(4): p. 357-371.

[22] Chen, S., Murphy, J., Herlehy, J., Bourell, D.L., and Wood, K.L., *Development of SLS fuel cell current collectors.* Rapid Prototyping Journal, 2006. **12**(5): p. 275-82.

[23] Ko, S.H., Heng, P., Grigoropoulos, C.P., Luscombe, C.K., Frechet, J.M.J., and Poulikakos, D., *Air stable high resolution organic transistors by selective laser sintering of ink-jet printed metal nanoparticles.* Applied Physics Letters, 2007. **90**(14): p. 141103-1.

[24] Ko, S.H., Pan, H., Grigoropoulos, C.P., Luscombe, C.K., Frechet, J.M.J., and Poulikakos, D., *All-inkjet-printed flexible electronics fabrication on a polymer substrate by low-temperature high-resolution selective laser sintering of metal nanoparticles.* Nanotechnology, 2007. **18**(34): p. 345202.

[25] Ko, S.H., Pan, H., Grigoropoulos, C.P., Frechet, J.M.J., Luscombe, C.K., and Poulikakos, D., *Lithography-free high-resolution organic transistor arrays on polymer substrate by low energy selective laser ablation of inkjet-printed nanoparticle film.* Applied Physics A: Materials Science and Processing, 2008. **92**(3): p. 579-587.

[26] Jana, S.C. and Jimenez, G.A., *Electrically conductive polymer nanocomposites of polymethylmethacrylate and carbon nanofibers prepared by chaotic mixing.* Composites Part A (Applied Science and Manufacturing), 2007. **38**(3): p. 983-93.

[27] Ezquerra, T.A., Bayer, R.K., and Balta Calleja, F.J., *Conductive PE-carbon black composites by elongational flow injection moulding.* Journal of Materials Science, 1988. **23**(11): p. 4121-4126.

[28] Bayer, R.K., Ezquerra, T.A., Zachmann, H.G., Balta Calleja, F.J., Martinez Salazar, J., Meins, W., Diekow, R.E., and Wiegel, P., *Conductive PE-carbon composites by elongation flow injection moulding.* Journal of Materials Science, 1988. **23**(2): p. 475-480.

[29] Martinez Salazar, J., Bayer, R.K., Ezquerra, T.A., and Balta Calleja, F.J., *Conductive polyethylene-carbon black composites by elongational-flow injection molding. Part 3. Study of the structure and morphology.* Colloid and Polymer Science, 1989. **267**(5): p. 409-413.

[30] Bigg, D.M., *Investigation of the effect of carbon black structure, polymer morphology, and processing history on the electrical conductivity of carbon-black-filled thermoplastics.* Journal of Rheology, 1984. **28**(5): p. 501-516.

[31] Pramanik, P.K., Khastgir, D., and Saha, T.N., *Effect of filler blend composition and temperature on the properties of electrically conductive rubber composites.* Plastics, Rubber and Composites Processing and Applications, 1991. **15**(3): p. 189-194.

[32] Drubetski, M., Siegmann, A., and Narkis, M., *Hybrid particulate and fibrous injection molded composites: Carbon black/carbon fiber/polypropylene systems.* Polymer Composites, 2005. **26**(4): p. 454-464.

[33] Foulger, S.H., *Reduced percolation thresholds of immiscible conductive blends.* Journal of Polymer Science, Part B: Polymer Physics, 1999. **37**(15): p. 1899-1910.

[34] Breuer, O., Tchoudakov, R., Narkis, M., and Siegmann, A., *Segregated structures in carbon black-containing immiscible polymer blends: HIPS/LLDPE systems.* Journal of Applied Polymer Science, 1997. **64**(6): p. 1097-1106.

[35] Li, B., Xu, X.-B., Li, Z.-M., and Song, Y.-C., *Manipulating the conductivity of carbon-black-filled immiscible polymer composites by insulating nanoparticles.* Journal of Applied Polymer Science, 2008. **110**(5): p. 3073-3079.

[36] Dong, X.M., Fu, R.W., Zhang, M.Q., Zhang, B., and Rong, M.Z., *Carbon black filled poly(2-ethylhexyl methacrylate) as a candidate for gas sensing material.* Journal of Materials Science Letters, 2003. **22**(15): p. 1057-1059.

[37] Jun Rong, L., Jia Rui, X., Ming Qiu, Z., and Min Zhi, R., *Carbon black/ polystyrene composites as candidates for gas sensing materials.* Carbon, 2003. **41**(12): p. 2353-60.

[38] Schueler, R., Petermann, J., Schulte, K., and Wentzel, H.-P., *Agglomeration and electrical percolation behavior of carbon black dispersed in epoxy resin.* Journal of Applied Polymer Science, 1997. **63**(13): p. 1741-1746.

[39] Koysuren, O., Yesil, S., and Bayram, G., *Effect of composite preparation techniques on electrical and mechanical properties and morphology of nylon 6 based conductive polymer composites.* Journal of Applied Polymer Science, 2006. **102**(3): p. 2520-2526.

[40] Pinto, G., Lopez-Gonzalez, C., and Jimenez-Martin, A., *Polymer composites prepared by compression molding of a mixture of carbon black and nylon 6 powder.* Polymer Composites, 1999. **20**(6): p. 804-808.

[41] Tchoudakov, R., Breuer, O., Narkis, M., and Siegmann, A., *Conductive polymer blends with low carbon black loading: Polypropylene/polyamide.* Polymer Engineering & Science, 1996. **36**(10): p. 1336-1346.

[42] Yacubowicz, J., Narkis, M., and Benguigui, L., *Electrical and dielectric properties of segregated carbon black-polyethylene systems.* Polymer Engineering and Science, 1990. **30**(8): p. 459-468.

[43] Coleman, J.N., Khan, U., Blau, W.J., and Gun'ko, Y.K., *Small but strong: A review of the mechanical properties of carbon nanotube-polymer composites.* Carbon, 2006. **44**(9): p. 1624-52.

[44] Wang, B., Wang, H., Hong, B., and Zhang, Y., *Fibers from multi-walled carbon nanotube/polyacrylonitrile composites.* Polymer Journal, 2005. **37**(5): p. 376-379.

[45] Choi, H.J., Zhang, K., and Lim, J.Y., *Multi-walled carbon nanotube/polystyrene composites prepared by in-situ bulk sonochemical polymerization.* Journal of Nanoscience and Nanotechnology, 2007. **7**(10): p. 3400-3403.

[46] Li, W.-H., Chen, X.-H., Chen, C.-S., Xu, L.-S., Yang, Z., and Wang, Y.-G., *Preparation and shear properties of carbon nanotubes/poly(butyl methacrylate) hybrid material.* Polymer Composites, 2008. **29**(9): p. 972-977.

[47] Kang, X., Ma, W., Zhang, H.-L., Xu, Z.-G., Guo, Y., and Xiong, Y., *Vinyl-carbon nanotubes for composite polymer materials.* Journal of Applied Polymer Science, 2008. **110**(4): p. 1915-1920.

[48] Chang, S., Gengchao, W., Farong, H., and Yanhua, S., *Effect of carbon black modified with polyaniline on resistivity behavior of polyethylene/carbon black composites.* Journal of Macromolecular Science-Physics, 2008. **47**(1): p. 65-75.

[49] Flandin, L., Prasse, T., Schueler, R., Schulte, K., Bauhofer, W., and Cavaille, J.Y., *Anomalous percolation transition in carbon-black-epoxy composite materials.* Physical Review B (Condensed Matter), 1999. **59**(22): p. 14349-55.

[50] Prasse, T., Flandin, L., Schulte, K., and Bauhofer, W., *In situ observation of electric field induced agglomeration of carbon black in epoxy resin.* Applied Physics Letters, 1998. **72**(22): p. 2903.

[51] Prasse, T., Schwarz, M.K., Schulte, K., and Bauhofer, W., *The interaction of epoxy resin and an additional electrolyte with non-oxidised carbon black in colloidal dispersions.* Colloids and Surfaces A: Physicochemical and Engineering Aspects, 2001. **189**(1-3): p. 183-188.

[52] Schwarz, M.K., Bauhofer, W., and Schulte, K., *Alternating electric field induced agglomeration of carbon black filled resins.* Polymer, 2002. **43**(10): p. 3079-82.

[53] Li, N., Huang, Y., Du, F., He, X., Lin, X., Gao, H., Ma, Y., Li, F., Chen, Y., and Eklund, P.C., *Electromagnetic Interference (EMI) shielding of single-walled carbon nanotube epoxy composites.* Nano Letters, 2006. **6**(6): p. 1141-1145.

[54] Sandler, J., Shaffer, M.S.P., Prasse, T., Bauhofer, W., Schulte, K., and Windle, A.H., *Development of a dispersion process for carbon nanotubes in an epoxy matrix and the resulting electrical properties.* Polymer, 1999. **40**(21): p. 5967-71.

[55] Sandler, J.K.W., Kirk, J.E., Kinloch, I.A., Shaffer, M.S.P., and Windle, A.H., *Ultra-low electrical percolation threshold in carbon-nanotube-epoxy composites.* Polymer, 2003. **44**(19): p. 5893-5899.

[56] Kirkpatrick, S., *Percolation and Conduction.* Reviews of Modern Physics, 1973. **45**(4): p. 574.

[57] Choi, Y.-K., Sugimoto, K.-I., Song, S.-M., Gotoh, Y., Ohkoshi, Y., and Endo, M., *Mechanical and physical properties of epoxy composites reinforced by vapor grown carbon nanofibers.* Carbon, 2005. **43**(10): p. 2199-2208.

[58] Zhang, B., Fu, R., Zhang, M., Dong, X., Wang, L., and Pittman Jr, C.U., *Gas sensitive vapor grown carbon nanofiber/polystyrene sensors.* Materials Research Bulletin, 2006. **41**(3): p. 553-562.

[59] Safadi, B., Andrews, R., and Grulke, E.A., *Multiwalled carbon nanotube polymer composites: Synthesis and characterization of thin films.* Journal of Applied Polymer Science, 2002. **84**(14): p. 2660-2669.

[60] Chuangchote, S., Sirivat, A., and Supaphol, P., *Mechanical and electro-rheological properties of electrospun poly(vinyl alcohol) nanofibre mats filled with carbon black nanoparticles.* Nanotechnology, 2007. **18**(14): p. 145705.

[61] Greiner, A. and Wendorff, J.H., *Electrospinning: a fascinating method for the preparation of ultrathin fibers.* Angewandte Chemie International Edition, 2007. **46**(30): p. 5670-3.

[62] Young Hee, L., Eun Ju, R., Kay Hyeok, A., Ki Kang, K., and Seung Yol, J., *Anisotropic electrical conductivity of MWCNT/PAN nanofiber paper.* Chemical Physics Letters, 2005. **413**(1-3): p. 188-93.

[63] Yu-Qin, W., Ji-Huan, H., and Jian-Yong, Y., *Carbon nanotube-reinforced polyacrylonitrile nanofibers by vibration-electrospinning.* Polymer International, 2007. **56**(11): p. 1367-70.

[64] Macossay, J., Leal, J.H., Anxiu, K., and Jones, R.E., *Electrospun fibers from poly(methyl methacrylate)/vapor grown carbon nanofibers.* Polymers for Advanced Technologies, 2006. **17**(5): p. 391-4.

[65] Ho, H.C.H., Gibson, I., and Cheung, W.L. *Effects of energy density on morphology and properties of selective laser sintered polycarbonate.* 1999. Switzerland: Elsevier.

[66] Partee, B., Hollister, S.J., and Das, S., *Selective laser sintering process optimization for layered manufacturing of CAPA 6501 polycaprolactone bone tissue engineering scaffolds.* Transactions of the ASME. Journal of Manufacturing Science and Engineering, 2006. **128**(2): p. 531-40.

[67] Yusheng, S., Yan, W., Jibing, C., and Shuhuai, H., *Experimental investigation into the selective laser sintering of high-impact polystyrene.* Journal of Applied Polymer Science, 2008. **108**(1): p. 535-40.

[68] Caulfield, B., McHugh, P.E., and Lohfeld, S., *Dependence of mechanical properties of polyamide components on build parameters in the SLS process.* Journal of Materials Processing Technology, 2007. **182**(1-3): p. 477-488.

[69] Thompson, M., Whalley, D., and Hopkinson, N. *Investigating Dielectric Properties of Sintered Polymers for Rapid Manufacturing*. in *Solid Freeform Fabrication Symposium*.August 4-6, 2008. Austin, Texas.

[70] Salmoria, G.V., Leite, J.L., Paggi, R.A., Lago, A., and Pires, A.T.N., *Selective laser sintering of PA12/HDPE blends: Effects of components on elastic/plastic behavior.* Polymer Testing, 2008. **27**: p. 654-659.

[71] Salmoria, G.V., Leite, J.L., and Paggi, R.A., *The microstructural characterization of PA6/PA12 blend specimens fabricated by selective laser sintering.* Polymer Testing, 2009. **28**(7): p. 746-751.

[72] Zhang, Y., Hao, L., Savalani, M.M., Harris, R.A., and Tanner, K.E., *Characterization and dynamic mechanical analysis of selective laser sintered hydroxyapatite-filled polymeric composites.* Journal of Biomedical Materials Research - Part A, 2008. **86**(3): p. 607-616.

[73] Schmidt, M., Pohle, D., and Rechtenwald, T., *Selective Laser Sintering of PEEK.* CIRP Annals - Manufacturing Technology, 2007. **56**(1): p. 205-208.

[74] Kim, J. and Creasy, T.S., *Selective laser sintering characteristics of nylon 6/clay reinforced nanocomposite.* Polymer Testing, 2004. **23**(6): p. 629-636.

[75] Zhang, Y., Hao, L., Savalani, M.M., Harris, R.A., and Tanner, K.E., *Characterization and dynamic mechanical analysis of selective laser sintered hydroxyapatite-filled polymeric composites.* Journal of Biomedical Materials Research-Part A, 2008. **86**(3): p. 607-616.

[76] Fan, K.M., Cheung, W.L., and Gibson, I., *Fusion behavior of TrueFormTM/SiO_2 composite powders during selective laser sintering.* Rapid Prototyping Journal, 2008. **14**(2): p. 87-94.

[77] Wang, Y., Shi, Y., and Huang, S., *Selective laser sintering of polyamide-rectorite composite.* Proceedings of the Institution of Mechanical Engineers, Part L: Journal of Materials: Design and Applications, 2005. **219**(1): p. 11-15.

[78] Mazzoli, A., Moriconi, G., and Pauri, M.G., *Characterization of an aluminum filled polyamide powder for applications in selective laser sintering* Materials and Design, 2007. **28**: p. 993-1000.

[79] Haizhong, Z., Jian, Z., Shiqiang, L., Gaochao, W., and Zhifeng, X., *Effect of core-shell composite particles on the sintering behavior and properties of nano-Al_2O_3/polystyrene composite prepared by SLS.* Materials Letters, 2006. **60**(9-10): p. 1219-23.

[80] Chunze, Y., Yusheng, S., Jinsong, Y., and Jinhui, L., *A nanosilica/nylon-12 composite powder for selective laser sintering.* Journal of Reinforced Plastics and Composites, 2009. **28**(23): p. 2889-2902.

[81] Lao, S.C., Koo, J.H., Morgan, A., Jor, H.-K., Nguyen, K., Wissler, G., Pilato, L., and Luo, Z. *Flame retardant intumescent polyamide 11-carbon nanofiber nanocomposites: Thermal and flammability properties*. 2008. Boston, MA, United states: Materials Research Society.

[82] Jinhui, L., Yusheng, S., Zhongliang, L., Yang, X., and Shuhuai, H., *Rapid manufacturing metal parts by laser sintering admixture of epoxy resin/iron powders.* Advanced Engineering Materials, 2006. **8**(10): p. 988-94.

[83] Evans, R.S., Bourell, D.L., Beaman, J.J., and Campbell, M.I., *Rapid manufacturing of silicon carbide composites.* Rapid Prototyping Journal, 2005. **11**(1): p. 37-40.

[84] Clare, A.T., Chalker, P.R., Davies, S., Sutcliffe, C.J., and Tsopanos, S., *Selective laser sintering of barium titanate-polymer composite films.* Journal of Materials Science, 2008. **43**(9): p. 3197-3202.

[85] Frenkel, J., *Viscous flow of crystalline bodies under the action of surface tension.* Journal of Physics, 1945. **9**: p. 385-291.

[86] Pokluda, O., Bellehumeur, C.T., and Vlachopoulos, J., *Modification of Frenkel's model for sintering.* AIChE Journal, 1997. **43**(12): p. 3253-3256.

[87] Sperling, L.H., *Introduction to Pyhsical Polymer Science*. 2006, New jeresey: John Wiley and Sons.

[88] Evonik Industries,Polyamide 12 Coating Powders,http://www.vestosint.com, February 2008

[89] King, J.A., Tucker, K.W., Meyers, J.D., Weber, E.H., Clingerman, M.L., and Ambrosius, K.R., *Factorial design approach applied to electrically and thermally conductive nylon 6,6.* Polymer Composites, 2001. **22**(1): p. 142-154.

[90] *Particulate-filled polymer composites*. Polymer science and technology series, ed. R.N. Rothon. 1995, Harlow, Essex, England :: Longman Scientific & Technical ;.

[91] Kalaitzidou, K., Fukushima, H., and Drzal, L.T., *Multifunctional polypropylene composites produced by incorporation of exfoliated graphite nanoplatelets.* Carbon, 2007. **45**(7): p. 1446-1452.

[92] Caulfield, B., McHugh, P.E., and Lohfeld, S., *Dependance of mechanical properties of polyamide components on build parameters in the SLS process.* Journal of Materials Processing Technology, 2007. **182**: p. 477-488.

[93] Schiaffino, S. and Sonin, A.A., *On the theory for the arrest of an advancing molten contact line on a cold solid of the same material.* Physics of Fluids, 1997. **9**(8): p. 2227-2233.

[94] Rasband, W.S. *ImageJ,U. S. National Institutes of Health*.Bethesda,Maryland, USA.http://rsb.info.nih.gov/ij/.1997-2010

[95] Deshmane, C., Yuan, Q., and Misra, R.D.K., *On the fracture characteristics of impact tested high density polyethylene-calcium carbonate nanocomposites.* Materials Science and Engineering A, 2007. **452-453**: p. 592-601.

[96] Majewski, C., Zarringhalam, H., and Hopkinson, N., *Effect of the degree of particle melt on mechanical properties in selective laser-sintered Nylon-12 parts.* Proceedings of the Institution of Mechanical Engineers, Part B: Journal of Engineering Manufacture, 2008. **222**(9): p. 1055-1064.

[97] Zarringhalam, H., Hopkinson, N., Camperman, N.F., and Vileger, J.J.D., *Effects of processing on microstructure and properties of SLS Nylon 12.* Materials Science and Engineering A, 2006. **435**.

[98] Chan, C.-M., Cheng, C.-L., and Yuen, M.M.F., *Electrical properties of polymer composites prepared by sintering a mixture of carbon black and ultra-high molecular weight polyethylene powder.* Polymer Engineering and Science, 1997. **37**(7): p. 1127-1136.

[99] Yacubowicz, J., Narkis, M., and Benguigui, L., *Electrical and dielectric properties of segregated carbon black-polyethylene systems.* Polymer Engineering & Science, 1990. **30**(8): p. 459-468.

[100] Woicke, N., Wagner, T., and Eyerer, P. *Carbon assisted laser sintering of thermoplastic polymers*. in *Annual Technical Conference - ANTEC*. 2005.

[101] Kim, J. and Creasy, T.S., *Selective laser sintering characteristics of nylon 6/clay-reinforced nanocomposite.* Polymer Testing, 2004. **23**(6): p. 629-636.

[102] Osswald, S., Behler, K., and Gogotsi, Y., *Laser induced light emission from carbon nanoparticles.* Journal of Applied Physics, 2008. **104**.

[103] *Carbon black-polymer composites : the physics of electrically conducting composites*. Plastics engineering ;, ed. E.K. Sichel. 1982, New York :: M. Dekker.

[104] Zhi Han, L., Lee, A., Yanwu, Z., Kim-Yong, L., and Chorng-Haur, S., *Sustained laser induced incandescence in carbon nanotubes for rapid localized heating.* Applied Physics Letters, 2009. **94**(7): p. 073106 (3 pp.).

[105] Zeng, H., Yang, C., Dai, J., and Cui, X., *Light-induced incandescence of single-walled carbon nanotubes.* Journal of Physical Chemistry C, 2008. **112**(11): p. 4172-4175.

[106] *GPC Final Report,*2009,Jordi Labs,Bellingham, USA

[107] *Envelope Density Report,*2009,Micromeritics Analytical Services,Norcross, Georgia, USA

[108] Young, R.J., *Introduction to Polymers*. 1983, London: Chapman and Hall.

[109] *Mechanical properties and testing of polymers : an A-Z reference*. Polymer science and technology series ;, ed. G.M. Swallowe. 1999, Dordrecht ;: Kluwer Academic.

[110] Xie, J.-J., *Kinetics of the solid-state polymerization of nylon-6.* Journal of Applied Polymer Science, 2002. **84**(3): p. 616-621.

[111] Gogolewski, S., Czerniawska, K., and Gasiorek, M., *Effect of annealing on thermal properties and crystalline structure of polyamides. nylon 12(polylaurolactam).* Colloid and Polymer Science, 1980. **258**(10): p. 1130-1136.

[112] Pham, D.T., Dotchev, K.D., and Yusoff, W.A.Y., *Deterioration of polyamide powder properties in the laser sintering process.* Proceedings of the Institution of Mechanical Engineers, Part C: Journal of Mechanical Engineering Science, 2008. **222**(11): p. 2163-2176.

[113] Giles, H.F., *Extrusion the definitive processing guide and handbook*. PDL handbook series, ed. J.R. Wagner and E.M. Mount. 2005, Norwich, NY :: William Andrew Pub.

[114] Sangkeun Rhee, J.L.W., *Crystal structure and morphology of biaxially oriented polyamide 12 films.* Journal of Polymer Science Part B: Polymer Physics, 2002. **40**(12): p. 1189-1200.

[115] Ramesh, C., *Crystalline transitions in Nylon 12.* Macromolecules, 1999. **32**(17): p. 5704-5706.

[116] Hiramatsu, N., Haraguchi, K., and Hirakawa, S., *Study of transformations among alpha , gamma and gamma prime forms in nylon 12 by x-ray and DSC.* Japanese Journal of Applied Physics, Part 1: Regular Papers & Short Notes, 1983. **22**(2): p. 335-339.

[117] Ayala, R.E., Hartley, P.A., and Parfitt, G.D., *Relevance of powder/liquid wettability to the cohesiveness of carbon black agglomerates.* Particle Characterization, 1986. **3**(1): p. 26-31.

[118] He, X., Yang, J., Zhu, L., Wang, B., Sun, G., Lv, P., Phang, I.Y., and Liu, T., *Morphology and melt rheology of nylon 11/clay nanocomposites.* Journal of Applied Polymer Science, 2006. **102**(1): p. 542-549.

[119] Bard, A.J., *Electrochemical methods : fundamentals and applications*, ed. L.R. Faulkner. 1980, New York :: Wiley.

[120] Pegel, S., Pötschke, P., Petzold, G., Alig, I., Dudkin, S.M., and Lellinger, D., *Dispersion, agglomeration, and network formation of multiwalled carbon nanotubes in polycarbonate melts.* Polymer, 2008. **49**(4): p. 974-984.

[121] Khan, J., Harton, S.E., Akcora, P., Benicewicz, B.C., and Kumar, S.K., *Polymer Crystallization in Nanocomposites: Spatial Reorganization of Nanoparticles.* Macromolecules, 2009. **42**(15): p. 5741-5744.

[122] Sun, M.M., *Physical Modeling of the Selective Laser Sintering Process*, PhD Thesis 1992, University of Texas, Austin

[123] Nelson, J.C., *Selective laser sintering: A definition of process and an empirical sintering model*, PhD Thesis 1993, University of Texas, Austin

[124] Vail, N.K., *Preparation and characterization of microencapsulated, finely divided ceramic materials for selective laser sintering*, PhD Thesis 1994, University of Texas, Austin

[125] Dong, L., Makradi, A., Ahzi, S., Remond, Y., and Sun, X., *Simulation of the densification of semicrystalline polymer powders during the selective laser sintering process: Application to Nylon 12.* Polymer Science - Series A, 2008. **50**(6): p. 704-709.

[126] Childs, T.H. and Tontowi, A., *Selective laser sintering of a crystalline and a glass-filled crystalline polymer: experiments and simulations.* Proceedings of the Institution of Mechanical Engineers, Part B: Journal of Engineering Manufacture, 2001. **215**(11): p. 1481-1495.

[127] Festa, R., Manca, O., and Naso, V., *Comparison between models of thermal fields in laser and electron beam surface processing.* International Journal of Heat and Mass Transfer, 1988. **31**(1): p. 99-106.

[128] Maquin, B., Goyheneche, J.-M., Derre, A., Trinquecoste, M., Chadeyron, P., and Delhaes, P., *Thermal conductivity of submicrometre particles: carbon blacks and solid solutions containing C, B and N.* Journal of Physics D: Applied Physics, 2000. **33**(1): p. 8-17.

[129] Akzo Nobel,Ketjenblack EC-600JD,2009,www.akzonobel.com

[130] Yagi, S. and Kunii, D., *Studies on effective thermal conductivities in packed beds.* Chemical Engineering Progress, 1957. **3**(3): p. 373-381.

[131] Tszeng, T.C., Im, Y.T., and Kobayashi, S., *Thermal analysis of solidification by the temperature recovery method.* International Journal of Machine Tools and Manufacture, 1989. **29**(1): p. 107-120.

[132] Balasubramanian, B., *Study of the selective laser sintering of metal-polymer powders*, PhD Thesis 1995, University of Texas, Austin

[133] Nielsen, L.E., *Mechanical properties of polymers and composites*. 1974, New York :: M. Dekker.